Journal of Applied Physics

REVIEW ARTICLE | SEPTEMBER 11 2023

Go with the flow: Rheological requirements for direct ink write printability

Peiran Wei (魏沛然) ; Ciera Cipriani ; Chia-Min Hsieh (謝佳旻) ; Krutarth Kamani ; Simon Rogers ; Emily Pentzer

J. Appl. Phys. 134, 100701 (2023)
https://doi.org/10.1063/5.0155896

AIP Publishing

Journal of Applied Physics REVIEW pubs.aip.org/aip/jap

Go with the flow: Rheological requirements for direct ink write printability

Cite as: J. Appl. Phys. **134**, 100701 (2023); doi: 10.1063/5.0155896
Submitted: 24 April 2023 · Accepted: 15 August 2023 ·
Published Online: 11 September 2023

Peiran Wei (魏沛然),[1,a)] Ciera Cipriani,[2] Chia-Min Hsieh (謝佳旻),[3] Krutarth Kamani,[4] Simon Rogers,[4] and Emily Pentzer[2,3,a)]

AFFILIATIONS

[1]Soft Matter Facility, Texas A&M University, 1313 Research Pkwy, College Station, Texas 77845, USA
[2]Department of Materials Science and Engineering, Texas A&M University, College Station, Texas 77840, USA
[3]Department of Chemistry, Texas A&M University, College Station, Texas 77843, USA
[4]Department of Chemical and Biomolecular Engineering, University of Illinois at Urbana-Champaign, Urbana, Illinois 61801, USA

[a)]**Authors to whom correspondence should be addressed:** peiran@tamu.edu and emilypentzer@tamu.edu

ABSTRACT

The rapid development of additive manufacturing, also known as three-dimensional (3D) printing, is driving innovations in both industry and academia. Direct ink writing (DIW), an extrusion-based 3D printing technology, can build 3D structures through the deposition of custom-made inks and produce devices with complex architectures, excellent mechanical properties, and enhanced functionalities. A paste-like ink is the key to successful printing. However, as new ink compositions have emerged, the rheological requirements of inks have not been well connected to printability, or the ability of a printed object to maintain its shape and support the weight of subsequent layers. In this review, we provide an overview of the rheological properties of successful DIW inks and propose a classification system based on ink composition. Factors influencing the rheology of different types of ink are discussed, and we propose a framework for describing ink printability using measures of rheology and print resolution. Furthermore, evolving techniques, including computational studies, high-throughput rheological measurements, machine learning, and materiomics, are discussed to illustrate the future directions of feedstock development for DIW. The goals of this review are to assess our current understanding of the relationship between rheological properties and printability, to point out specific challenges and opportunities for development, to provide guidelines to those interested in multi-material DIW, and to pave the way for more efficient, intelligent approaches for DIW ink development.

I. INTRODUCTION

Three-dimensional printing (3DP), the largest subset of additive manufacturing, has gained much attention in the past two decades as a method for producing complex, customized three-dimensional structures with excellent mechanical properties and/or functionalities. Direct ink writing (DIW), also known as robocasting,[1–3] is one of the most commonly used techniques to accomplish this goal due to its low cost, ease of use, and ability to tailor feedstock composition.[4] In recent years, substantial advances have been made in DIW, specifically for bio-related[5–11] and conductive[12–17] materials. As shown in Fig. 1, the use of DIW to produce functional devices is rapidly growing, with an increasing annual number of publications on advanced applications, such as printed structural components,[18–21] electronics,[12–17,22] flexible materials,[17,23,24] biomedical materials,[5–11] and catalysis materials,[25–27] among others.

DIW feedstocks, also referred to as "inks," are a key component in DIW as they determine not only the internal structure and performance of resultant objects but also the success of printing. Similar to fused deposition modeling (FDM), the rheology of which was discussed by Mackay,[31] DIW is an extrusion-based additive manufacturing method; however, DIW and FDM use different principles to print, and hence, the rheological requirements for their feedstocks differ. An FDM printer heats a thermoplastic filament to the melt/liquid state, and the extruded filament cools rapidly after extrusion onto a substrate and solidifies [Fig. 2(a)].[32,33] The rheology of the melt state is, therefore, important, but the thermal properties of the FDM filament, which solidifies as it cools after printing, are what enables FDM to build fully 3D objects. In contrast, DIW is most commonly performed at room temperature, meaning that the isothermal rheology plays a

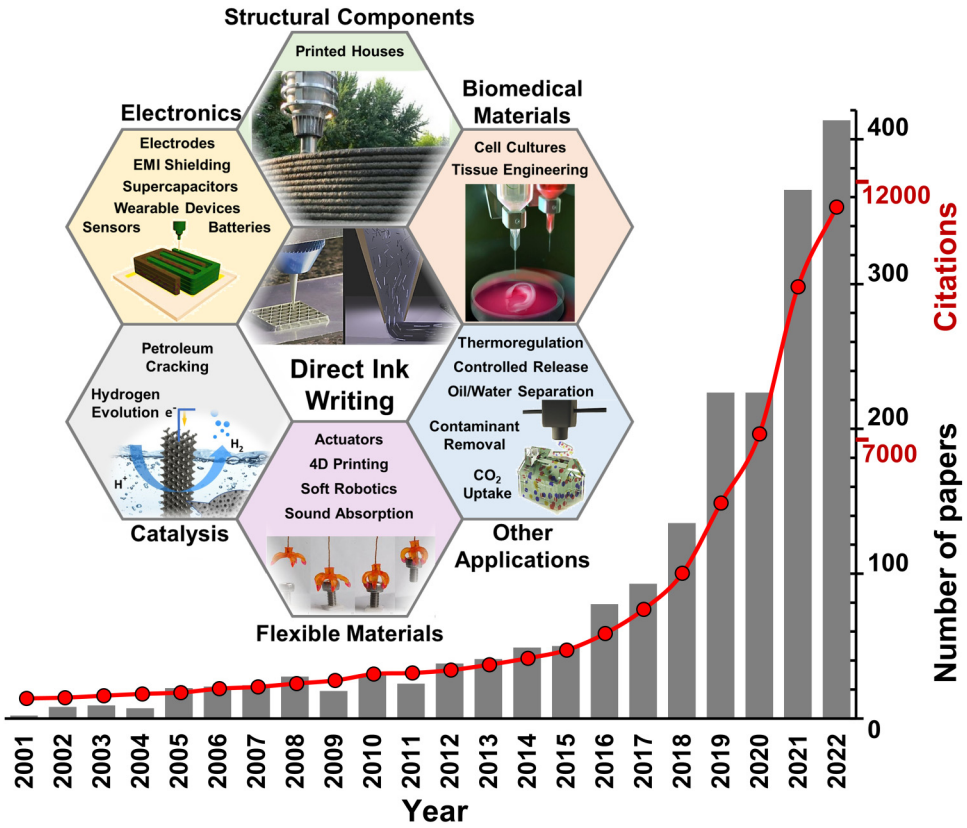

FIG. 1. Both the number of papers and citations have increased exponentially in the field of DIW over the past 20 years[28] (data acquired from Web of Science, search keyword: "direct ink writing." Date: July 22, 2023). The honeycomb diagram illustrates the main applications of DIW.[18,22,24,27,29,30] Reproduced with permission from Compton *et al.*, Adv. Mater. **26**, 5930–5935 (2014). Copyright 2014 John Wiley and Sons; Shen *et al.*, Adv. Energy Mater. **8**, 1800408 (2018). Copyright 2018 John Wiley and Sons; Ge *et al.*, Sci. Rep. **6**, 31110 (2016). Copyright 2016 Springer Nature; Li *et al.*, J. Energy Power Technol. **2**(2), 7 (2020). Copyright 2020 Author(s), licensed under a Creative Commons Attribution (CC BY) license; Wei *et al.*, Matter **4**(6), 1975–1989 (2021). Copyright 2021 Elsevier; Hager *et al.*, Proc. Eng. **151**, 292–299 (2016). Copyright 2016 Elsevier.

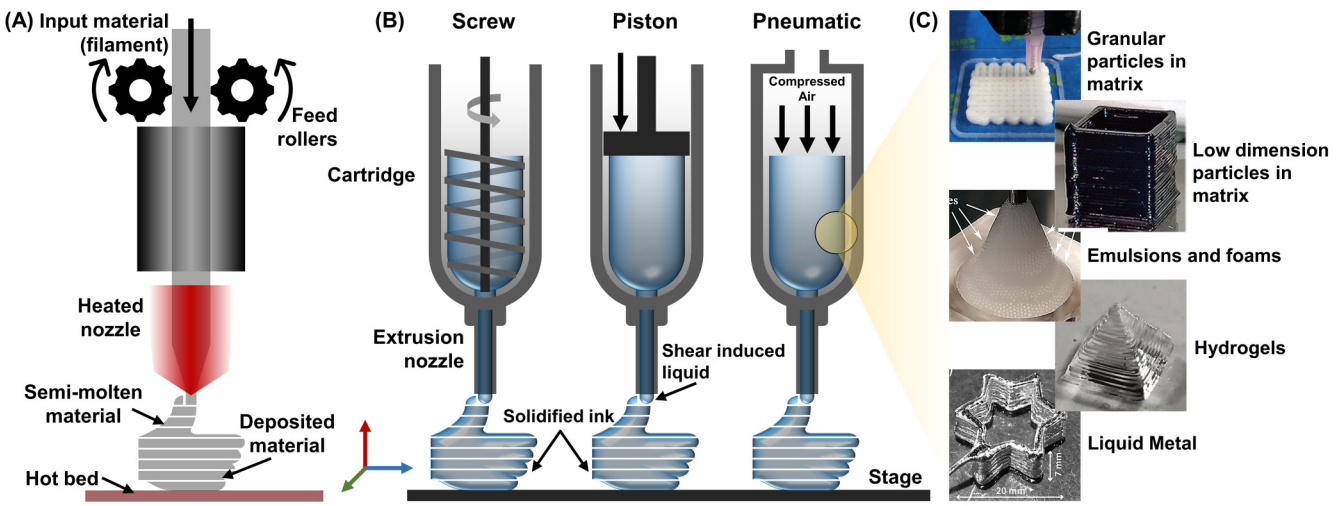

FIG. 2. Comparison of the FDM technique (a) and the DIW technique (b). (c) Illustration of the five most common ink categories for DIW.[33,45,49,58–60] Reproduced with permission from Gomez-Gras *et al.*, Mater. Des. **140**, 278–285 (2018). Copyright 2018 of Elsevier; Chen *et al.*, Adv. Funct. Mater. **29**(20), 1900971 (2019). Copyright 2019 John Wiley and Sons; Daalkhaijav *et al.*, Adv. Mater. Technol. **3**, 1700351 (2018). Copyright 2018 John Wiley and Sons; Malda *et al.*, Adv. Mater. **25**(36), 5011–5028 (2013). Copyright 2013 John Wiley and Sons; Costantini *et al.*, Angew. Chem. Int. Ed. **131**, 7702–7707 (2019). Copyright 2019 John Wiley and Sons; Yang *et al.*, Adv. Mater. **31**(37), 1902725 (2019). Copyright 2019 John Wiley and Sons.

larger role than in FDM. Since the room temperature process eliminates heat transfer considerations, nozzles for DIW can vary greatly in size, ranging from as small as 0.1 μm in diameter, as used in microfabrication, to as big as several dm for concrete printing, as in building applications.[34] An ideal DIW feedstock "ink" should be extrudable at moderate pressures and should maintain its shape after extrusion. Further, multiple layers must be stackable without significant structure slumping [Fig. 2(b)].

As illustrated in Fig. 2(c), DIW inks are usually composed of highly filled polymer solutions,[35–37] emulsions,[38–42] hydrogels,[10,43–45] or liquid metals.[46–50] Printable inks are viscous, paste-like materials which are able to be extruded through a syringe, stackable to form 3D-printed structures, and may be solidified during/after printing by solvent drying,[36,37] ultraviolet curing,[23,29,36,51–53] chemical curing,[54,55] or heating/cooling[56,57] the printed ink. Since these curing methods can enable access to inks having a wider scope of rheological behavior (i.e., inks which would typically slump if not post-processed), the present review focuses on inks which are printable at room temperature without additional curing during printing and that can form structures at least 5 mm tall. Real inks almost always deviate in some meaningful manner from the idealized requirements elucidated above, leading to compromised prints. Therefore, a detailed understanding of ink rheology will allow for ink-specific printing protocols to be applied to achieve higher quality final objects.

Although a great number of studies have been dedicated to the investigation of novel functional DIW inks and their applications, few address the fundamental questions:

How is "printability" defined?
What rheological properties are required for a successful DIW ink?
How does the composition of the DIW ink determine the rheological properties that define the printability and fidelity of the final printed objects?

The successful answers to these questions will (1) lead to a simple way to predict the printability based on ink rheology and the constituent components, (2) help researchers better tune printing parameters and print fidelity, and (3) facilitate the development of inks that have special rheological requirements, such as bioinks containing live cells[5,61,62] or emulsion inks[38–42] composed of thermodynamically unstable phase separated systems.[63,64] In this review, we first describe the rheological requirements of DIW inks (Sec. II) and then discuss the quantitative methods to describe ink printability using rheology and print resolution (Sec. III). We follow this by proposing a new classification for ink composition and discuss factors influencing the rheology of different types of inks (Sec. IV). Finally, we address the evolving techniques in the study of ink rheology (Sec. V) and propose immediate areas for focus (Sec. IV). This description paves the way for more efficient, intelligent approaches to DIW ink development, including high-throughput rheological measurements, machine learning, and materiomics.

II. RHEOLOGICAL REQUIREMENTS FOR DIW INKS

A DIW printer consists of a syringe-based dispensing system which contains the feedstock ink and which is moved in three dimensions relative to a build platform such that the ink is dispensed in a predefined pattern. During printing, the ink is subjected to stress (σ) and acquires strain, γ, at a rate of $\dot{\gamma}$ as it is pushed through a nozzle onto the build surface to create the three-dimensional object. Strictly speaking, the strain, strain rate, and stress are all tensorial quantities, but typically, only one or two components are investigated at a time. An adequate ink for DIW requires homogeneous dispersion of its components and must have appropriate rheological behavior to be printable. Here, a printable ink is defined as being capable of being extruded and of supporting some mass indefinitely without continued distortion. The extrusion requirement relates to viscous or plastic behavior, while the ability to support mass without continued distortion is a solid-like property. Specifically, a DIW ink should have a yield stress (σ_y) above which the ink will flow.[4] From this, yield stress follows a high viscosity (η) at low rates [usually between 10^2 and 10^6 mPa s when measured at a shear rate ($\dot{\gamma}$) of 0.1 s^{-1}].[65–68] The high viscosity enables the ink to maintain a paste-like consistency.[4,62] Additionally, shear-thinning behavior permits the ink to be extruded, and thixotropy contributes to recovery of the high viscosity after extrusion.[67,69,70] As such, the presence of a yield stress facilitates DIW printing and the ability of the ink to maintain the shape of a printed object.

To illustrate the connection between shear stress, yield stress, shear rate, and viscosity, we present the example of the simple Bingham model for yield stress fluids, which additively combines a yield stress and a simple (Newtonian) flow rule,

$$\sigma_{\text{Bingham}} = \sigma_y + \eta_B \dot{\gamma}, \tag{1}$$

where η_B is the Bingham plastic viscosity and all other terms have their usual meaning.[71] Below the yield stress, the model is perfectly rigid. Other models, such as those of Casson[72] or Herschel and Bulkley[73] use similar formulations but make different choices for the flow rule. The Herschel–Bulkley model, for instance, generalizes the Bingham model by allowing for power-law flow with an exponent n. When $n = 1$ in the Herschel–Bulkley model, the Bingham model is obtained.

Viscosity describes a fluid's resistance to flow when a force is applied and results from internal friction.[34,62,74,75] For different inks, there are different origins of internal friction, including interactions between particles/particle flocs,[4,67,69,70,76–78] polymer entanglement,[79–81] non-covalent bonds (e.g., van der Waals interactions),[77,78] etc. (see Sec. IV). Apparent viscosity is defined as the ratio of the shear stress to the shear rate, which for the Bingham model is

$$\eta_{\text{Bingham}} = \sigma_{\text{Bingham}}/\dot{\gamma} = \sigma_y/\dot{\gamma} + \eta_B. \tag{2}$$

A number of simple observations can be drawn from this. First, the viscosity is dominated at low rates by the $\sigma_y/\dot{\gamma}$ term in Eq. (2), which makes the viscosity very large. In fact, in the limit of zero shear rate, the viscosity diverges. Second, the viscosity decreases with increasing shear rate, showing shear-thinning because of the presence of the yield stress term. Additionally, if the viscosity is plotted as a function of the shear rate (both on logarithmic scales), it will show a shear-thinning slope of −1 at low rates. Third, for simple models like the Bingham model, when the stress drops below the yield stress, all flow ceases, and the material resolidifies. The factors of high viscosity, shear-thinning behavior, and thixotropy are commonly referred to as the three main

requirements of a DIW ink; however, as illustrated by Eqs. (1) and (2), these factors are all contained in the statement, "A DIW ink must have a yield stress."

Printability of a DIW ink goes beyond the simple presence of a yield stress because filaments need to be able to support the mass of the same ink extruded layer-by-layer atop one another. The yield stress of an ink must, therefore, be larger than the forces due to gravity, which are dictated by the density of the ink. As a result, denser inks require larger yield stresses to be printable. If the gravitational force on a printed element exceeds the yield stress, the lower layer of material will yield and flow until the cross-sectional area increases enough to reduce the stress to the yield stress.[82] Thus, the ratio of gravitational stress to the yield stress sets the maximum vertical dimensions of what can be printed before slumping occurs and additional post-processing is required. This requirement can be summarized by the dimensionless group that relates gravitational stresses to the yield stress, which resembles a plastic Galilei number (typically the ratio of gravitational to viscous forces) or an inverse gravitational Bingham number (typically the ratio of yield stress to viscous forces). Printability is obtained when

$$\frac{\rho g h}{2\sigma_y} < 1, \tag{3}$$

where h is the height of the print with a maximum value set by $2\sigma_y/\rho g$ before slumping occurs. The reason for the factor of 2 in the denominator was noted by Pashias *et al.*, that for an ideal elastic solid the maximum shear stress that can act on a body when a pressure is applied to it in a normal direction is equal to half the pressure.[82,83] A simple analysis of how much a cylinder of material will slump was presented by Pashias *et al.* in their work introducing their "50 cent rheometer."[82] The goal of their work was to allow for field measurements of yield stresses, but their analysis of slump heights also holds for the modern application of DIW printing.

As with this printability requirement, it is convenient to compare similar properties across complex fluids using dimensionless groups that summarize the essential physics. Two dimensionless groups, known as the Deborah and Weissenberg numbers,[84–88] quantify the extent to which a material's rheological response is elastic or viscous at a particular observation time, along with the strength of the flow. The Deborah number is defined as the ratio of a material timescale, such as a relaxation time, and an experimental timescale and is large for elastic responses and small for viscous responses. The Weissenberg number is often defined as the product of the relaxation time and the characteristic rate of deformation and describes the degree to which nonlinearity is exhibited.[89] For example, flowing polymer in the melt at high Weissenberg number disentangles, and polymer chains are aligned along the direction of applied shear, resulting in a decrease in the apparent viscosity. In colloidal suspensions, fluid droplets align and deform, solid particle aggregates break apart, or low-dimensional particles align in the direction of the applied shear. These are the mechanisms behind shear-thinning behavior within various DIW inks at high Weissenberg numbers, which will be further detailed in Sec. III.

Applying this framework to the direct ink writing (DIW) process, we observe the following phenomena: (1) if the ink possesses a yield stress and is sitting in a nozzle, it will exhibit a high Deborah number and low Weissenberg number, thereby preventing dripping out of the nozzle; (2) during extrusion, flow occurs once the stress exceeds the yield stress, resulting in a low Deborah number and a (typically) high Weissenberg number; (3) once the ink exits the nozzle, it enters a zero-stress condition, allowing for the elastic strain acquired during the extrusion process to recover; consequently, the Deborah number transitions back to a high value, while the Weissenberg number becomes low once again.

For a printing nozzle with diameter of 1 mm, application of a stress that leads to an extrusion rate of $1\ s^{-1}$ results in a filament that grows in length at a rate of 1 mm/s. As such, modulating the value of the applied stress controls the rate of filament growth; stresses that are closer to the yield stress will cause the filaments to grow even slower, in some cases by orders of magnitude. The applied stress should be tuned to achieve the desired material extrusion rate. In the 1 mm nozzle case, extrusion of a filament at a rate of 1 cm/s, therefore, corresponds to a shear rate of $10\ s^{-1}$. Printing with smaller nozzles, therefore, requires pushing the ink rheology to higher shear rates. The connection between printing and rheology is, therefore, intimately related to the timescales over which a printing result will be allowed to occur, and yield stress fluid rheology is key to the printing process.

A. Brief history of yield stress fluid rheology

In the DIW process, inks with yield stresses undergo a transition from being viscoelastic solids, where deformations are recoverable, to deforming viscoplastically, where deformation is unrecoverable, as the applied load exceeds a certain threshold. This phenomenon is commonly referred to as "yielding." The existence of the yield stress has been vigorously debated over the years,[90] with some authors pointing out that determination of a yield stress depends on waiting long enough to determine whether very slow flows are stable. However, the yield stress has since become accepted as an engineering reality.

Early attempts to model the rheology of yield stress fluids, such as those of Bingham, Herschel and Bulkley, and Casson, focused solely on creating a flow rule for the steady flowing state.[71–73,91] These attempts implied an instantaneous yielding process and infinitely rigid pre-yielding behavior. Oldroyd's work expanded on these early attempts by explicitly modeling both the unyielded and yielded regimes. Oldroyd proposed that yield stress fluids behave as elastic solids when the applied stress is below the yield stress and flow plastically above it, following the flow behavior described by Bingham. This two-regime behavior is now known as the Oldroyd–Prager formalism.[92–95] Several models utilize this formalism and distinguish between unyielded solid and yielded viscoplastic behaviors using distinct physics, with the most prominent models proposed by Saramito.[96,97]

Recently, models have been developed that move beyond the Oldroyd–Prager formalism. Dimitriou and McKinley constructed a model based on the idea of kinematic hardening,[98] which describes the yielding condition as a function of the intensity of the past plastic strain.[99] Kamani *et al.* proposed a five-parameter model that accounts for all the major rheological observations of yield stress fluids, including the transient nature of the yielding transition.[100]

Their model incorporates a relaxation time that is dependent on the rate of deformation and a framework where plastic flow is enhanced by rapid elastic deformation. In the context of DIW, this model indicates that plastic flow of an ink can begin at stresses below the yield stress, but stress should be maintained above the yield stress for stable flow. The ink composition, nozzle diameter, and material extrusion rate can be modulated to account for this phenomenon and achieve stable extrusion throughout the extent of a print.

III. ASSESSING PRINTABILITY FROM RHEOLOGY AND FIDELITY PERSPECTIVE

Unlike FDM feedstocks which tend to be commercialized and standardized, new DIW inks are constantly being developed and are often formulated using a guess-and-check approach. This variability in ink composition makes it challenging to directly compare ink performance from study to study. To both expedite DIW ink development and improve reproducibility, ink properties and, thus, printability must be quantified. Printability can be described by two interlinked metrics: rheology of the ink and fidelity of the printed object. Methods for evaluating these metrics are elaborated below.

A. Rheological experiments

The commonly employed rheometers to evaluate ink rheology are torsional and capillary. In a torsional rheometer, a sample is sheared between two surfaces, one of which rotates about an axis and the other of which is stationary.[34] Based on the nature of this rotation, various rheological properties can be determined. In contrast, capillary rheometers perform measurements while pushing a sample through a capillary die. As such, capillary rheometry can achieve higher shear rates (~100–1000 s^{-1})[101] which are similar to those experienced during DIW,[102] and this technique can also be used at elevated temperatures and pressures compared to torsional rheometry.[101,103,104] Although capillary rheometers possess these advantages, they typically only provide access to steady state flow behavior at zero Deborah number and not the transient rheology which is important for DIW. Additionally, the influence of the high pressure used for testing on the sample rheology must be accounted for, and torsional rheometers are more commonly available. Therefore, rheological studies of DIW inks are most commonly performed using torsional rheometers with either parallel plate or cone-and-plate geometries.

Based on rheological measurements, fluids can be classified as either Newtonian or non-Newtonian. Newtonian fluids have a linear relationship between stress and shear rate, as shown in Fig. 3(a), whereas non-Newtonian fluids exhibit rate-dependent viscosities.[34,62,78,105] Shear-thickening materials show an increase in viscosity with increasing stress due to hydrocluster formation which leads to continuous shear-thickening or frictional contacts that cause discontinuous shear-thickening. Shear-thinning materials, in contrast, show decreased viscosity at high Weissenberg number as the alignment of fluid components (e.g., particles or polymer chains) dominate the rheological behavior.[62,105]

Transient nonlinear rheology is key to DIW processes; therefore, when measuring ink rheology, it is best to use geometries that

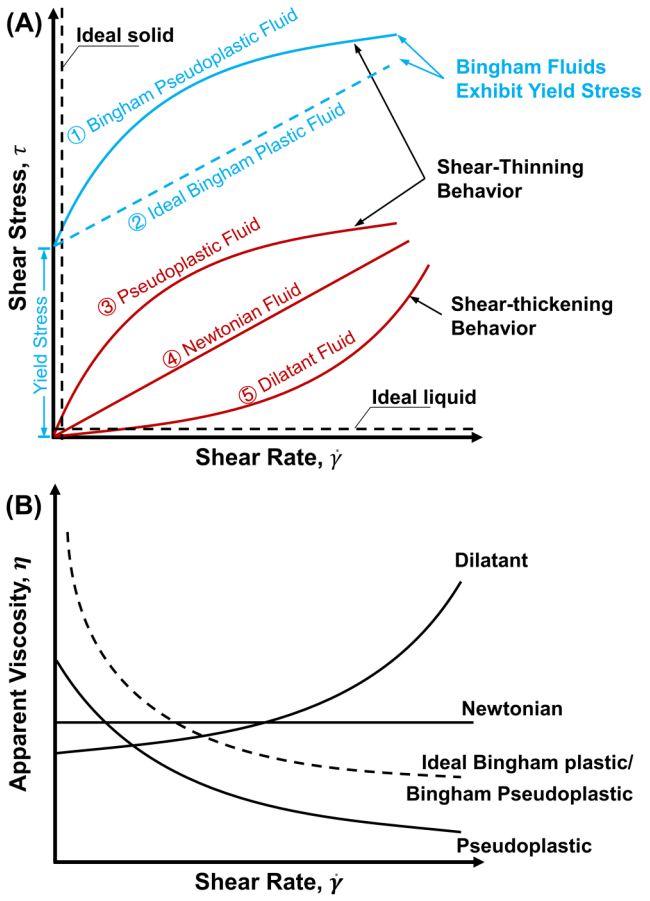

FIG. 3. (a) Shear stress vs shear rate profiles of different types of fluids. (b) Viscosity vs shear rate profiles of different types of fluids. Note: Bingham fluids are also called yield-stress fluids. Depending on the model used to approximate the rheological data, these may also be called Herschel–Bulkley fluids, Casson fluids, etc.

accurately measure nonlinear properties without the need for corrections. While parallel plate rheometry is attractive for ease of loading, measuring nonlinear properties with this geometry requires well-known corrections to account for the heterogeneous shear rate across the gap.[106–112] Better geometries include cone-and-plate and concentric cylinder Couette tools. As such, if a single viscosity value is reported for a DIW ink, the shear condition, including geometry, must also be reported. To quantify viscosity over a wide range of rates, shear rate sweeps are generally performed, where the rate is increased in a stepwise manner throughout the experiment, and the viscosity is reported over the course of the measurement in a plot like that in Fig. 3(b).[34,105] The extent of any shear-thinning behavior can be described by the slope of this curve or by a shear-thinning index, where the value of the ratio of the low-rate viscosity to the high-rate viscosity is reported.[113] Since these are steady state measurements, the Deborah number is zero and one can only interpret the rheology in terms of the strength of the flow that is described by

the Weissenberg number. However, the DIW process involves variation in the Deborah number as well. In other words, shear rate sweeps only provide information about the flowing state and not about the transient yielding or unyielding processes crucial to successful printing.

To describe how an ink yields and unyields during DIW, it is important to acknowledge that the shear strain and rate are composite parameters made of recoverable and unrecoverable components,

$$\gamma(t) = \gamma_{rec}(t) + \gamma_{unrec}(t), \tag{4a}$$

$$\dot{\gamma}(t) = \dot{\gamma}_{rec}(t) + \dot{\gamma}_{unrec}(t), \tag{4b}$$

where γ_{rec} and γ_{unrec} are the recoverable and unrecoverable shear strains and $\dot{\gamma}_{rec}$ and $\dot{\gamma}_{unrec}$ are their rates. Elastic processes are related to the recoverable component, whereas the plastic behavior is linked to the unrecoverable component. To study both the unyielded elastic and yielded plastic behaviors, oscillatory tests are typically used. The constant variation of strain and rate provides the ability to investigate the impact of both the timescale and extent of deformation. The average energy stored is proportional to the storage modulus, which is usually denoted by G' and is associated with recoverable strains only. Acknowledging the composite nature of the deformation rates, there are two methods of dissipating energy—one associated with the rate at which recoverable elastic strain is acquired, G''_{solid}, and the other with the rate at which unrecoverable plastic strain is acquired, G''_{fluid}.[114,115] The sum of these dissipation mechanisms gives the traditional loss modulus, G'', which is defined as the average energy dissipated normalized by the square of the total strain rate. Donley *et al.* used recovery rheology to elucidate the composite nature of G'', comprised of both viscoelastic solid and fluid energy dissipation pathways, leading to a clearer understanding of transient yielding.

The dynamic moduli, G' and G'', and the components, G''_{solid} and G''_{fluid}, represent average measurements over a single period of oscillation.[114,115] However, to gain a more comprehensive understanding of the DIW process, it is crucial to investigate the transient behavior of inks. Only recently, with the development of recovery rheology techniques, have methods emerged that allow for clear interrogation of transient nonlinear rheological behaviors.[88]

Yield stress fluids behave as viscoelastic solids at stresses below their yield stresses. The viscoelasticity is typically characterized by the dynamic moduli that we introduced previously. While the energetic definitions are true in both the linear and nonlinear regimes, there is also a geometric relation that holds in the linear regime. The dynamic moduli can be thought of as the real and imaginary parts of a complex modulus, G^*,

$$G^* = G' + iG''. \tag{5}$$

In a similar manner, a complex viscosity, η^*, can be defined as[105]

$$\eta^* = G^*/\omega. \tag{6}$$

A plot of the sinusoidally varying stress and strain during an oscillatory test of a viscoelastic material is plotted at the top of Fig. 4(a). From these data, the phase lag δ is observed. The relationship between G', G'', and G^* is also plotted at the bottom of Fig. 4(a). For all viscoelastic materials in the linear regime, $0° < \delta < 90°$ with the lower end corresponding to a purely elastic response and the upper bound corresponding to a viscous one. For DIW inks, which are viscoelastic, the strain lag has a strain amplitude-dependent intermediate value.

In oscillatory tests designed to probe the nonlinear rheology of inks, the stress response to oscillatory straining is often non-sinusoidal. It is, therefore, difficult to define a unique phase angle to retain the geometric interpretation. However, the energetic interpretation of the dynamic moduli holds true at all amplitudes. When the strain amplitude is small, the viscoelastic solid behavior of the ink dominates the response and $G' > G''$. As the amplitude increases, G'' typically increases and then decreases again, and the moduli cross [Fig. 4(a)]. Many measures of the yield stress have been inferred from such responses: as the point at which G' begins to deviate from linearity (sometimes called the yield point with stress σ_y); the point at which the stress–strain response deviates from linearity; the point at which $G' = G''$ (sometimes called the flow point with stress σ_f), or other measures; even so, these descriptions provide an incomplete understanding of yielding.[116] To illustrate whether the yielding process is more gradual or closer to instantaneous (i.e., brittle fracture), a flow transition index (FTI) may be reported, where

$$FTI = \frac{\sigma_f}{\sigma_y}. \tag{7}$$

The closer that the FTI is to 1, the more brittle the material.[117] Although the FTI is a useful shorthand way of describing the fracture behavior of a material, the calculation still depends on the definition of the yield stress. The previously discussed work by Donley *et al.* indicates that while the various measures of the yield stress each have different interpretations, recovery rheology can unambiguously identify yielding and shows that yielding is a gradual process both in terms of time and deformation.[114] Another study using recovery rheology has shown that all yielding behaviors can be described using only the yield stress determined from the steady shearing response.[100] This modern understanding of yielding should be considered when developing DIW inks which must flow to be printed and unyield to be built upon.[34,62]

A third method for quantifying how quickly a DIW ink resolidifies is by evaluating the change in viscosity or stress upon a change in applied shear rate.[69,118,119] When the syringe plunger is pressed, the shear rate suddenly increases, and the stress becomes large. When the ink is extruded, the rate rapidly decreases, and the stress drops to zero. This scenario is demonstrated experimentally using the three-interval thixotropy test (3ITT) shown in Fig. 4(c). Broadly speaking, thixotropy is the name given to time-dependent rheological behaviors that saturate on timescales different than those due to viscoelasticity. In a thixotropic material, a rapid decrease in viscosity occurs when shear is applied, and a time-dependent recovery in viscosity begins when the shear rate is reduced.[34,62,119] A simple yield stress fluid that obeys Bingham's model [Eq. (1)] will resolidify the instant the stress drops below the yield stress. The amount of time required to restore the initial value of viscosity is proportional to the resolidification time.[120] Results

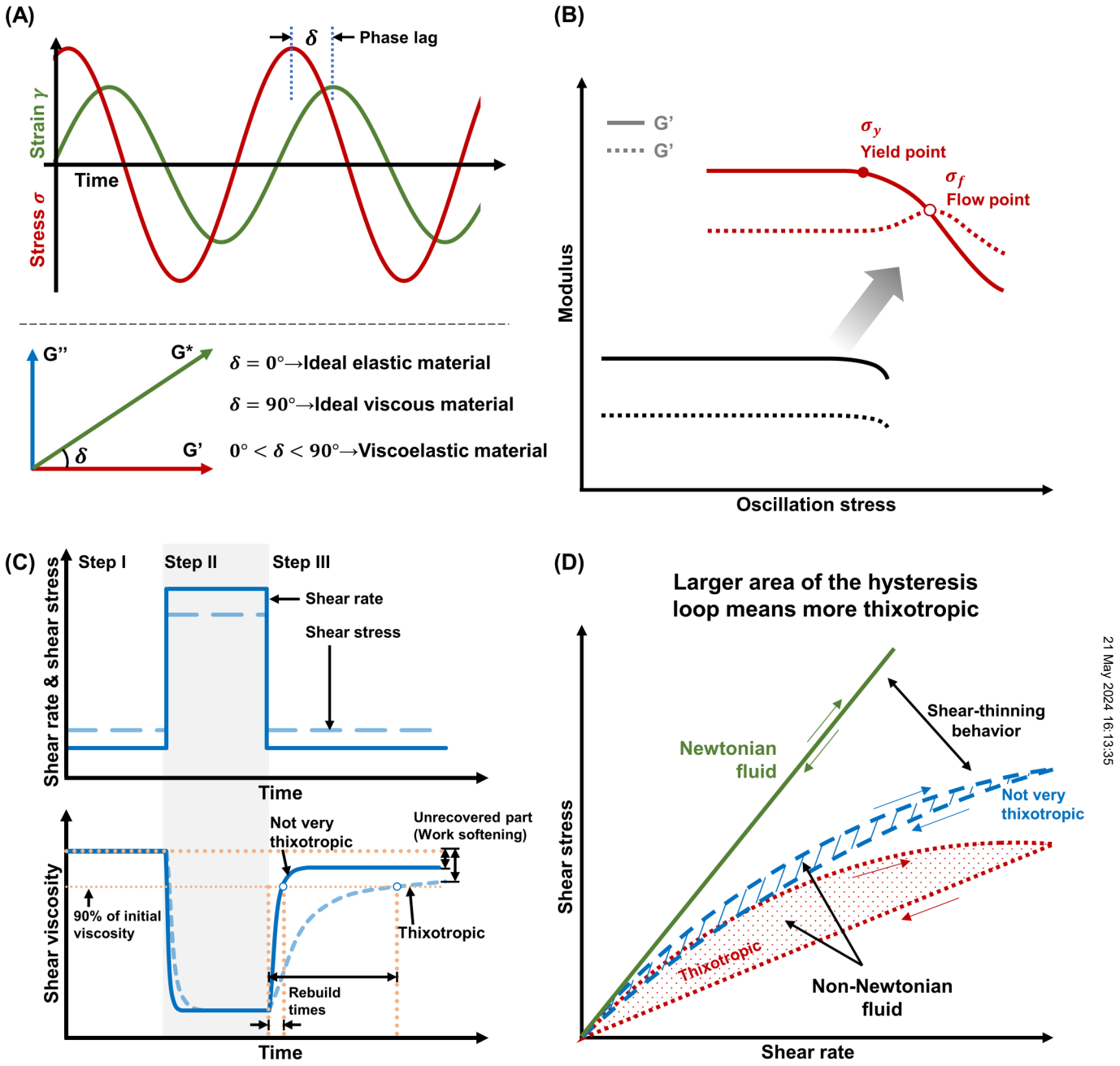

FIG. 4. (a) For viscoelastic behavior, the sine curves of strain and stress show a phase shift δ, as can be seen from the time lag between the two amplitude values. (b) G' and G'' during large-amplitude oscillatory shear experiments on a nonyielding fluid and a yielding fluid. (c) 3ITT data, with applied strain rate and measured stress plotted at top and the effect on apparent viscosity at bottom. (d) Stress vs strain rate during a hysteresis cycle of a Newtonian fluid and two thixotropic fluids.

from this experiment are generally reported as a percent recovery of the initial (first interval) viscosity at a specified time in the third interval. During this recovery period, the unrecovered portion of viscosity is termed "work softening."[119]

Another parameter commonly used to describe thixotropy is the degree of hysteresis in the shear stress during a rate-controlled experiment.[62,69,118–120] In a hysteresis test, the shear rate is swept from low to high or high to low. To neglect effects of time-

dependent factors and elasticity, Divoux *et al.*[121] have shown that it is better to begin at a high rate and wait for steady state and then sweep down and up at prescribed rates. In this test, a thixotropic material will follow different paths downward and upward in shear rate, with the degree of thixotropy being determined by the area between the curves (i.e., hysteresis), which is dependent on the rate at which shear rates are swept [Fig. 4(d)]. A challenge with these experiments is that two variables—rate and time—are modulated concurrently. Thixotropy is a function of both of these variables, and a lag in the material response compared to the applied shear may occur. Therefore, interpretation of hysteresis loop results can be challenging, and care must be taken in interpreting their results.[69]

B. Fidelity tests

Under ideal conditions, each extruded filament of a Bingham yield stress fluid would demonstrate a well-defined morphology with a smooth surface and constant cross-sectional dimensions. In the case of a printed lattice structure, this would result in regular grids and square voids in the fabricated constructs. However, an incomplete understanding of the complex rheology of real inks can result in printed filaments that exhibit distortions in terms of filament width, pore geometry, layer height, etc. Therefore, fidelity tests are commonly employed as a complement to rheology tests to quantify the printability of an ink. These fidelity tests can be grouped into three different categories: (1) single filament evaluation, (2) filament fusion evaluation, and (3) pore geometry evaluation.

The single filament test evaluates the morphology or smoothness of the extruded ink filament and its sagging behavior under the action of gravity. As shown in Fig. 5(ai), filament diameters can be measured on images of the filament at different locations (d_1, d_2, and d_3), which indicates the homogeneity of the filament. Another common test on a single extruded filament is called the filament collapse test, which was developed by Therriault *et al.*[122] Here, a single filament is extruded over a series of pillars with increasing spacing between them (in the absence of post-printing processing). An ink with ideal Bingham rheology would either not sag at all because of the absence of elasticity or would collapse completely if the force due to gravity exceeds the yield stress. For real inks, the filament exerts a force F_s which results in some sagging as shown in Fig. 5(aii). The collapse of the filament is quantified by measuring the angle of deflection θ at the edge of the suspended filament using optical microscopy, under the assumption that deformation is negligible and forces on the filament have achieve equilibrium at the time of measurement. The angle of deflection can then be related to the yield stress of the ink by[123]

$$\theta = \sin^{-1}\left(\frac{\rho g L}{\sigma_y}\right), \tag{8}$$

where ρ is the density of the material, g is the gravitational acceleration, and L is half the distance between two pillars. In the absence of further experimentation, the cause of the sagging cannot be decoupled between recoverable and unrecoverable processes, as indicated by Eq. (4). If the sagging is recoverable, then it can be said to be due to elastic effects, as an elastic filament would sag an amount proportional to its modulus. If the sagging is unrecoverable, then some plasticity has occurred, which may be indicative of partial yielding.

Alternatively, the collapse area factor C_f can be calculated.[123,124] This calculation requires extruding filament strands across a ridged scaffold, then measuring the cross-sectional area formed between the filament and the scaffold walls, as shown in Fig. 5(aii). An ink with simple Bingham rheology that is perfectly rigid below the yield stress would have no collapse across the scaffold, and, thus, a rectangle would form between the filament and the scaffold walls. The area of this rectangle is the theoretical area A_t^c, and the actual measured area is A_a^c. Then, C_f is calculated using the following equation:[124]

$$C_f = \frac{A_a^c}{A_t^c} \times 100\%. \tag{9}$$

In the ideal scenario with no filament collapse, $A_a^c = A_t^c$ and $C_f = 100\%$. In reality, however, C_f decreases with increasing filament collapse. This calculation provides a quantitative measure of the level of filament sagging that may occur when ink is extruded and spans a structure.

A common method to quantify the spreading and merging behavior of the ink is the filament fusion test,[123] as shown in Fig. 5(b). One version of the test consists of printing a zigzag pattern composed of parallel strands at decreasing spacing F_d and measuring the length of the portions of adjacent filaments that are fused together (F_s) as shown in Fig. 5(bi). Inks with lower yield stresses tend to have larger F_s, as adjacent filaments spread and merge, even at higher F_d, causing a loss of resolution in the x–y plane. Another variant of the test shown in Fig. 5(bii) consists of printing two layers of the zigzag pattern which are orthogonal to each other.[124] By measuring the area of the variably sized pores of the fabricated scaffold, the effect of filament fusion and pore closure can be quantitatively assessed for different ink compositions.

Pore geometry is evaluated using semiquantitative assessments of the pore and lateral pore size, circularity of printed filaments, and shape fidelity of the pores, which rheologically correspond to acquisition of recoverable and unrecoverable strains during the printing process. Using this approach, the perimeter and area of pores are used to derive a printability index [P_r, Fig. 5(c)].[5,125] An ideal axial porosity in a lattice made from orthogonal filaments should display a squared profile in the x–y plane (or rectangular, depending on the designed strand-to-strand distances). In this case, high geometric accuracy would result in a printability index of $P_r = 1$ (square-shaped transversal pore geometry), while $P_r < 1$ and $P_r > 1$ correspond to a more round or irregularly shaped transversal geometry, respectively. Thus, the measurement of pore circularity and the deviation from an ideal square can provide an estimation of shape fidelity in the x–y plane. In a similar vein, the lateral shape fidelity can be described quantitatively in terms of the lateral porosity, as shown in Fig. 5(cii). The lateral collapse area factor C_f^l, that is, the percentage of the actual lateral area of each lateral pore with respect to the theoretical lateral pore area, is determined using the following equation:[124]

$$C_f^l = \frac{A_a^l}{A_t^l} = \frac{A_a^l}{F_d \times L_t - 0.25\pi d_f^2} \times 100\%, \tag{10}$$

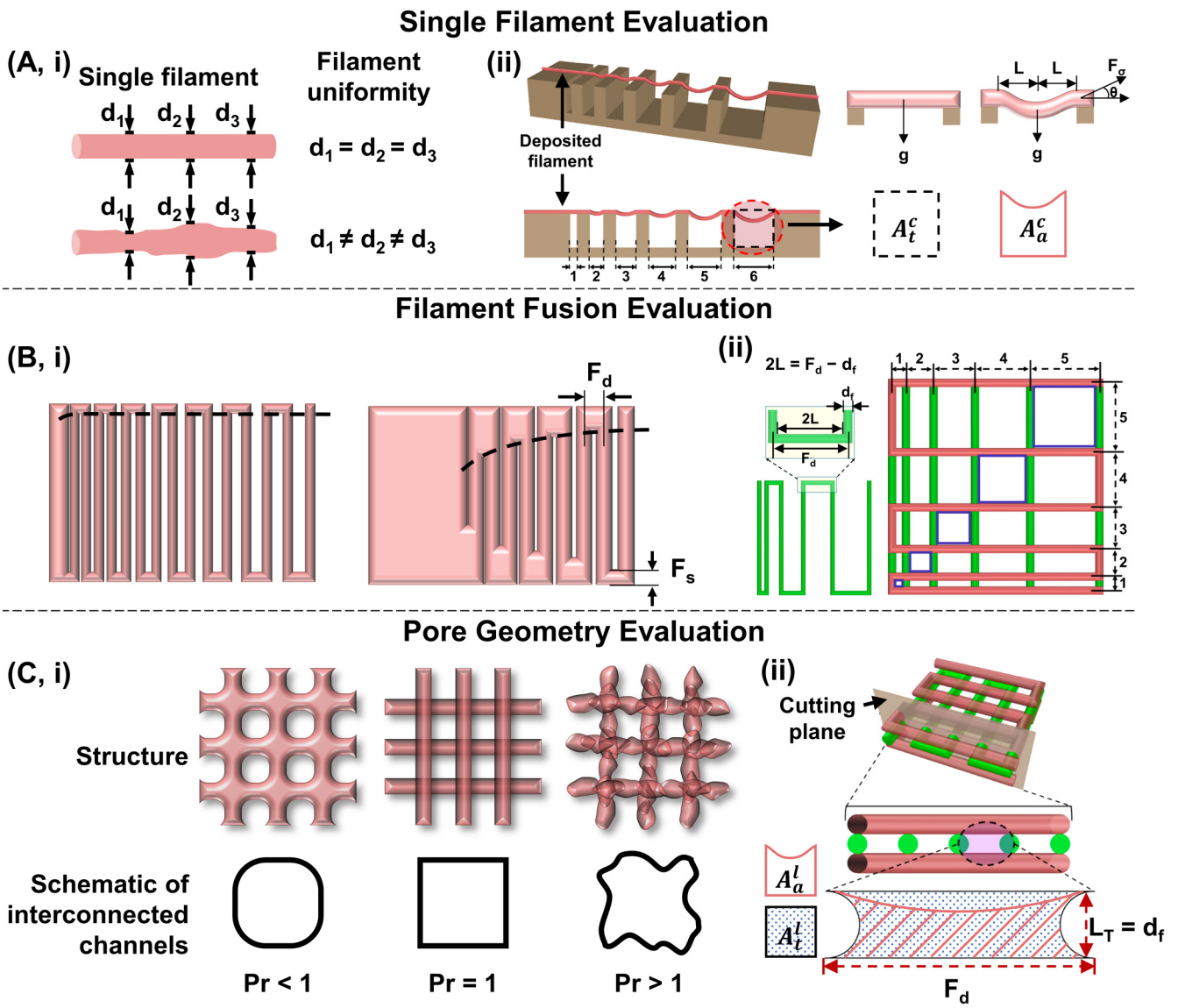

FIG. 5. Quantitative tests to assess the shape fidelity of an ink during printing. (ai) Filament uniformity evaluation. (aii) Filament collapse test to assess sagging of support-free structures due to gravity.[124] (bi) Filament fusion test.[123] (bii) A filament fusion test where two layers of filament are deposited orthogonally. (ci) Transversal pore geometry of printed structure having various P_r values. Reproduced with permission from Refs. 5 and 125. (cii) Diagram of pore dimensions used to determine C_f^l.[124] Reproduced with permission from Habib *et al.*, Materials **11**(3), 454 (2018). Copyright 2018 Author(s), licensed under a Creative Commons Attribution (CC BY) license; Ribeiro *et al.*, Biofabrication **10**, 014102 (2018). Copyright 2018 IOP Publishing, Ltd; Ouyang *et al.*, Biofabrication **8**(3), 035020 (2016). Copyright 2016 IOP Publishing, Ltd; Soltan *et al.*, ACS Biomater. Sci. Eng. **5**(6), 2976–2987 (2019). Copyright 2019 American Chemical Society.

where A_a^l is the actual area of the lateral pore, A_t^l is the theoretical pore area, F_d is the distance between adjacent filaments, L_t is the theoretical layer thickness, and d_f is the theoretical filament radius, as shown in Fig. 5(cii). If the lateral pore size completely collapses after fabrication of the scaffold, $A_a^l = 0$ and $C_f^l = 0$. A higher value of C_f^l reflects better preservation of lateral pore size and, therefore, improved scaffold shape fidelity, with perfect fidelity achieved at $C_f^l = 100\%$. In addition to pore shape fidelity, the quality of layer stacking in a multi-layered setup can be measured by the maximal height reached for printing a defined geometry, often described as critical height.[126] The critical height is related to the amount of mass that a single extruded filament can support. As additional filaments are extruded atop one another, the mass that each filament is supporting increases. This can lead to structure slumping and, ultimately, print failure.

As detailed above, the rheology of DIW inks is necessary to characterize and understand how composition can be tuned to enhance the ability to print an object. In complement, print fidelity can be evaluated by characterizing filament collapse, filament fusion, and pore collapse, which may be more accurately compared to measured rheological parameters through recoverable and unrecoverable parameters. Taken together, these two classes of characterization dictate printability and can provide insight into new avenues to improve ink development to expedite new ink formulations from diverse feedstocks. However, these fidelity tests do not always correlate to bulk rheological predictions, and a rigorous mathematical model has not been established. This indicates that we do not have a complete understanding of the rheology of DIW inks.

IV. FACTORS THAT INFLUENCE THE RHEOLOGY OF DIFFERENT TYPES OF INKS

Since the first ceramic slurry ink,[127] scientists have expanded DIW feedstocks to print polymers,[35–37] food[128,129] and biomass,[130] phase change materials,[29] metals[131,132] and liquid metals,[46–50] etc. From a microscopic perspective, DIW inks can be grouped into five categories based on the origins of the interactions within the materials. These include (i) granular (three-dimensional) particles in a fluid matrix, (ii) low-dimensional particles in a fluid matrix, (iii) emulsions and foams, (iv) hydrogels, and (v) liquid metals. Below we provide a detailed review of factors which influence printability for each system.

A. Granular particles in matrices

Inks composed of highly jammed granular particles in fluid matrices are one of the most common feedstocks for DIW. An illustration of the extrusion of this type of ink is provided in Fig. 6, where the brown granular particles are suspended in a blue fluid matrix. The particles are shown as size-disperse spheres with some surface roughness, although the size and size distribution, shape, surface roughness, and loading level all depend on the particle identity. To understand the non-Newtonian rheology of colloidal dispersions, it is useful to consider suspension microstructure. For suspensions of spherical particles, the microstructure is defined by the relative positions of the suspended particles. It is now generally accepted that the non-Newtonian behavior of dense suspensions results from changes in microstructure under shear. Particles form "flocs" (they flocculate together) because of steric stabilization, hydrogen bonding, and/or electrostatic forces.[69,70,77,78,119] Applied σ overcomes these attractive forces are overcome and lead to flocs breaking apart. Increasing σ breaks flocs down further, which is the cause of shear-thinning behavior. When stress is removed, particles re-bond to one another, and a network can be reformed.[67,69,70,77,78] Inks comprised of 3D particles in fluid matrices can be classified into two major categories: (i) geopolymers or ceramics in water and (ii) filler particles in liquidous polymers.

The basic rheology-determining parameters of a particle-filled ink are the rheology of the matrix material, loading of the filler particles, physical properties of the particles such as the surface roughness, which relates to modes of shear-thickening, and the nature of particle–particle and particle–matrix interactions.[133]

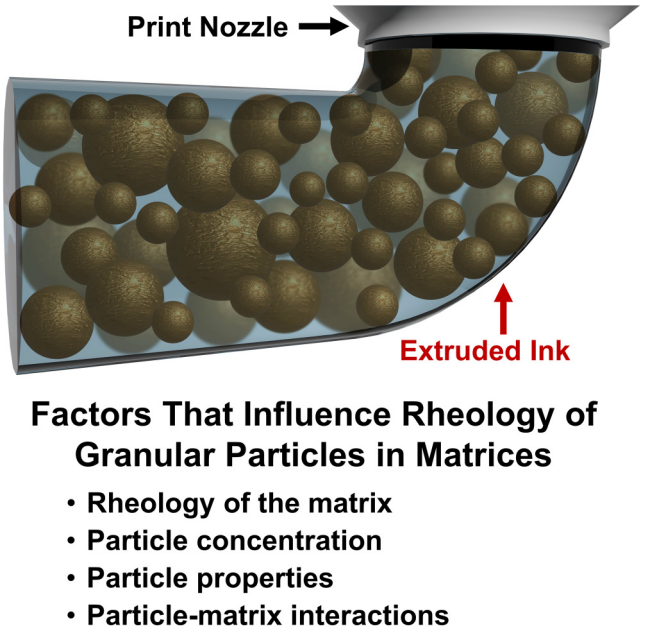

FIG. 6. Illustration of an ink composed of highly jammed granular particles in a fluid matrix. The factors that may influence the ink rheology are listed at the bottom.

1. Rheology of the matrix

The rheological properties of the viscous matrix material can greatly influence the consistency of the resulting DIW ink, as indicated by existing rheological models for solid particles suspended in viscous matrices. In 1906, Einstein[134] described a mathematical relationship between matrix viscosity and relative viscosity of an infinitely dilute suspension of solid particles,

$$\eta = \eta_0(1 + [\eta]\Phi), \tag{11}$$

where η is the relative viscosity of the suspension, η_0 is the matrix viscosity, $[\eta]$ is the intrinsic viscosity (2.5 for rigid spherical particles), and Φ is the volume fraction of solid particles. This equation is only applicable to very dilute suspensions where interparticle interactions are negligible. To expand the use of this relationship, Batchelor[135] incorporated a third term, including the Huggins coefficient k_H (6.2 for repulsive spherical particles), which accounts for repellant interparticle interactions,

$$\eta = \eta_0(1 + [\eta]\phi + k_H\Phi^2). \tag{12}$$

Krieger and Dougherty[136] expanded the use of this model to more concentrated suspensions, as well as a range of shear rates, by accounting for the maximum solid fraction in the suspension, Φ_{max},

$$\eta = \eta_0\left(1 - \frac{\Phi}{\Phi_{max}}\right)^{-[\eta]\Phi_{max}}. \tag{13}$$

Based on this relationship, the viscosity of a viscous matrix material used for DIW inks can be considered a "baseline," and the

ink viscosity increases upon addition of solid particles, in addition to the potential emergence of a yield stress. Such matrices are generally Newtonian fluids, with the shear stress being linearly proportional to the shear rate, and the viscosity independent of shear rate. The viscosity of the matrix can have drastic effects on the rheological performance of an ink. As the matrix viscosity changes, the particle loading level required to make a printable ink also changes: the more viscous the matrix, the lower the required loading of particle filler necessary for the emergence of a yield stress, and, thus, a less viscous matrix can be used to maximize particle concentration.[137] Therefore, there is a balance between matrix viscosity and particle concentration, and if the matrix viscosity can be tuned, then a desired amount of particle filler within an ink can be achieved. With this said, only a range of acceptable ink properties is feasible for DIW. Specifically, an ink must have a yield stress to hold its shape after extrusion, but not be so viscous that the printer cannot exert enough force to extrude it through the desired size nozzle.

2. Particle concentration

A key factor in the printability of polymer composite inks containing 3D fillers is particle concentration or filler loading level. As shown in Fig. 7, for spherical particles of monodisperse size, the theoretical Φ_{max} is 74 vol. % with a hexagonal close-packed or face-centered cubic stacking structure. The maximum particle concentration is even higher for polydisperse particles where smaller particles can occupy the space between larger particles, and particle shape and interparticle interactions also influence the value of Φ_{max} for a given system.[76,105,137–140] The 3D particle concentrations of printable inks have been reported across a large range from as low as 23[141] to as high as 73 vol. %.[23] Generally, the ideal concentration is dependent on the rheological properties of the ink so that good print fidelity is achieved, as well as the end use of the printed object. As such, a range of concentrations may be printable. However, if too low a particle loading is used, the viscosity of the suspension will increase compared to the neat fluid matrix, but the degree of interparticle interactions will be too low to produce a yield stress, so the ink rheology will be dominated by the Newtonian matrix fluid. As the particle concentration increases, it becomes statistically more likely that particles will interact with one another, thus increasing the interparticle friction and resistance to an applied stress, and thus viscosity, of the suspension.[137] Another consideration is the interconnectivity of the matrix; if the particle concentration is too high, the matrix material will not form an interconnected network within the ink, and the structure will crumble under its own weight.[29]

Regardless of filler identity, increased volume fraction is expected to result in an increase in the viscosity, as reflected in the aforementioned mathematical descriptions of suspension viscosity. This increase is due to a higher degree of interparticle and particle–matrix interactions. Furthermore, the emergence of a yield stress brings with it an enhanced degree of shear-thinning (a slope of −1 in the viscosity vs shear rate curve). This has been illustrated for many particle–matrix systems. For example, Huang *et al.*[143] evaluated the influence of particle concentration on the printability of SiOC ceramic parts. The authors produced inks from solutions of polymethylsiloxane in isopropanol mixed with spherical poly (methyl methacrylate) (PMMA) particles and a crosslinker. Figure 8(a) indicates that increasing the concentration of 25 μm diameter PMMA particles from 50 to 80 vol. % caused the viscosity to increase by over an order of magnitude at low rate, whereas the extent of shear-thinning (i.e., the magnitude of the slope of the viscosity–shear rate curve) also increased. Furthermore, the high volume fraction of 80 vol. % enabled a flow point to be observed in the plot of G' and G'' against the strain amplitude [Fig. 8(b)]. Similar phenomena were observed in studies by Cipriani *et al.*[23,144] on paraffin microbeads (mean diameter = 26 μm) in photopolymer resin [Figs. 8(c) and 8(d)]. Here, the authors also demonstrated that the viscosity recovery of paraffin-photopolymer inks was dependent upon the particle concentration by shearing at a rate of 50 s^{-1}, then rapidly decreasing the shear rate to 0.1 s^{-1}. Higher particle loading produced inks with shorter recovery times as shown in Fig. 8(e).[144]

3. Particle properties

a. Shape. Thus far, particle fillers within DIW inks have been considered as perfectly smooth spheres except for the brief

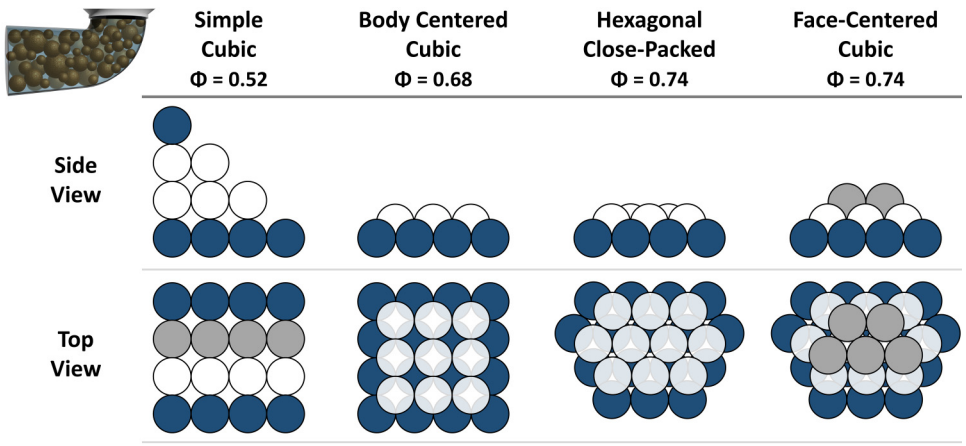

FIG. 7. Sphere stacking schemes with different maximum occupied volume solid fractions. Reproduced with permission from Ref. 142.

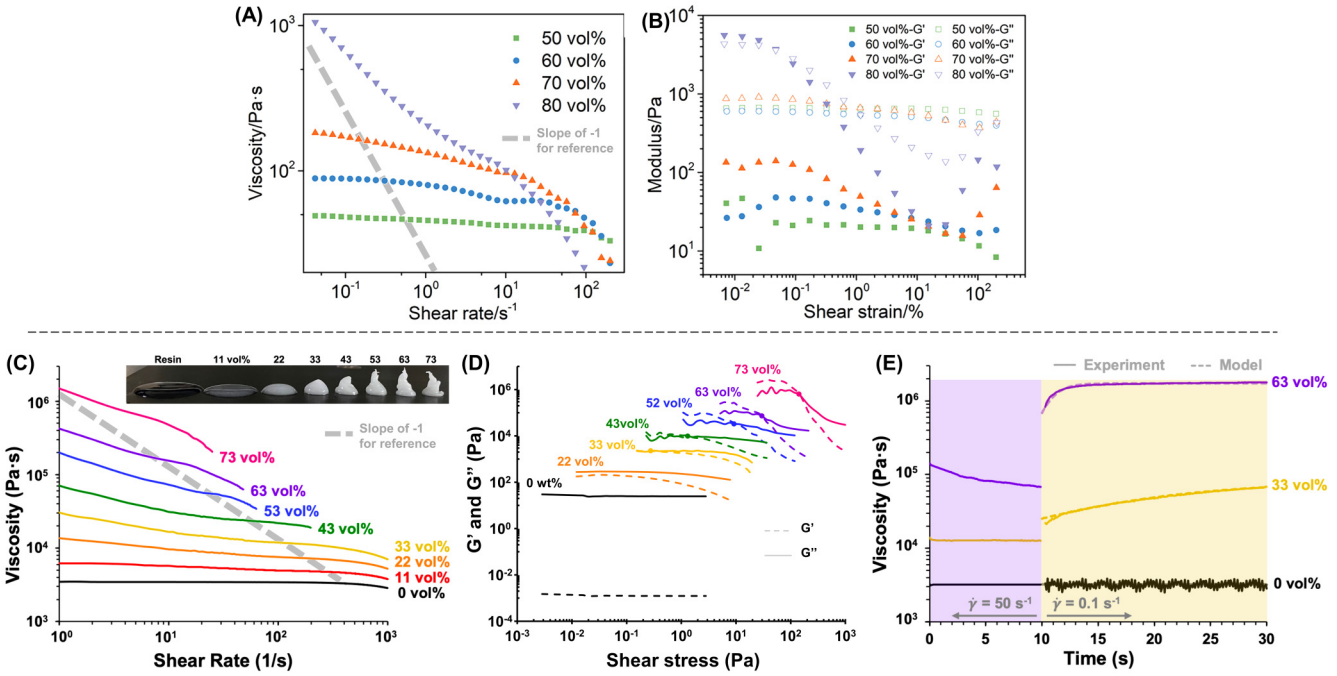

FIG. 8. (a) Viscosity as a function of shear rate for suspensions of 25 μm PMMA particles in polymethysiloxane solution, at Φ from 50 to 80 vol. %. (b) Dynamic moduli as a function of strain for suspensions of 25 μm PMMA particles in polymethysiloxane solution, at particle concentrations ranging from 50 to 80 vol. %.[143] (c) Viscosity as a function of shear rate for suspensions of paraffin microbeads in photopolymer resin at particle concentrations ranging from 0 to 73 vol. %.[144] (d) Dynamic moduli as a function of strain for suspensions of paraffin microbeads in photopolymer resin at particle concentrations ranging from 0 to 73 vol. %.[23] (e) Viscosity recovery of suspensions of paraffin microbeads in photopolymer resin at particle concentrations of 0, 33, and 63 vol. % after the shear rate was decreased from 50 to 0.1 s^{-1} at time = 10 s.[144] Reproduced with permission from Huang *et al.*, Addit. Manuf. **36**, 101549 (2020). Copyright 2020 Elsevier; Cipriani *et al.*, Phys. Fluids **34**(9), (2022). Copyright 2022 AIP Publishing LLC; Cipriani *et al.*, ACS Mater. Au **1**(1), 69–80 (2021). Copyright 2021 American Chemical Society.

discussion of shear-thickening. In reality, granular, three-dimensional particle fillers may be regular or irregular, oblate or prolate, and faceted or smooth. They may also be spherical, cubic, oblong, or another geometry. Particle shape is often defined by aspect ratio (AR), with a perfect sphere having $AR = 1$ (i.e., height equal to width) while oblate particles have $AR < 1$ and prolate particles have $AR > 1$. The previously discussed Einstein, Batchelor, and Krieger–Dougherty models only apply to spherical particles. For non-spherical particles, the intrinsic viscosity must be modified. Pabst[145] developed the following equation for the lower bound of the intrinsic viscosity, $[\eta]_\infty$, of a suspension of particles with aspect ratios varying from 1 to 50,

$$[\eta]_\infty = 2.5 + 0.123(AR - 1)^{0.925}. \tag{14}$$

In general, suspensions of ellipsoidal particles (i.e., round particles with $AR > 1$) have higher viscosities at low rates due to a higher degree of interparticle interactions. As the rate increases, ellipsoidal particles orient in the direction of shear, producing a higher maximum particle loading. This results in lower viscosity values at high rates and more exaggerated shear-thinning effects.[146]

To mathematically describe the effect of non-sphericity, An *et al.*[147] measured the apparent viscosity of suspensions containing particles having various degrees of sphericity, calculated from the particle dimensions, at multiple particle loading levels. The degree of sphericity (s) and the viscosity were found to be inversely related, which the authors attributed to changes in the degree of interparticle interactions. As sphericity increases, interparticle friction decreases, so the suspension is more amenable to shear deformation, and the viscosity is lowered. The authors incorporated s into the previously developed Batchelor and Krieger–Dougherty models relating the apparent viscosity of a suspension η to the solvent viscosity η_0 and volume fraction of particles Φ,

$$\eta = \eta_0(1 + 2.5\Phi s + 6.2s\Phi^2), \tag{15}$$

$$\eta = \eta_0\left(1 - \frac{s\Phi}{\Phi_{max}}\right)^{-2.5\Phi_{max}}. \tag{16}$$

At particle fractions above 0.18, the modified models more closely matched experimental data than their counterparts based on hard spheres, which points to the usefulness of such modifications for highly filled DIW inks.

b. Size and size distribution. Particle size has a large effect on ink rheology, and the cases of monodisperse and polydisperse particle sizes must be considered separately. As shown in Fig. 9, for noninteracting particles with a monodisperse size distribution, particle size can be directly related to surface area and, thus, η. In theory, if the total volume of particles is held constant, smaller particles have a higher surface area-to-volume ratio; therefore, the degree of friction between particles and matrix should increase, and the viscosity should increase correspondingly,[148] although the results of some DIW studies conflict with this expected trend.[128,143] At lower rates, this effect is more pronounced, because as the rate increases, particles rearrange in the direction of the applied shear, and the difference in viscosity between suspensions of large particles and small particles decreases. Most suspensions of solid particles in liquid matrices are not perfectly uniform in particle diameter, and commonly, filler particles possess a polydisperse size distribution as shown in the middle of Fig. 9. In this case, the maximum possible volume fraction of particles can be increased to above 0.74 since smaller particles can occupy the spaces between large particles. Therefore, a broader size distribution results in a higher maximum concentration of particles. Smaller particles can also behave as lubricants between larger particles,[149] and a polydisperse suspension will have a lower viscosity than monodisperse suspensions with the same particle concentration, regardless of particle size.[150] Although polydispersity reduces the viscosity of a suspension, the yield stress can remain high.[149] Therefore, the viscosity of a DIW ink may be modulated using both particle size and polydispersity, while having a high enough yield stress to avoid dripping from the nozzle.

The relationship between particle size and rheological behavior was reported in the work by Huang *et al.*[143] referenced in Sec. IV A 2, in which inks were made from solutions of polymethylsiloxane in isopropanol mixed with spherical PMMA particles (diameters of either 0.46, 5, 10, 25, or 50 μm) and crosslinker. As displayed in Fig. 10(a), the viscosity of the ink containing 80 vol. % 0.46 μm particles was the highest at nearly 10^6 Pa s at the start of the shear rate sweep, whereas at higher rates (>50 s^{-1}), the viscosity values of all the inks approached one another. Notably, the viscosities of inks containing 80 vol. % of 5, 10, or 50 μm particles did not follow the expected size-based trend, nor did the dynamic moduli of the inks. Although the smallest particles resulted in the highest dynamic moduli [Fig. 10(b)], as expected, for larger particles, no clear trend between particle size and dynamic moduli was observed. Clearly, additional factors must be considered to explain these deviations from the predicted behavior of the inks. For example, the samples of particles may also have different size distributions, the particles may be deformable, or particle–matrix interactions may complicate the rheological behavior, as discussed below.

c. Hardness and particle–particle interactions. So far, the particles within DIW inks have been assumed to be non-deformable hard spheres, i.e., that they have no overlap in space. In the hard-sphere model, repulsive and attractive forces are not considered, and the rheology of a suspension is described by Brownian diffusion and hydrodynamic forces. Particles are treated as hard spheres with some hard-sphere particle radius R_{HS}, and at distances $D > R_{HS}$, no interaction occurs; once D between two particles reaches $2R_{HS}$, interactions significantly increase and approach infinity, as shown in Fig. 11(a). The aforementioned rheological models assume hard-sphere behavior to relate particle concentration to the viscosity of a suspension. In reality, nearly all particles affect one another; in fact, interparticle interactions are a key component of ink rheology. Tadros[77,78] classified the contributing factors to interparticle friction into four types: (i) hard-sphere interactions (previously discussed), (ii) electrostatic interactions arising from double layer repulsion, (iii) steric repulsion based on adsorbed or grafted species, and (iv) van der Waals attraction.

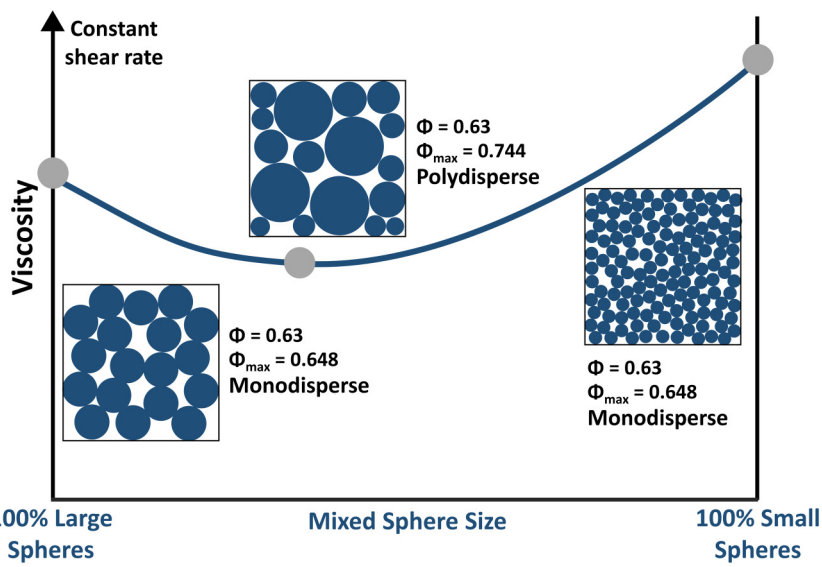

FIG. 9. Relationship between viscosity, particle size, and size dispersity with constant particle concentration and constant shear rate. Reproduced with permission from Ref. 142.

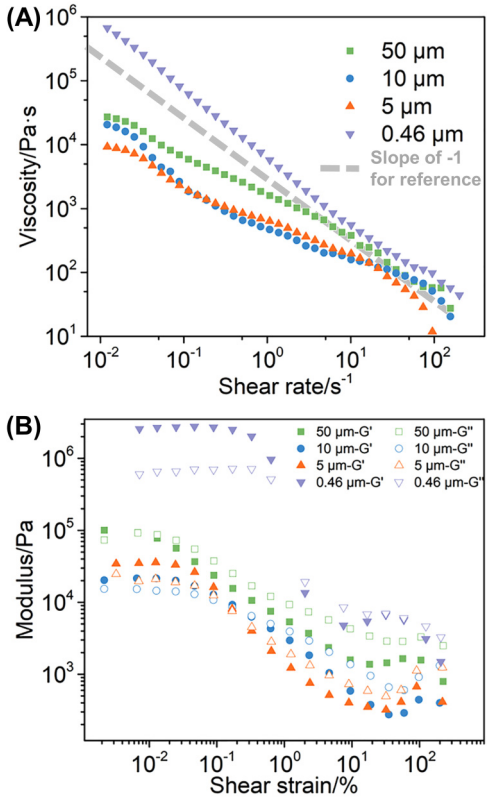

FIG. 10. (a) Viscosity as a function of shear rate for 80 vol. % suspensions of PMMA particles of varying sizes. (b) Dynamic moduli as a function of shear strain for 80 vol. % suspensions of PMMA particles of varying sizes.[143] Reproduced with permission from Huang *et al.*, Addit. Manuf. **36**, 101549 (2020). Copyright 2020 Elsevier.

Factors accounting for the chemical functionality of particles can be considered "soft" interactions since these factors result in deviations from hard-sphere behavior. For example, electrostatic forces are present for particles with surface charges, including ionized surface groups or adsorbed ionic surfactants. In these cases, counterions aggregate on the particle surface, and co-ions aggregate onto the counterion layer to form a double layer. As displayed in Fig. 11(b), this increases the effective radius of the particles (R_{eff}), and as particles of the same charge approach one another, their double layers overlap, leading to increasing repulsion.[77,78,150] Similarly, steric effects increase the effective radius [Fig. 11(c)]. Steric effects apply to particles with strongly adsorbed (or covalently attached) nonionic species, such as nonionic surfactants or polymer chains, forming a layer with thickness r. If the matrix is a good solvent for the adsorbed species, interactions between these surface species are unfavorable; therefore, at interparticle distances $D < (R + r)$, particles repel one another and steric repulsion increases. Once $D = R$, the interaction energy goes to infinity as in the hard-sphere model. For adsorbed species that can interact with one another via intermolecular interactions or simply due to high particle concentrations, these interactions must be overcome by sufficient shear to induce flow.[151,152] Finally, van der Waals attraction is considered when determining the degree of interparticle interactions within a solid–liquid suspension. van der Waals forces can be separated into dipole–dipole interactions, dipole-induced dipole interactions, and London dispersion forces (i.e., induced dipole-induced dipole). For polar compounds, dipole-related interactions must be considered, whereas London dispersion forces arise from changes in electron density dispersion and apply to both polar and nonpolar compounds. As shown in Fig. 11(d), the van der Waals attractive forces increase sharply below some critical distance, termed the "capture distance," at which all particles are strongly attracted to one another and flocculate.[77,78]

Particle characteristics, which dictate these four categories of interparticle interactions, can greatly influence suspension rheology. Hard-sphere suspensions are dominated by Brownian diffusion at low shear rates and exhibit solid-like behavior. As the shear rate increases, layers form within the flowing suspension, and at high rates, these layers move freely, resulting in viscous fluid-like behavior.[77,78,105] Similarly, suspensions of particles with electrostatic interaction are dominated by Brownian diffusion at low rates; as the rate increases, hydrodynamic interactions between the double-layered particles dominate, and the viscosity decreases. However, with sufficiently high particle loading, a critical value is reached, and pseudoplastic flow is observed.[77,78] Alternatively, particles of sterically influenced suspensions are affected by both viscous and steric forces. Particle suspensions with nonpolar species adsorbed onto particles achieve high η at lower Φ as compared to hard spheres. Increased steric interactions also tend to increase the value of the storage modulus, producing more elastic behavior within the suspension.[77,78] Finally, flocculation arising from van der Waals attraction between particles can result in thixotropy.[77,78,105] As flocculated aggregates are sheared, attractive forces are overcome after a certain amount of time, and as the aggregates break apart, entrapped liquidous matrix is freed. This reduces the effective volume of particles within the suspension, corresponding to a time-dependent decrease in effective viscosity and resulting in thixotropic behavior.[77,78]

4. Particle–matrix interactions

a. Surface roughness of particles. Although particle fillers are typically modeled as smooth spheres, in practice, surface roughness can drastically influence ink rheology. For instance, the surface roughness leads to increased geometric friction, and, therefore, requires smaller number of particles to achieve the same shear-thickening strength as compared to smooth particles.[153] Concentrated suspensions exhibit strong continuous shear-thickening, where the viscosity increases continuously with increasing shear rate. However, at volume fractions above a critical value, an abrupt increase in viscosity may occur, which leads to discontinuous shear-thickening.[154–156] The design of shear-thickening strength for a wide range of colloidal suspensions was recently demonstrated using a single parameter: the distance to jamming.[157]

Rough particles have higher surface area-to-volume ratios than smooth particles, which is expected to lead to a higher degree of interparticle interactions. Additionally, rough particles physically

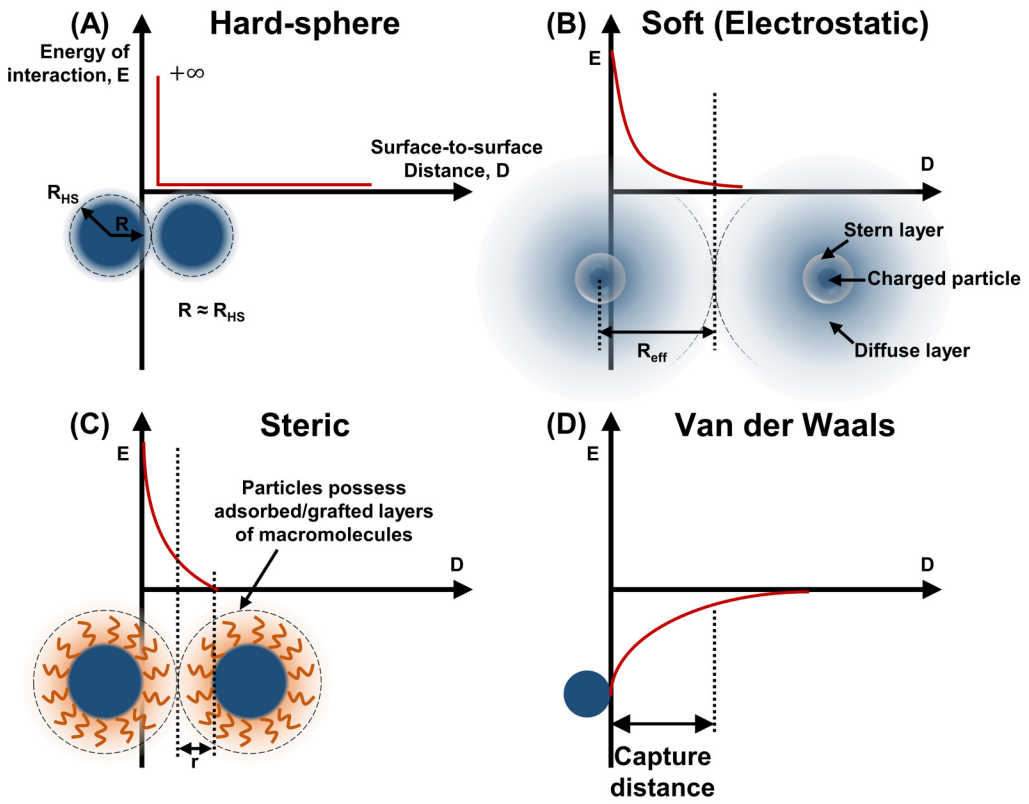

FIG. 11. Types of interparticle interactions in suspensions: (a) "hard-sphere"; (b) "soft" (electrostatic); (c) steric; (d) van der Waals. [77] Reproduced with permission from Tadros *et al.*, Adv. Colloid Interface Sci. **68**, 97–200 (1996). Copyright 1996 Elsevier.

disrupt the flow path of the liquid matrix compared to smooth particles which facilitate the flow of the matrix around them. Thus, suspensions of rough particles are generally accepted to be more viscous than suspensions of smooth particles.[139,158,159] For example, Moon and co-workers[139] prepared silicone oil suspensions of 80 μm spherical particles of polystyrene with roughness ratios of either 5.1% (resulting from a grinding process) or 0.13% (unground) and particle concentrations of 30, 40, or 50 vol. %. Regardless of particle concentration, the viscosity increased with increased roughness, as shown in Fig. 12(a), which is attributed to increased interparticle friction.

Recent studies have elucidated some effects of particle roughness in non-colloidal suspensions (that is, suspensions containing particles > 1 μm in diameter) which give an alternate perspective to friction effects. These studies have placed greater emphasis on the clustering, or flocculation, of solid particles in suspensions. For example, Lin and co-workers[160] prepared suspensions of PMMA particles of different roughnesses or smooth hollow glass spheres in silicone oil [SEM images shown in Fig. 12(b)]. Rougher particles were found to decrease the viscosities of these shear-thinning suspensions across the range of shear rates, as shown in Fig. 12(c). The authors attribute this behavior to decreased flocculation of rougher particles. In suspensions of granular particles, shear-thinning behavior is thought to arise from the breakdown of flocs as the shear rate increases; as such, less flocculation would result in a lower degree of shear-thinning. Further work is required to accurately model the effects of particle roughness and account for potentially contradictory factors.

b. Particle–matrix chemical compatibility. Alongside physical interactions between particles and liquid matrices, non-covalent forces such as polar interactions, hydrogen bonding, and van der Waals interactions also influence ink rheology. In a useful comparison, Cai and Salovey[161] performed a rheological study on suspensions made from liquid polysulfide polymer as the matrix combined with monodisperse spherical particles of either PS, crosslinked vinylphenol modified polystyrene (PSVP), all monodisperse with diameters of 0.315 μm, or crosslinked PMMA 0.344 μm in diameter. The degree of particle–matrix interactions was expected to increase from PS to PMMA to PSVP: PS should have only non-polar, dispersive intermolecular interactions with the matrix, PMMA should exhibit dipole–dipole interactions and weak hydrogen bonding, and PSVP should have the strongest intermolecular hydrogen bonding due to the hydroxyl groups. The authors

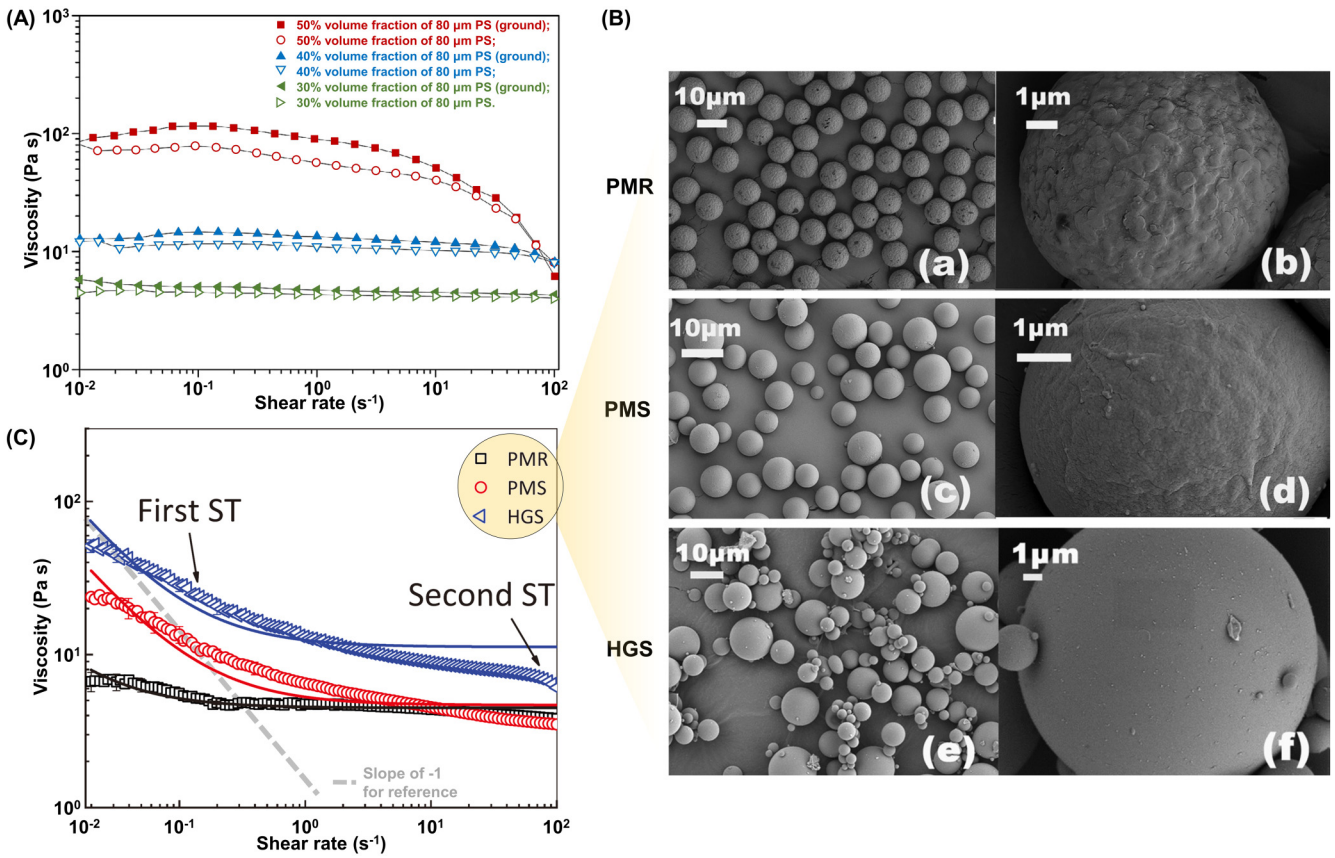

FIG. 12. (a) Viscosities of suspensions of ground and unground PS spheres in silicone oil at particle concentrations of 30, 40, and 50 vol. %.[139] (b) Viscosities of suspensions containing 40 vol. % rough PMMA particles, smooth PMMA particles, or hollow glass particles in silicone oil. The traces are curves fit to the experimental results. ST indicates shear-thinning. (c) SEM images of rough PMMA particles (i), smooth PMMA particles (ii), and hollow glass particles (iii).[160] Reproduced with permission from Moon *et al.*, J. Non-Newton. Fluid Mech. **223**, 233–239 (2015). Copyright 2015 Elsevier; Lin *et al.*, Phys. Fluids **33**(4), 043104 (2021). Copyright 2021 AIP Publishing LLC.

explained that, for a suspension with a polymer melt as the matrix, polarity and hydrogen bonding cause polymer chains to adsorb or entangle and form a layer on the particle surface. With increased interfacial interactions, the thickness of this layer grows, and the effective concentration of particles increases, raising the viscosity, both dynamic moduli, and yield stress of the suspension.

c. Density difference between ink components. A final, and critical, consideration in DIW inks is the difference in density between particles and the suspending matrix. A general understanding of this factor leads to the conclusion that granular particles denser than the liquid matrix will sink due to gravitational force, g, and particles which are less dense than the matrix will float. However, the size of the particles and viscosity of the matrix (η_0) must also be considered, since in the colloidal range (diameters $< 1\,\mu$m), the effects of diffusion (osmotic pressure, Brownian motion, electrostatic repulsion or attraction, and convection)[162] have non-negligible impacts in resisting g. Above the colloid size range, these effects are lessened in comparison to the magnitude of g.[78] Over the timescale of ink formulation and printing, which may take hours, this can result in noticeable phase separation within an ink such that the particle concentration gradates throughout the process (and thus the printed object). Phase separation is commonly mentioned in studies on DIW inks, and many reports leverage additional ink components to mitigate phase separation. For example, Cai *et al.*[163] produced suspensions of ceramic powders in an aqueous solutions of high- and low-molecular weight polyethylenimine, and methylcellulose was added to increase the matrix viscosity, thus counteracting the gravitational pull which contributes to phase separation. Yang *et al.*[164] used triethanolamine to increase surface interactions between a variety of suspended particles and an aqueous rubber latex matrix, primarily via hydrogen bonding. Polymer additives can also be used to entrap particles and inhibit phase separation.[165] Notably, phase separation may also impact the scale of ink preparation such that small batches of ink can be printed, but attempts to scale ink preparation and use are met with limited success. Whereas priority has been placed on avoiding phase separation, the impact of density mismatch has not been

thoroughly studied in the context of DIW either during ink formulation and storage or the printing process itself.

B. Low-dimensional particles in matrix

Low-dimensional (1D or 2D) materials are those that have at least one dimension at the nanoscale (e.g., nanorods or nanosheets). In the past few decades, low-dimensional particles (LDPs) have garnered interest for a variety of applications due to their distinct and complementary properties resulting from their high AR values compared to those of more common granular particles (e.g., 3D). Among many applications of LDPs, printable electronics and wearable devices are of considerable interest and have undergone explosive growth in recent years.[12,13,16] Typical LDPs include 1D carbon nanotubes,[16] self-assembled nanowires of poly(3,4-ethylenedioxythiophene) polystyrene sulfonate (PEDOT:PSS),[12] and 2D LDPs include graphene (as well as graphene oxide and reduced graphene oxide),[13–16,63,166] cobalt oxide,[167,168] hexagonal boron nitride,[169] clays,[169,170] boron carbide,[171,172] MXenes (i.e., transition metal carbides or nitrides),[60,173,174] and transition metal dichalcogenides.[175] The low dimensionality of these particles (i.e., one dimension shorter than 100 nm) causes distinct behavior when incorporated into DIW inks as compared to inks with 3D particles. Unlike granular particles which interact by "pushing" each other in the matrix, LDPs commonly entangle or buckle when interacting with other particles due to softness (e.g., flexibility) in their longest dimension.[176,177] The high *AR* also endows a high surface area-to-volume ratio to the particle, so the particles are more sensitive to changes in pH or ionic strength. The chemical composition of these particles is also a necessary consideration, particularly for oxygen-containing particles which can exhibit strong hydrogen bonding between particles or between particles and a matrix.

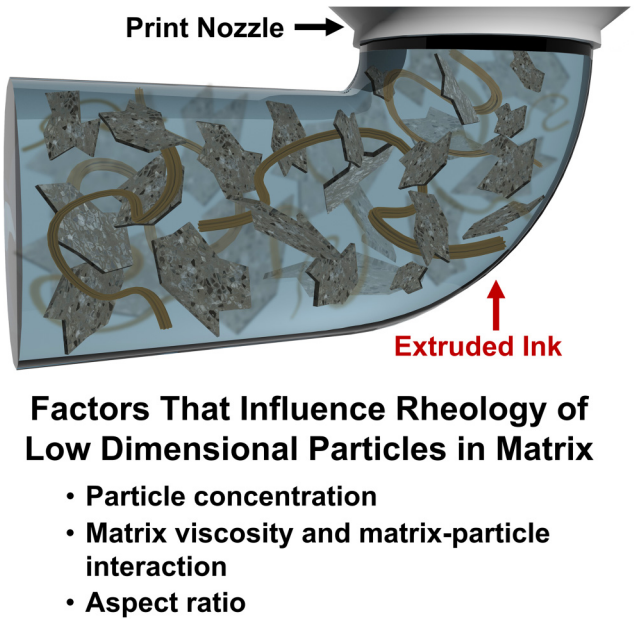

FIG. 13. Illustration of an ink composed of low-dimensional (1D and 2D) particles in a fluid matrix. The factors that may influence the ink rheology are listed at the bottom.

A visualization of LDPs suspended in a fluid matrix is shown in Fig. 13. Some empirical formulas have been proposed to assess the rheological properties of fluids containing LDPs. For example, in 1999, Jogun and Zukoski[178] studied the flow properties and microstructure of dense kaolin clay suspensions in water. The authors revealed a relationship between the critical volume fraction Φ^* at which a transient network forms and various properties of charged disk-shaped particles,

$$\Phi^* \propto \frac{h}{d}\left(1+\frac{2}{d\kappa}\right)^{-1}. \tag{17}$$

Here, h/d is the flake aspect ratio (thickness/diameter) and κ^{-1} is the Debye screening length (cf. DLVO theory). Thus, the critical volume fraction, and by extension, the rheology of a dispersion, is strongly dependent on both the surface charge of the particles and the electromagnetic permittivity of the matrix. Experimentally, this dependence can be accounted for by measuring the ζ-potential of the particles. Although this empirical formula is based on relatively rigid, disk-like particles with aspect ratios of only 10–12, it is apparent that the rheology of LDP-containing inks is highly dependent on both the particle aspect ratio and the particle–matrix interactions. Furthermore, factors such as particle concentration and matrix viscosity play a role, as discussed above for granular particle-based inks. Below we further describe the major factors influencing LDP ink rheology.

1. Particle concentration

In DIW inks, LDPs must form a transient network within the matrix to create a yield stress that imparts printability, consistent with inks containing granular particles. Therefore, the concentration of the LDPs (Φ), which determines the number of interparticle junctions, is one of the most important factors to the rheological properties of the inks. Unlike granular particles, most LDPs achieve percolation (i.e., the formation of a continuous 3D network throughout the entire sample) at a relatively low concentrations (i.e., <10 vol. %).[179] For example, Corker *et al.*[117] found that graphene oxide (GO) suspensions in water show yield stresses at concentrations as low as 0.3 vol. %, as determined by amplitude sweeps [Figs. 14(a) and 14(b)]. It is in this work that the authors linked the previously discussed flow transition index (FTI) [Eq. (7)] to the printability of DIW inks. More recent studies have shown that these yield and flow parameters conflate recoverable and unrecoverable processes, but the connection remains an interesting one. In a similar vein, for inks containing PEDOT:PSS nanofibers, a yield stress appeared at 1 wt. % fiber loading [Figs. 14(c)–14(e)].[12] In these cases, the LDPs may interact at very long distances via electrostatic forces, likely due to the high density of hydrophilic functional groups on the flake or fiber surface. On the contrary, if the LDPs possess a low density of polar functional groups (e.g., carbon nanotubes, graphene, graphite), then they cannot form hydrogen bonds or electrostatic attractions with the matrix. Further, if hydrophobic solvents are used in the matrix, then a higher particle concentration would be needed to produce the desired rheological response for DIW inks. This can be found in the recent work on 3D printing of carbon nanotubes[180] and graphite flakes.[13,14,181]

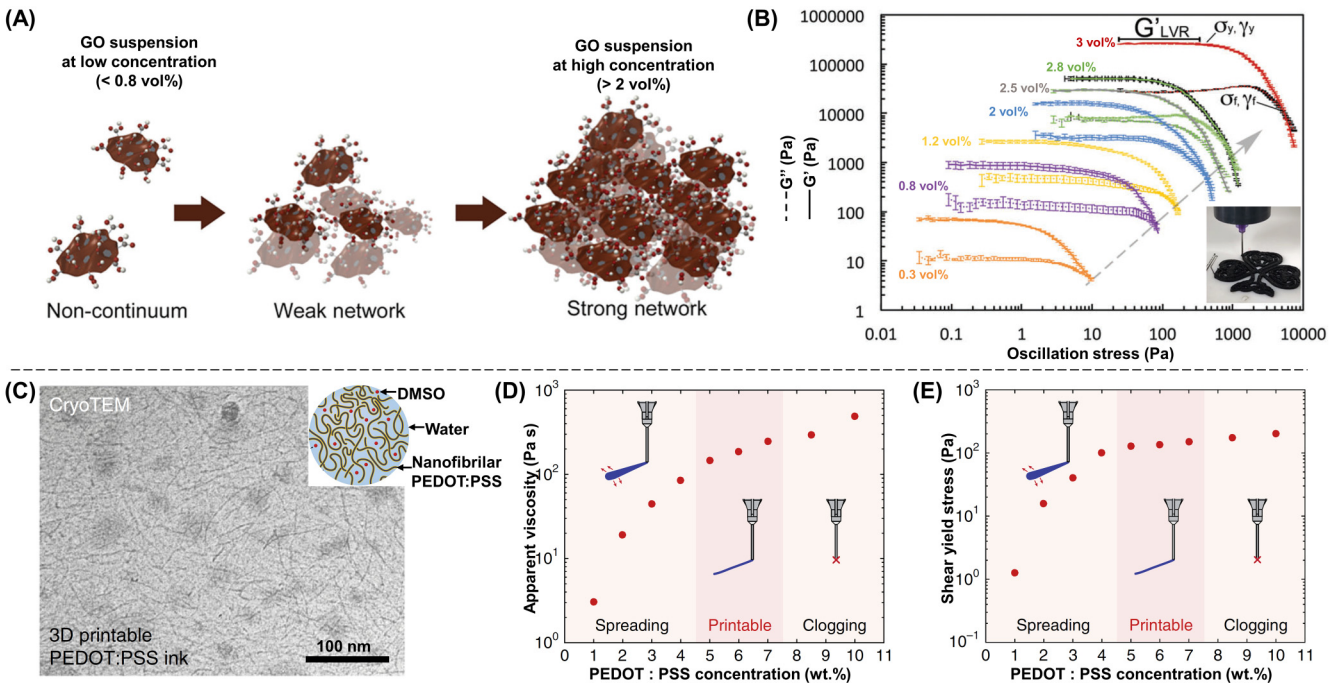

FIG. 14. (a) Schematic of the aggregation state of GO particles at different particle concentrations. (b) Amplitude sweeps showing the LVER and yielding region for GO suspensions with increasing concentration. G' (solid lines) and G'' (dashed lines) are plotted against the oscillation stress to visualize the evolution of the yield and flow stresses as concentration increases.[117] (c) Transmission electron cryomicroscopy image of a 3D printable conducting polymer ink. (d) Apparent viscosity of conducting polymer inks as a function of PEDOT:PSS nanofibril concentration. (e) Yield stress of conducting polymer inks as a function of PEDOT:PSS nanofibril concentration.[12] Reproduced with permission from Corker *et al.*, Soft Matter **15**(6), 1444–1456 (2019). Copyright 2019 The Royal Society of Chemistry; Yuk *et al.*, Nat. Commun. **11**, 1604 (2020). Copyright 2020 Springer Nature.

Though LDP suspension inks may exhibit solid-like behavior at low particle concentrations, the yield stress of the ink is usually not sufficient to meet the requirements of DIW printing because the solid-like behavior results mainly from long-range electrostatic interactions or hydrogen bonding which results in forces due to gravity that are larger than the yield stress. Generally, the particle concentration must be increased far above the critical concentration such that the particles form a highly jammed structure due to an increased number of interactions per particle. Various groups report the rheological behavior of inks composed of polymer matrices with 1D or 2D particles, including graphite nanoparticles,[13,14,181] GO,[15,166] and MXenes.[60] Taken together, these results reveal that an increase in LDP concentration leads to an emergence of a yield stress that also brings with it more pronounced shear-thinning behavior and increased dynamic moduli, in line with granular particles, although the high aspect ratios of LDPs contribute to long-range interactions dominating the particle behavior and printability at lower concentrations than in granular particle inks.

2. Matrix viscosity and matrix–particle interaction

Like inks with granular particles, the properties of the fluid matrix also have a great influence on LDP composite inks. In 2019, Mirkhani *et al.*[174] studied the dynamic moduli of a suspension of MXene nanosheets in an aqueous solution of polyvinyl alcohol (PVA). As shown in Fig. 15(a), a 5 wt. % MXene dispersion in water showed no yield stress, indicating fluid-like behavior (unlike the GO suspension discussed above). Adding the water-soluble polymer PVA (20 mg/ml) into the MXene suspension increased both G' and G'' by two orders of magnitude and led to a crossover point at strain amplitudes of approximately 30% [Fig. 15(b)]. Since PVA is a charge-neutral polymer, the change in the rheology of this ink is likely due to the increase in the matrix viscosity, though the influence of LDP–polymer interactions cannot be ruled out.

The high surface area-to-volume ratios of LDPs can increase particle–matrix interactions, such as electrostatic interactions and hydrogen bonding, particularly in oxygen-containing LDPs, and, thus, provide additional control compared to the matrix rheology alone. In recent work by Jiang *et al.*,[166] aqueous GO inks were used to produce ultralight aerogels; the oxygen-containing functional groups of GO, such as −COOH and −OH, enable Ca^{2+} ions to effectively crosslink the nanosheets via coordination interactions and form a hydrogel, as shown in Fig. 15(c). Thus, the rheological behaviors of the inks can be controlled by adjusting the concentration of Ca^{2+} ion. As shown in Figs. 15(d) and 15(e), both the GO dispersion and GO hydrogel ink exhibited the same shear-thinning,

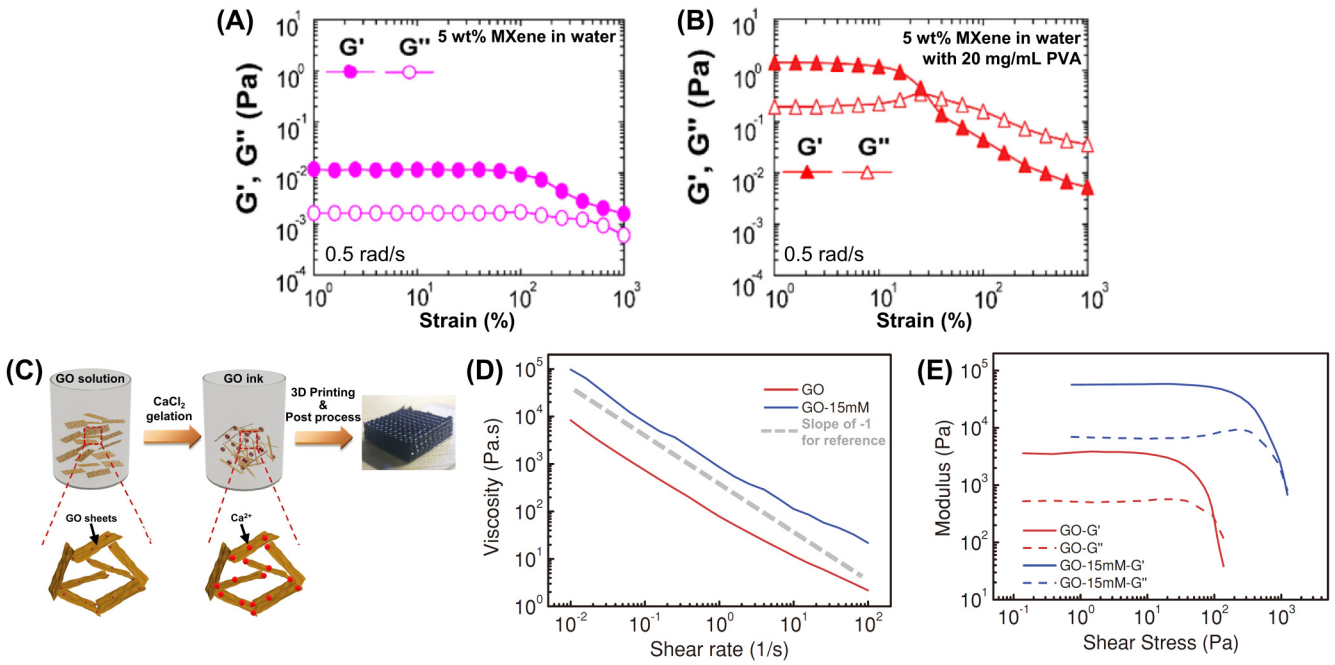

FIG. 15. Oscillatory strain amplitude sweep response of a 5 wt. % MXene aqueous solutions (a) without and (b) with 20 mg/ml PVA.[174] (c) Schematic illustration of the gelation and printing of aqueous GO suspensions with $CaCl_2$ added. (d) Viscosity response with increasing shear rate. (e) Dynamic moduli vs shear stress during oscillatory testing of the pure GO solution and Ca^{2+}-containing GO gel ink.[166] Reproduced with permission from Mirkhani *et al.*, ACS Appl. Mater. Interfaces **11**(20), 18599–18608 (2019). Copyright 2019 American Chemical Society; Jiang *et al.*, Adv. Funct. Mater. **28**(16), 1707024 (2018). Copyright 2018 John Wiley and Sons.

non-Newtonian fluid behavior, but the GO ink with Ca^{2+} ions showed one order of magnitude higher apparent viscosity than the pure GO dispersion and, correspondingly, brought a remarkable increase of the dynamic moduli and, thus, the yield stress.

3. Aspect ratio

Aspect ratio also plays an important role in the rheological properties of LDP inks. In 2020, Zhang *et al.*[182] reported the self-assembly of $Ti_3C_2T_x$ MXenes of different aspect ratios into nematic liquid crystals suitable for wet spinning; notably, the authors did not evaluate the material as an ink for DIW printing, but the study nonetheless sheds light on the relationship between LDP aspect ratio and rheological properties of dispersions. The study reported that the nematic phase formed above a critical transition concentration, C_t, and that this critical concentration was related to the MXene aspect ratio. Aqueous dispersions comprising large MXene flakes with a high aspect ratio of approximately 3.1 μm were compared to those containing MXene flakes with a lower aspect ratio of approximately 0.31 μm; as displayed in Fig. 16(a), although both dispersions exhibited nematic phases with similar rheological behavior, Ct was approximately one order of magnitude larger for the smaller nanosheets. Therefore, the use of smaller MXenes should require a much higher concentration to reach the same viscosity and G'/G'' ratio compared to the use of larger nanosheets, which is verified by Yang *et al.*[60] As shown in Figs. 16(b)–16(e), the authors developed two MXene inks with different lateral flake sizes (8 and 3.7 μm) for DIW printing. To achieve similar viscosity and G'/G'' values, the concentration of smaller aspect ratio MXene flakes must be two to three times higher than the concentration of their large aspect ratio counterpart.

C. DIW of emulsions and foams

Hierarchical cellular structures are ubiquitous in nature and have low densities, high active surface areas, and multifunctionality.[183] In the past decade, porous materials have gained increased attention due to their promising applications in energy storage, wearable sensors, heat insulation, bone regeneration, etc. Emulsion and foam templating has emerged as a popular technique for creating porous polymers because such approaches offer excellent control over pore size and interconnectivity. In 2016, the Cosgriff-Hernandez[38,39] and Studart[40–42] groups pioneered the use of emulsions and foams as inks in DIW printing as a route to produce lightweight porous structures without the need for complicated porogen removal.

Emulsions range from low-viscosity, milk-like Newtonian liquids, to thicker shear-thinning liquids, to thick and cream-like fluids, the latter of which have ratios of gravitational forces to their yield stress suitable for DIW. Most of the printable emulsion inks are highly concentrated emulsions, or so called high internal phase emulsions (HIPEs), defined by having an internal phase fraction Φ

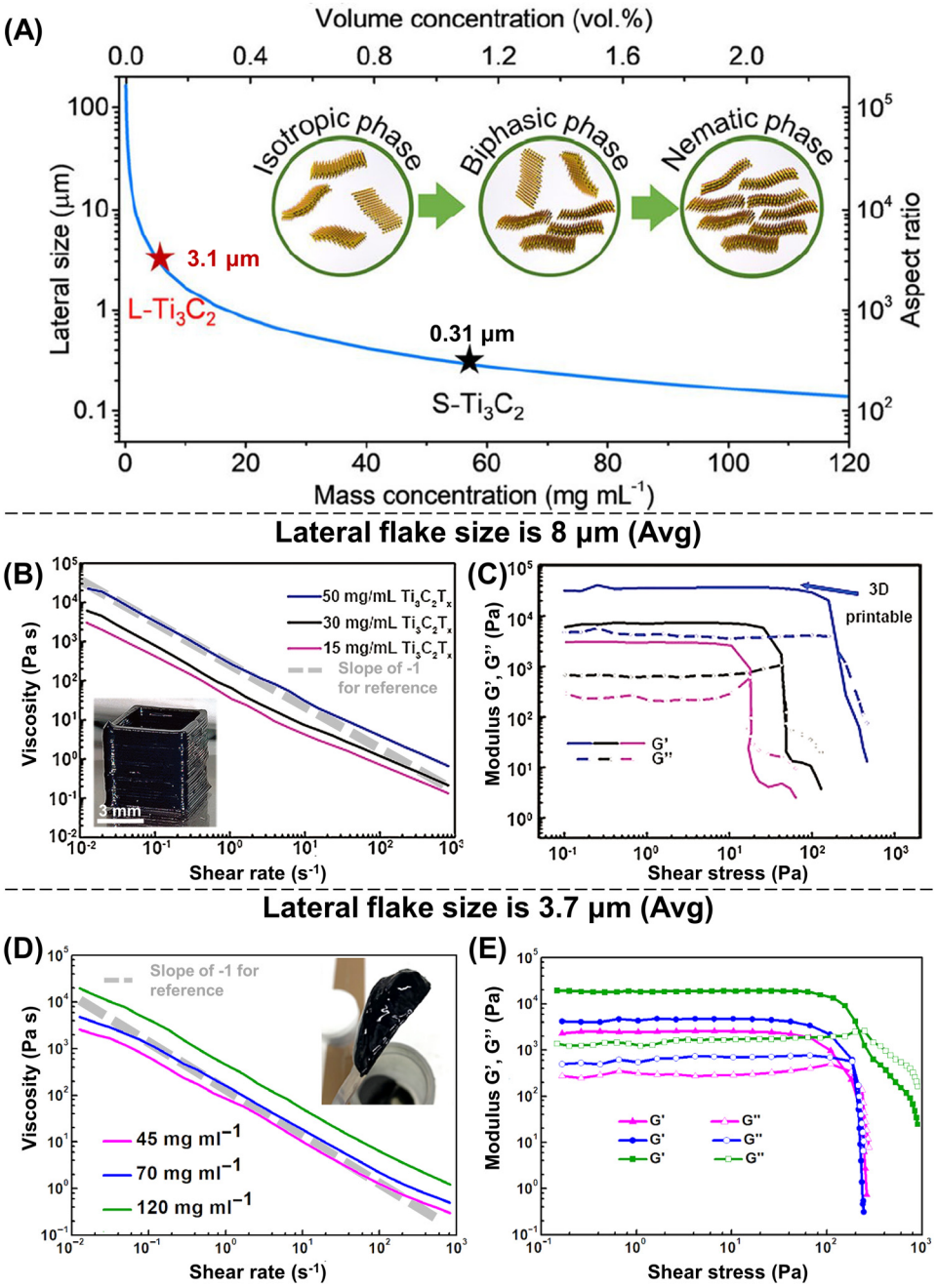

FIG. 16. (a) Theoretical calculations of the relationship between the MXene ink concentration (volumetric and mass) and the flake dimensions for isotropic to nematic phase transformation (inset), with stars indicating C_f for large (L-Ti_3C_2) and small (S-Ti_3C_2) MXene flakes.[182] (b) Viscosity vs shear rate of aqueous suspensions of 8 μm flakes of $Ti_3C_2T_x$ at various concentrations. (c) Dynamic moduli vs stress during oscillatory testing of 8 μm flakes of $Ti_3C_2T_x$ at various concentrations. (d) Viscosity vs shear rate of aqueous suspensions of 3.7 μm flakes of $Ti_3C_2T_x$ at various concentrations. (e) Dynamic moduli vs stress during oscillatory testing of 3.7 μm flakes of $Ti_3C_2T_x$ at various concentrations.[60] Reproduced with permission from Zhang *et al.*, ACS Cent. Sci. **6**(2), 254–265 (2020). Copyright 2020 American Chemical Society; Yang *et al.*, Adv. Mater. **31**(37), 1902725 (2019). Copyright 2019 John Wiley and Sons.

greater than 74% (Φ_{max}).[64] The emulsion composition is of great importance for both the rheological properties for printing and emulsion stability under the shear of extrusion. However, due to the lack of suitable model systems that account for droplet deformability and changing droplet size, a quantitative description of the rheology of the jammed emulsions with yield stress values is still missing.[184,185] The basic rheology-determining parameters of an emulsion are (i) continuous phase rheology; (ii) characteristics of the droplets including size distribution, deformability, internal viscosity, and concentration; and (iii) nature of droplet–droplet interactions.

1. Rheology of the continuous phase

In terms of microstructure, emulsions are composed of two immiscible liquids, in which a continuous phase of one contains

dispersed domains of the other (i.e., droplets). A visualization of an emulsion ink is shown in Fig. 17. Emulsions are thermodynamically unstable, but the interface between the two liquids can be tailored to endow kinetic stability,[186] and the interface can also shield the internal liquid from velocity gradients in the continuous phase liquid. If the interface stiffness and/or viscosity of the dispersed phase are high enough, the droplets can behave as a dispersion of solid particles within a liquid matrix. Under these conditions, the Krieger–Dougherty equation [Eq. (10)] can be applied to get insight into the viscosity of the emulsion system. In this case, the viscosity of the emulsion is related to that of the continuous phase so that changes in the environment which influence the continuous phase viscosity change the emulsion viscosity proportionally. Furthermore, the emulsion viscosity is related to the particle concentration Φ so that for $\Phi > 0.3$, the emulsion viscosity becomes highly sensitive to phase volume. Due to the exponential relationship described in Eq. (10), as particle loading increases, the viscosity becomes increasingly sensitive to the value of Φ_{max}.[133] This is supported by the work of Cosgriff-Hernandez and co-workers.[39] This team reported a series of HIPEs (75 vol. % water as the dispersed phase, 25 vol. % oil as the continuous phase) with the continuous phase containing a low-viscosity component, poly (propylene glycol) dimethacrylate (PPGDMA), and 0, 20, or 40 mol. % of a high-viscosity component, diurethane dimethacrylate (DUDMA). As shown in Fig. 18(a), for inks with the same volume ratio of dispersed to continuous phase, the ink with higher continuous phase viscosity exhibited a higher overall viscosity, even at continuous phase proportion as low as 25 vol. %. Additionally, as the continuous phase viscosity increased, both G' and G'' increased, and, thus, of the ink increased [Fig. 18(b)]. The increase in the yield stress indicates the destruction of a temporary 3D network of jammed droplets upon shear, with the strength of the network proportional to the yield stress.

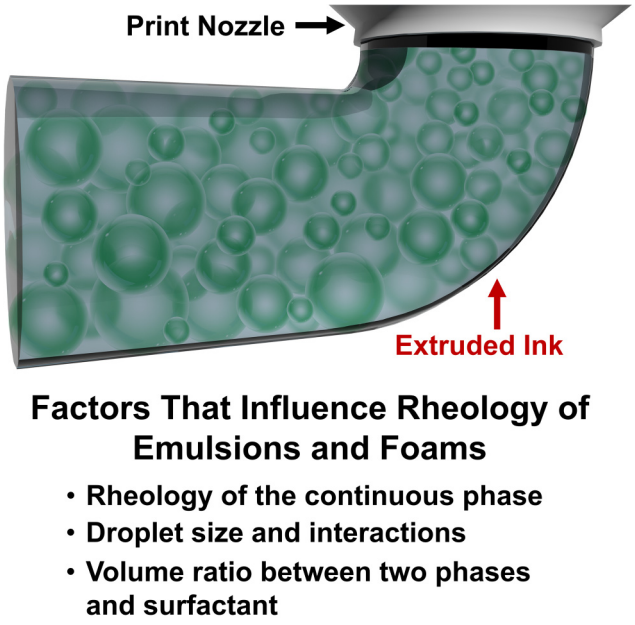

FIG. 17. Illustration of an ink composed of emulsion. The factors that may influence the ink rheology are listed at the bottom.

2. Droplet size and droplet–droplet interactions

The droplet size in emulsion-based inks is also an important variable in emulsion rheology. As proposed by Prince[188] increasing the droplet size decreases viscosity and the dynamic moduli, in line with particle size in granular particle-based inks. In research focused on colloidal particle-stabilized emulsion paste inks [Figs. 18(c) and 18(d)], Franks and co-workers[187] developed a 3D printable oil-in-water emulsion ink consisting of sunflower oil, PVA aqueous solution, co-surfactant sodium 1-heptane sulfonate (C7), and alumina particles and evaluated the effects of mixing speed on rheological properties of the emulsions produced. The authors found that increasing mixing speed during emulsification led to emulsions with higher storage modulus and yield stress [Fig. 18(d)]. This is because higher mixing speeds produce smaller-sized droplets with higher surface area-to-volume ratios, and, thus, increase colloidal interactions between droplets, as well as interactions of a droplet with the continuous phase (i.e., higher overall interfacial area). Another factor that may contribute to differences in rheological performance is that droplet deformability decreases with decreased droplet size. Notably, the impact of mixing speed also depends on the surfactant concentration. As shown in Fig. 18(d), inks with a low loading of co-surfactant (large initial droplet size) exhibited a larger increase in the storage modulus after high power emulsification, whereas the ink with a high loading of co-surfactant (small initial droplet size) was hardly changed.

3. Volume ratio between two phases

The formulation of an emulsion ink determines both its rheological properties and its emulsion properties (e.g., stability, internal phase volume fraction, droplet shape, etc.). As such, the relationship between formulation and rheology of an ink is not straightforward. A good rule of thumb is that with a similar formulation, emulsions with harder droplets (e.g., smaller radius, higher viscosity of the dispersed phase, etc.) and a greater extent of droplet interaction (e.g., higher number of droplets, etc.) will have higher viscosity, storage modulus, and yield stress. For example, Franks and co-workers[187] evaluated the effects of formulation on rheology of particle-stabilized emulsion inks and found that an increase in the volume percent of the oil led to an increase in the dynamic moduli and yield stress for the oil-in-water emulsion [Figs. 18(e) and 18(f)]. This is an outcome of two opposite effects: (1) increasing the proportion of the dispersed oil phase increases the size of droplets, as indicated by the larger voids observed in the SEM images of the printed and sintered inks in Fig. 18(e), which results in lower values for the dynamic moduli; and (2) increasing the oil fraction increases the number of droplets and, thus, increases jamming between droplets, which increases the dynamic moduli. According to the authors, the latter likely has a larger influence, resulting in higher values of the dynamic moduli as seen in Fig. 18(f). Therefore, when interpreting effects from variations in

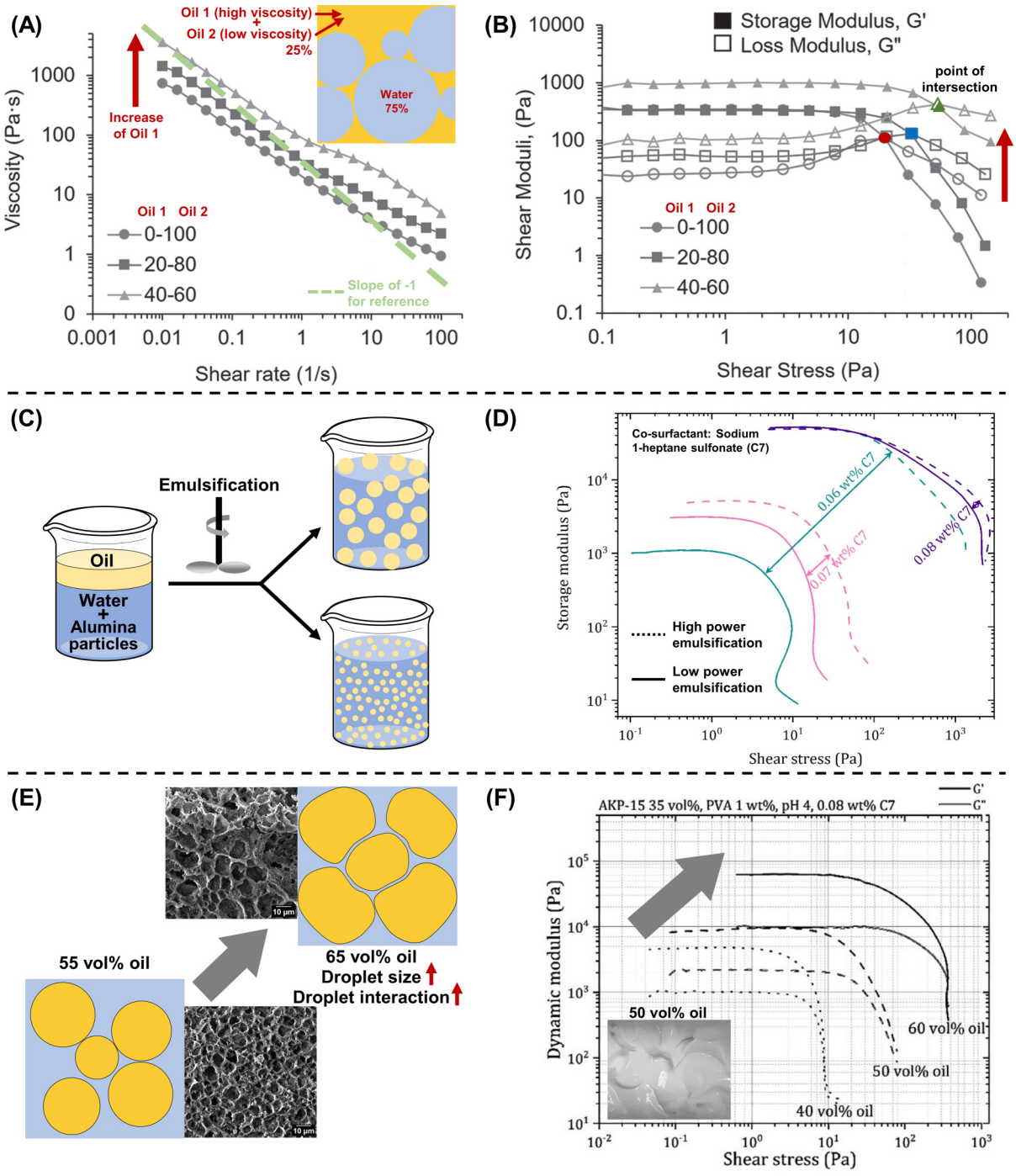

FIG. 18. (a) Viscosity as a function of shear rate and (b) dynamic moduli as a function of shear stress for water-in-oil HIPEs having varying continuous phase viscosities.[39] (c) Schematic of emulsification of an oil-in-water system stabilized by alumina particles. (d) Storage modulus vs shear stress for emulsions having varying concentrations of C7 surfactant emulsified at high or low power. (e) Schematic and scanning electron microscopy images of sintered DIW-printed filaments demonstrating changes in pore size by varying oil fraction. (f) Dynamic moduli vs shear stress with varying oil fraction in an oil-in-water emulsion ink.[187] Reproduced with permission from Sears *et al.*, Macromol. Rapid Commun. **37**(16), 1369–1374 (2016). Copyright 2016 John Wiley and Sons; Chan *et al.*, J. Am. Ceram. Soc. **103**(10), 5554–5566 (2020). Copyright 2020 John Wiley and Sons.

formulation, care should be taken to consider both competing and synergistic effects from multiple variables.

4. 3D printing of air–liquid foams

Recently, researchers have pushed the limits of fluid-fluid emulsion inks for 3D printing by developing air–liquid foams as feedstocks to produce porous structures. In 2019, Lewis and co-workers[189] reported a new 3D printing technique using polymer foams with locally programmed bubble size, volume fraction of voids, and connectivity. As shown in Fig. 20(a), a core–shell nozzle was used for the rapid generation and patterning of droplets containing a gas core and liquid shell [Fig. 19(b)]. This foam ink was composed of polyethylene glycol-diacrylate, a photoinitiator, surfactant, and deionized water; whereas the ink did not possess suitable rheology for self-supported stacking since the outer shell was composed of a low-η monomer, rapid UV-initiated polymerization upon deposition enabled the printed shape to be retained [Fig. 19(c)]. Alternatively, Costantini *et al.*[59] employed a valve-based flow-focusing (vFF) junction in which the size of the orifice can be adjusted in real time to generate foams with online controlled bubble size. The vFF chip was mounted on a robotic XYZ platform [Figs. 19(d) and 19(e)] and used to fabricate tailored macroporous structures with pore size varying from 80 to 800 μm. As shown in Figs. 19(f) and 19(g), this foam ink can hold its shape against gravity without instant curing, which indicates suitable rheological properties common to many DIW inks.

As described above, the development of foam inks for DIW brought new challenges to the rheology of foams. However, characterization of the rheological properties of foams is complicated; numerous parameters, such as foam quality, the size of the measurement apparatus compared to bubble size, and the influence of foam production methods, have to be considered and controlled.[190] Although many experimental studies and theoretical models of foams have been reported, the bridge that connects the rheological behaviors and DIW technique is still required. With a better understanding of the factors that dictate printability of foams, both the composition and the resolution of printed objects can be tailored for desired applications.

D. Hydrogel inks

Hydrogels are an appealing class of polymeric 3D networks that are typically formed by crosslinked hydrophilic chains swollen in water or, in the case of organogel, another organic solvent. Within the context of additive manufacturing, non-covalently

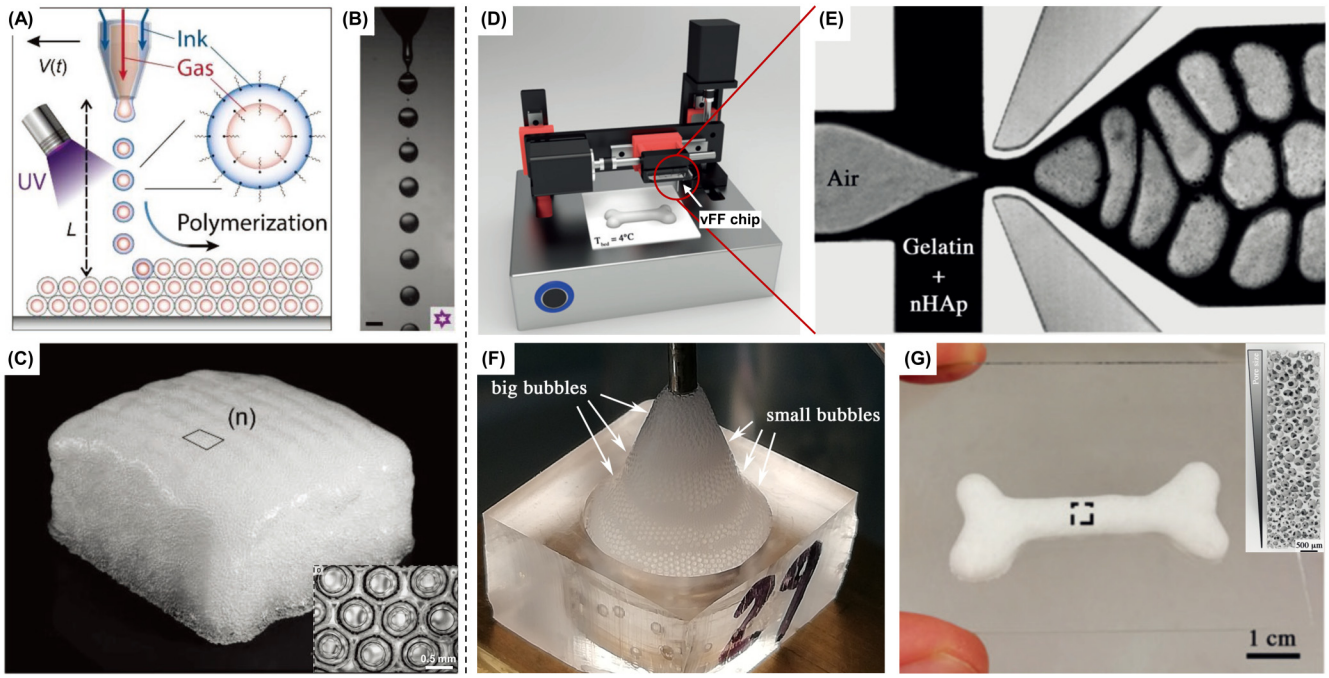

FIG. 19. (a) Schematic illustration of bubbles composed of a fluid shell–gas core, which are ejected from the core–shell nozzle onto the substrate and rapidly photopolymerized. (b) Monodisperse bubbles are ejected at intermediate gas pressures. (c) Optical image of a polymer foam (70 × 70 × 35 mm^3) fabricated by direct bubble writing. (Inset) Optical microscopy image of voids at the top surface.[189] (d) vFF-based 3D printing setup: vFF chip is mounted on the *x* axis and used as the extruder. (e) Contrasted image of gelatin/nHAp solution during foaming within vFF chip. (f) The vFF chip during the production of bi-disperse layered foams. Bubbles with different sizes do not mix but form separated layers which can be attributed to the solid-like behavior of concentrated foams. (g) A 3D-printed dog-bone of graded foam. Inset: 3D reconstruction obtained from microcomputed tomography scan of the boxed region.[59] Reproduced with permission from Visser *et al.*, Adv. Mater. **31**(46), 1904668 (2019). Copyright 2019 John Wiley and Sons; Costantini *et al.*, Angew. Chem. Int. Ed. **131**, 7702–7707 (2019). Copyright 2019 John Wiley and Sons.

crosslinked hydrogels are perhaps the most well studied polymeric system. These possess a wide range of material properties and functionalities including high water content, shape changing, multiple stimuli response, self-healing, and, commonly, biocompatibility. These materials are particularly attractive for use in biological[44,45,191–195] and energy applications[192,193] from soft actuators[44,45,191–193] to sensors.[192,193] Given that hydrogel-based inks are widely used for bioprinting, in which inks contain live cells, the rheological properties of the ink are of critical importance to minimize the stress experienced by the cells.[62]

In hydrogel/organogel inks, no particles or flocs are present, as with the aforementioned ink families, yet the same rapid dissociative/associative network is required for printability. As shown in Fig. 20, such a network is formed on a molecular scale by multivalent interactions between polymer chains. In general, hydrogels only form if the number of junction zones is sufficient to hold the entrained liquid. The non-covalent network which features rapid responsive association/dissociation[191] is a balance between competing forces that favor assembly (e.g., hydrophobic interactions, hydrogen bonding, electrostatic attraction, and/or guest–host interaction)[196,197] and forces that act against assembly (e.g., electrostatic repulsion, Brownian motion, and solvation).[193] Figure 20 summarizes the four major types of interactions that form the network for DIW.[196] These interactions are generally weak individually, but collectively can lead to stable network formation. Due to the dynamic and transient nature of these weak physical associations, the formed networks can quickly dissociate under applied shear and then rapidly recover to the original state once the shear force is removed. This leads to desired rheology of inks for 3D printing. For hydrogels, factors, such as temperature, pH, ion strength, etc., can dramatically influence interchain physical interaction density or strength and will, thus, affect the rheological properties of the ink, so long as the polymer concentration and molar mass are kept constant. Below we list the three factors that are most impactful to ink rheology.

1. Concentration of the gelation reagent

Hydrogels only form in the presence of enough gelling agents (i.e., network-forming molecules). For all four gelation mechanisms, the increase in the number of junction zones leads to increased viscosity and yield stress, alongside improved shape retention and print fidelity.[196] In 2019, Cheng *et al.*[191] developed an ink for 3D-printed soft robotics by introducing an ionic crosslinked network (alginate polymer/Ca^{2+}) into the functional hydrogel precursors to enable the rheological tuning of inks. In a model ink composed of acrylamide and alginate, the desired shear-thinning behavior resulted from the mechanically reversible ionic cross-links between Ca^{2+} and alginate. Increasing the amount of alginate led to inks with higher viscosities and yield stresses, as well as better shape retention of extruded filaments, as shown in Figs. 21(a)–21(c). The same trend was observed in a dynamic network based on hydrogen bonding: in 2020, Jiang *et al.*[10] developed a hydrogel ink using PVA and κ-carrageenan ($\kappa - CA$) [Fig. 21(d)]. The plentiful –OH and $-SO_3^-$ functionalities meant that hydrogen bonding and van der Waals forces were the predominant interactions between PVA and $\kappa - CA$, resulting in hydrogel inks with shear-thinning behavior. With an increased amount of $\kappa - CA$, the viscosity increased [Fig. 21(e)], and shear-thinning behavior and a yield stress were realized [Fig. 21(f)]. Recently, Emiroglu *et al.* studied the effect of altering the stiffness of the microgel building blocks on printing of granular hydrogels. The study revealed that printing of softer microgel packings required increased pressures, offering a means to customize the flow properties and printability.[198] Furthermore, the study highlighted the

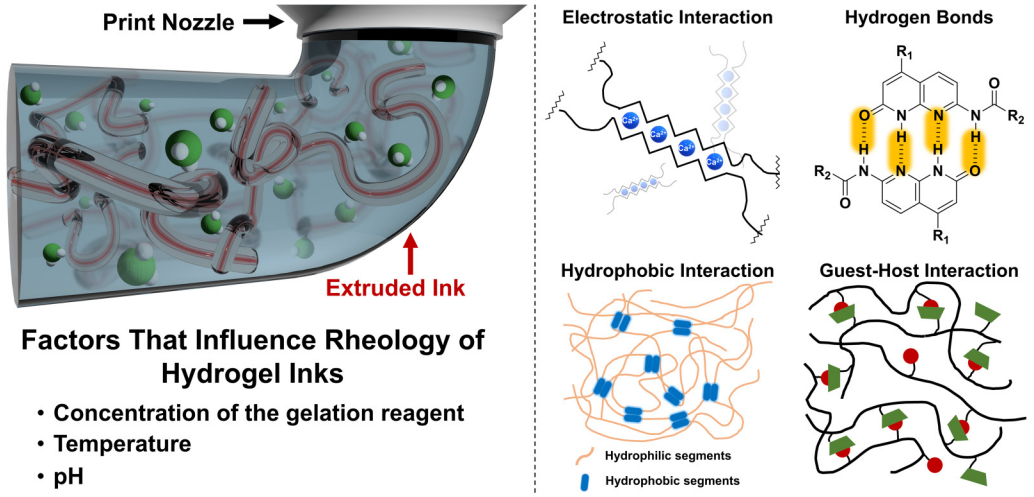

FIG. 20. (Left) Illustration of an ink composed of hydrogel. The factors that may influence the ink rheology are listed at the bottom. (Right) Four major types of interactions that help form a polymer network to impart printability.[196] Reproduced with permission from Cui *et al.*, Adv. Healthc. Mater. **9**(15), 1901648 (2020). Copyright 2020 John Wiley and Sons.

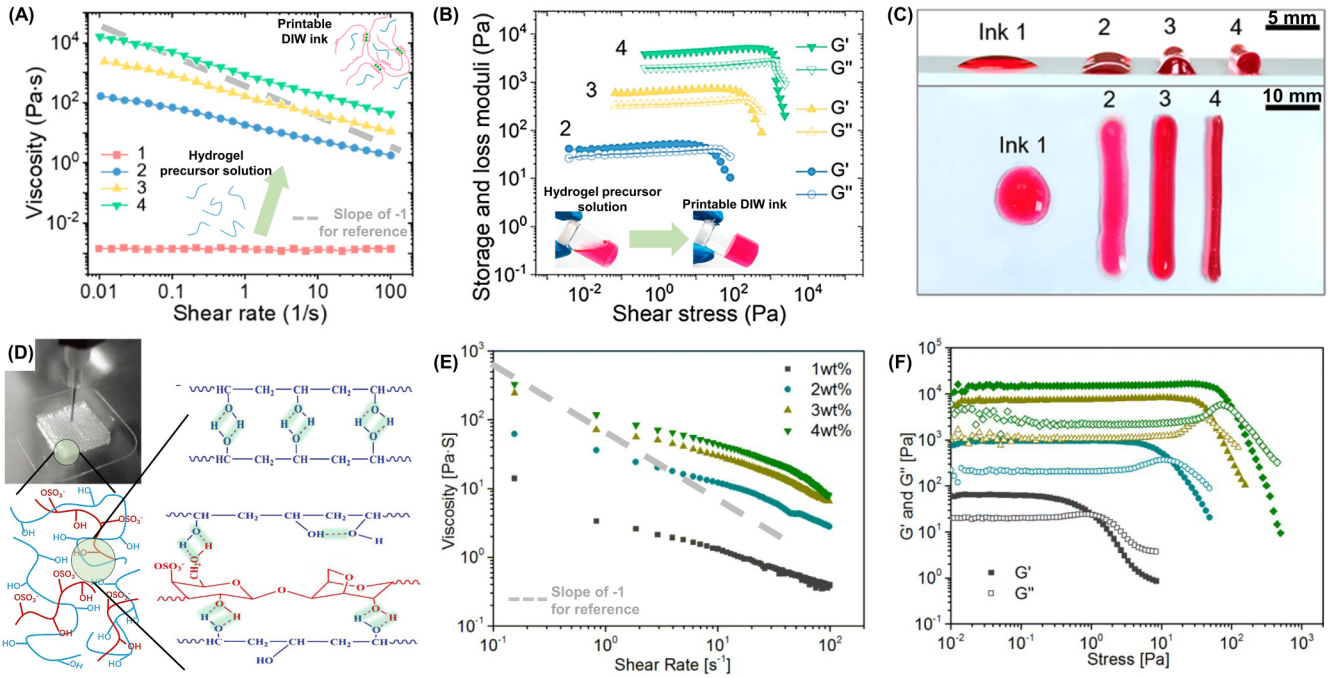

FIG. 21. Rheological tuning of DIW inks and mechanical enhancement characterization. (a) Viscosity as a function of shear rate for the hydrogel precursor (1) and inks containing 1.7, 3.3, or 6.5 wt. % alginate (2, 3, and 4, respectively). (b) Dynamic moduli as a function of shear stress for inks 2–4. (c) Top and side views of manually printed lines from inks 1–4 (nozzle diameter of 1.8 mm).[191] (d) Printed structures from hydrogel inks of PVA/κ-CA. (e) Viscosity as a function of shear rate for PVA/κ-CA inks having different concentrations of κ-CA. (f) Dynamic moduli as a function of shear stress for PVA/κ-CA inks having different concentrations of κ-CA.[10] Reproduced with permission from Cheng *et al.*, ACS Nano **13**(11), 13176–13184 (2019). Copyright 2019 American Chemical Society; Jiang *et al.*, Biomater. Sci. **7**, 1805–1814 (2019). Copyright 2019 The Royal Society of Chemistry.

usefulness of micromechanical models[199–203] in enhancing printing outcomes.

2. Temperature

Hydrogels which are formed based on physical associations are often temperature dependent (e.g., they dissociate at elevated temperatures); therefore, change in temperature significantly affects the rheological behavior of these inks. Polymers which form hydrogels mainly through hydrogen bonding tend to possess a gel transition temperature below which the solution gels; common examples include agarose, methylcellulose, gelatin, and collagen.[204] This is because increased temperature weakens the bonding between chains. Therefore, solutions of these polymers can be printed at slightly elevated temperatures onto a cooled stage such that the sample traverses its gel transition temperature upon deposition and solidifies. Two examples are provided by Ouyang *et al.*[5] and Sarker and Chen[6] where inks were formed from aqueous gelatin and alginate solutions, respectively. In Ouyang's work, a hydrogel ink for the printing of embryonic stem cells was developed. Gelatin was chosen as the major gelation reagent and had the largest contribution to the change in temperature-dependent complex modulus and, thus, complex viscosity of the ink. As shown in Fig. 22(a), aqueous alginate (1% w/v) did not experience gelation, whereas 7.5% w/v aqueous gelatin did, as indicated by the increase in complex viscosity with decreasing temperature. A similar gelation transition was observed in a mixture containing 1% w/v alginate and 7.5% w/v gelatin in water. In Sarker's work, the flow behavior of an aqueous alginate ink was evaluated under different conditions. As shown in Fig. 22(b), an increase in the yield stress was noted as the alginate concentration increased from 1% to 4% w/v, and for a given alginate concentration, the yield stress decreased with increasing temperature, which indicates elevated temperature reduces the initial flow resistance. However, such temperature-dependent behavior can be inversed when different polymer systems are used. In work by Müller *et al.*,[61] Pluronic, a thermo-sensitive polymer which gels below an upper critical solution temperature, was introduced to a biocompatible ink and the temperature-driven dehydration of the hydrophobic blocks transformed the Newtonian ink precursor to a material with shear-thinning behavior at elevated temperatures, suitable for 3D printing [Fig. 22(c)].

3. pH

The pH response of hydrogels is typically due to the presence of pH-dependent ionizable groups on the polymer backbone or side chains. In 2019, Yang and co-workers[45] studied carbomer 940 as a rheology modifier for 3D printing; this is a high molecular

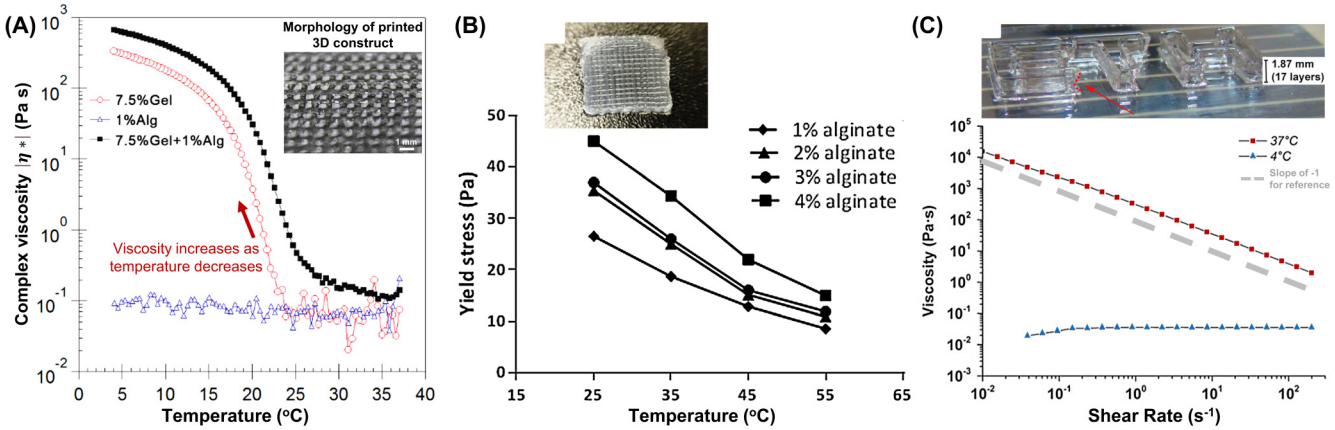

FIG. 22. (a) The magnitude of complex viscosity ($|\eta^*|$) with increasing temperature sweep tests for aqueous gelatin, aqueous alginate, and an aqueous gelatin-alginate mixture.[5] (b) Yield stress of aqueous alginate inks (1–4 w/v%) at various temperatures (25–55 °C). Photographs show a printed alginate scaffold.[6] (c) Flow curves for Pluronic ink at 4 and at 37 °C. Photograph shows side view of the printed 3D text with single layers visible.[61] Reproduced with permission from Ouyang *et al.*, Biofabrication **8**(3), 035020 (2016). Copyright 2016 IOP Publishing, Ltd.; Sarker *et al.*, J. Manuf. Sci. Eng. **139**, 081002 (2017). Copyright 2017 The American Society of Mechanical Engineers; Müller *et al.*, Biofabrication **7**(3), 035006 (2015). Copyright 2015 IOP Publishing, Ltd.

weight polymer of acrylic acid which possesses pH dependence. As shown in Figs. 23(a) and 23(b), varying the pH from 5 to 8 had no impact on the yield stress of a 0.5% w/v carbomer dispersion in water, but the yield stress decreased at pH below 5 or above 8. In neutral environments, the polymer chains of carbomer aggregate into clusters, and the carboxyl groups partially ionize. Upon the addition of NaOH, more carboxyl groups are ionized, leading to electrostatic repulsion between negatively charged groups and stretching of the chains. As the carbomer chains unfold, microgels form, then stack, and swell. This phenomenon imparted these inks with the ability to resist shear stress. In another study, Lim *et al.*[205] evaluated the impact of pH on the rheological properties of composite hydrogel inks composed of hyaluronic acid (HA) and 0.02 wt. % surface-modified nanodiamond (ND). The carboxylation and hydroxylation of NDs (ND–COOH and ND–OH, respectively) alter the surface functional groups and, thus, surface charge (i.e., ζ-potentials). When added into the HA hydrogel ink (HA/ND), the NDs act as junctions to interact with HA [Fig. 23(c)]. As shown in Fig. 23(d), upon changing the pH from 7 to 8, both the dynamic moduli of the ink increased, thus improving printability. Of note, the pH change had a larger impact on in the ink with ND–COOH than the other inks tested which indicates that the deprotonated ND–COOH surface became hydrophilic ($-COO^-$) and, thus, had increased electrostatic interactions with the carboxyl and hydroxyl functionalities of the HA chains.

E. Liquid metal

Liquid metals (LMs) are useful for stretchable, self-healable circuits,[46–49,206,207] strain sensors,[48,49] and soft materials like wearable electronics[48,49,207] and soft robotics.[48] Unlike regular metal powders or particles, DIW of LMs does not require sintering, so it offers a facile and scalable procedure for making complicated structures without using specialized accessories like stencils, microchannels, or stamps.[48] The term "liquid metals" refers generically to alloys of gallium, which are used because of their low toxicity[207,208] and low melting points (mercury is excluded due to its toxicity). Gallium has a melting point of ~30 °C, and its alloys with indium and other metals can reduce the melting point to 15.5 °C or lower,[206] which facilitates use in DIW printing at ambient temperatures. The ability to print LMs at room temperature, alongside their low vapor pressure and toxicity, improve the safety and compatibility of liquid metal parts with soft and bio-based materials.[48] DIW of liquid metals differs from ceramic and polymer-based materials because liquid metals have very low viscosities (near that of water),[209] and their high densities and low affinities to non-metal materials make it difficult to use common particle rheology modifiers such as clay, fumed silica, lignin, etc.

Two major techniques have been developed to DIW liquid metals. Eutectic gallium indium (EGaIn) can form a thin layer of metal oxide (0.5–5 nm) on the surface upon exposure to oxygen (as low as 1 ppm), as illustrated in Fig. 24. This layer endows the liquid metals with shear-thinning properties.[206,210–212] Specifically, the low-viscosity metal can flow when the thin oxide shell ruptures under shear or tension beyond a critical surface stress [~0.3–0.5 N m^{-1}, Fig. 25(a)].[48] After the liquid is extruded, the oxide forms rapidly, which maintains the printed shape and prevents the metal from flowing or slumping. A common challenge with printing liquid metals is the formation of droplets at the tip of the print nozzle resulting from the high surface tension of liquid metals. This causes expansion in all directions and may even interrupt extrusion.[49] Thus, the nozzle head should be suitably close to the substrate so that the LM can flow when the nozzle moves parallel to the substrate (shear) or away from the surface (tension) to break the oxide.[48] Figures 25(b)–25(d) show various free-standing structures printed by DIW of LMs without support material.[46,47]

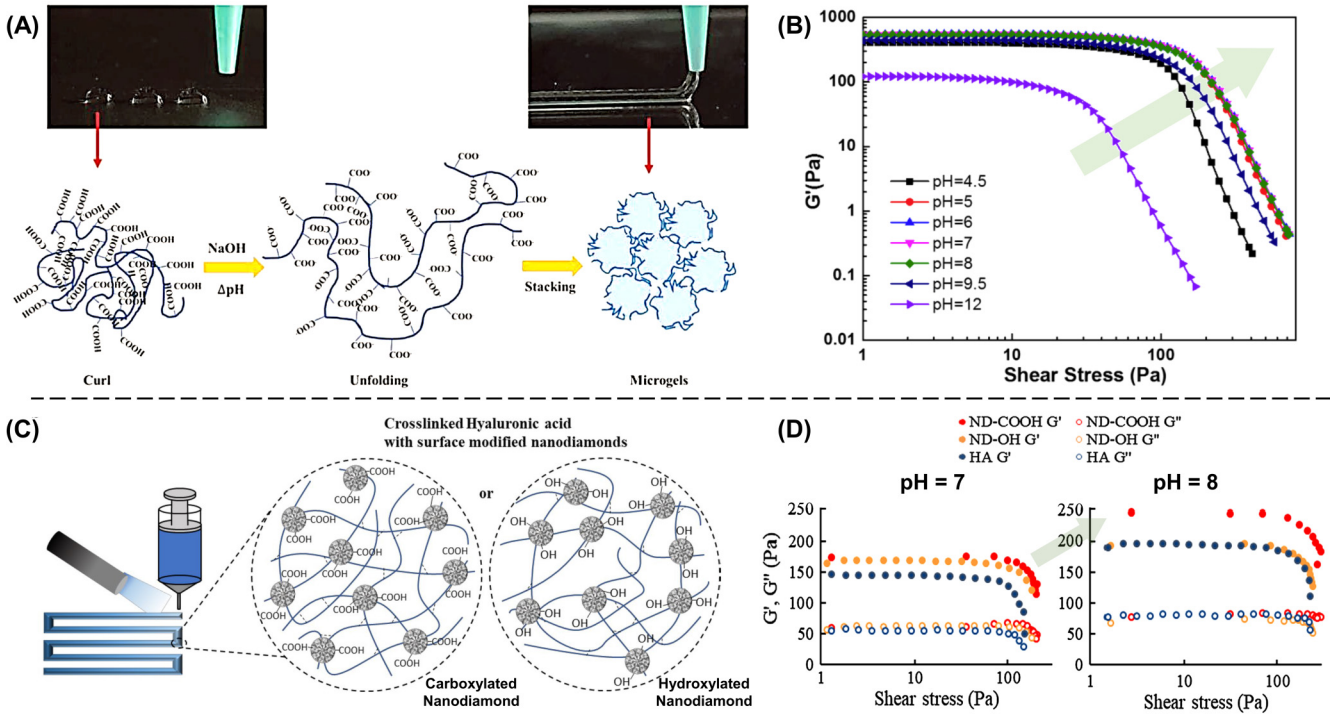

FIG. 23. (a) Schematic of the fluid-to-gel transition of carbomer ink by changing the pH from slightly acidic due to the dissociation of carbomer chains (left) to neutral via the addition of NaOH (center), resulting in microgel formation (right). (b) Storage modulus as a function of shear stress for an aqueous carbomer colloid (0.5 w/v%) at various pH values.[45] (c) Schematic of the interaction of HA with ND–COOH and ND–OH. (d) Dynamic moduli of HA hydrogel precursor, HA/ND–COOH, and HA/ND–OH (0.02 wt. % ND) as function of shear stress at pH 7 and pH 8.[205] Reproduced with permission from Chen *et al.*, Adv. Funct. Mater. **29**(20), 1900971 (2019). Copyright 2019 John Wiley and Sons; Lim *et al.*, J. Nanobiotechnology **18**, 88 (2020). Copyright 2020 Springer Nature.

Recently, a handful of reports address using carbon nanotubes[48] or metal/metal oxide particles[49,213] as rheology modifiers for LMs to improve printability. The synergy of particle–LM interactions and the metal oxide shell for enhanced performance in DIW makes it difficult to predict the rheological behavior of LM inks. Currently, these works focus on the viscosity and shear-thinning properties of the inks,[47–49,206] and only a few reports cover thixotropy and yielding.[48,49,206] The unique and exciting capabilities of LMs inspire a broader discussion of the printability and rheological properties of these materials.

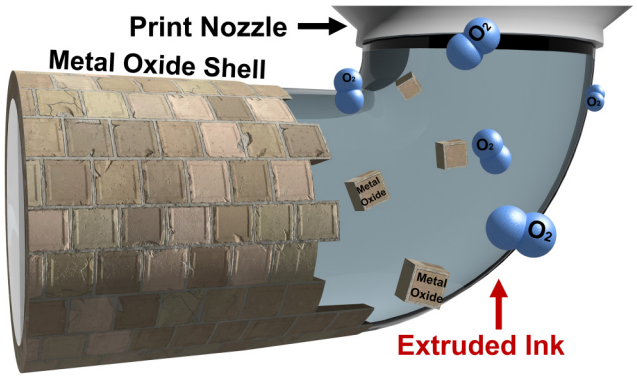

FIG. 24. Schematic of the formation of metal oxide shell that helps the extruded filament maintain its shape.

F. Other types of ink

1. Capillary suspensions

While the rheology of particle-filled suspensions is controlled primarily through the rheology of the matrix and the volume fraction of solids, researchers reported in 2011 that the addition of a small amount of a secondary fluid which is immiscible with the continuous phase (i.e., matrix) can cause particle agglomeration and dramatically alter the bulk rheology.[214] As shown in Fig. 26(a), capillary suspensions have been divided into two distinct states: the pendular state where the minority liquid preferentially wets the particles, and the capillary state where the secondary fluid wets the particles less well than the primary fluid. In both states, the capillary forces of the two fluids on the solid particles leads to particle bridging and network formation.[214–216] The phenomenon increases the yield stress and viscosity by several orders of magnitude as the

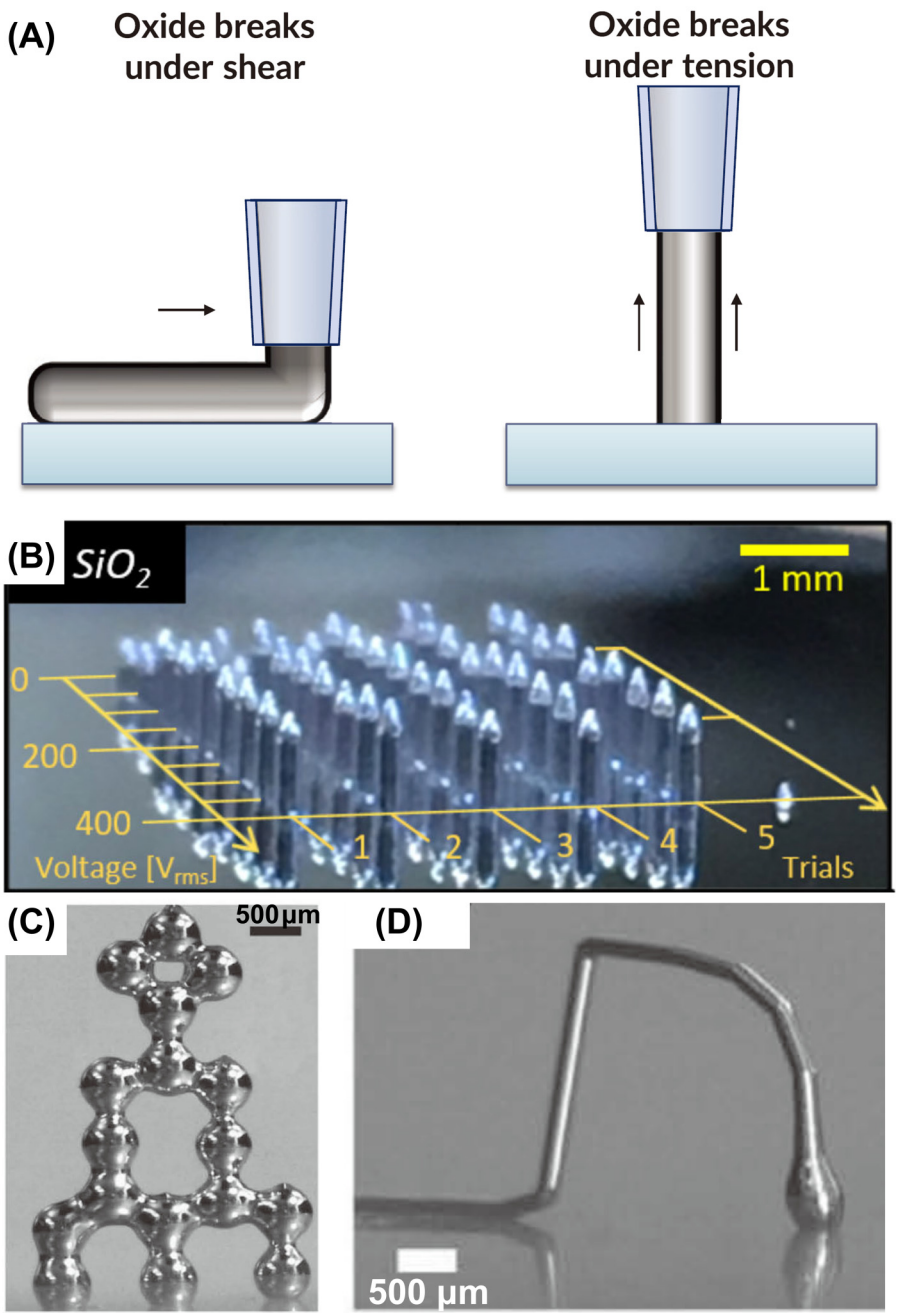

FIG. 25. (a) Rupturing the oxide layer of an LM through shear or tension arising from the combined effects of oxide adhesion to the substrate and motion of the nozzle.[48] (b) Vertical Z-printing by extrusion of EGaIn onto an oxide surface (SiO_2).[46] (c) Photograph of a free-standing tower structure printed from LM. (d) Free-standing arch printed from LM.[47] Reproduced with from permission Neumann *et al.*, Adv. Mater. Technol. **5** (9), 2000070 (2020). Copyright 2020 John Wiley and Sons; Watson *et al.*, Adv. Eng. Mater. **21**, 1900397 (2019). Copyright 2019 John Wiley and Sons; Ladd *et al.*, Adv. Mater. **25**(36), 5081–5085 (2013). Copyright 2013 John Wiley and Sons.

volume fraction of the second fluid increases and, therefore, has been successfully used to develop DIW inks. For example, Fig. 26(b) shows the transition from weakly elastic, fluid-like behavior to highly elastic, gel-like behavior for a capillary state suspension with the addition of a small amount of water to hydrophobically modified calcium carbonate/diisononyl phthalate suspension ($\Phi_{solid} = 0.11$).[214,216] Similarly, Ding *et al.* reported a capillary suspension ink composed of carboxymethyl cellulose and graphene nanoflakes. By adding 2 vol. % octanol, a wetting fluid of graphene, the viscosity and yield stress increased by more than one order of magnitude, as shown in Fig. 26(c). Other capillary ink compositions have included polydimethylsiloxane (PDMS) microbeads with uncured PDMS precursor with water as a continuous phase,[217,218] graphite in glycerol with epoxy resin as a secondary fluid,[219] and aluminum oxide suspended in a blend of waxes with aqueous sucrose as a secondary fluid.[141] Capillary suspensions

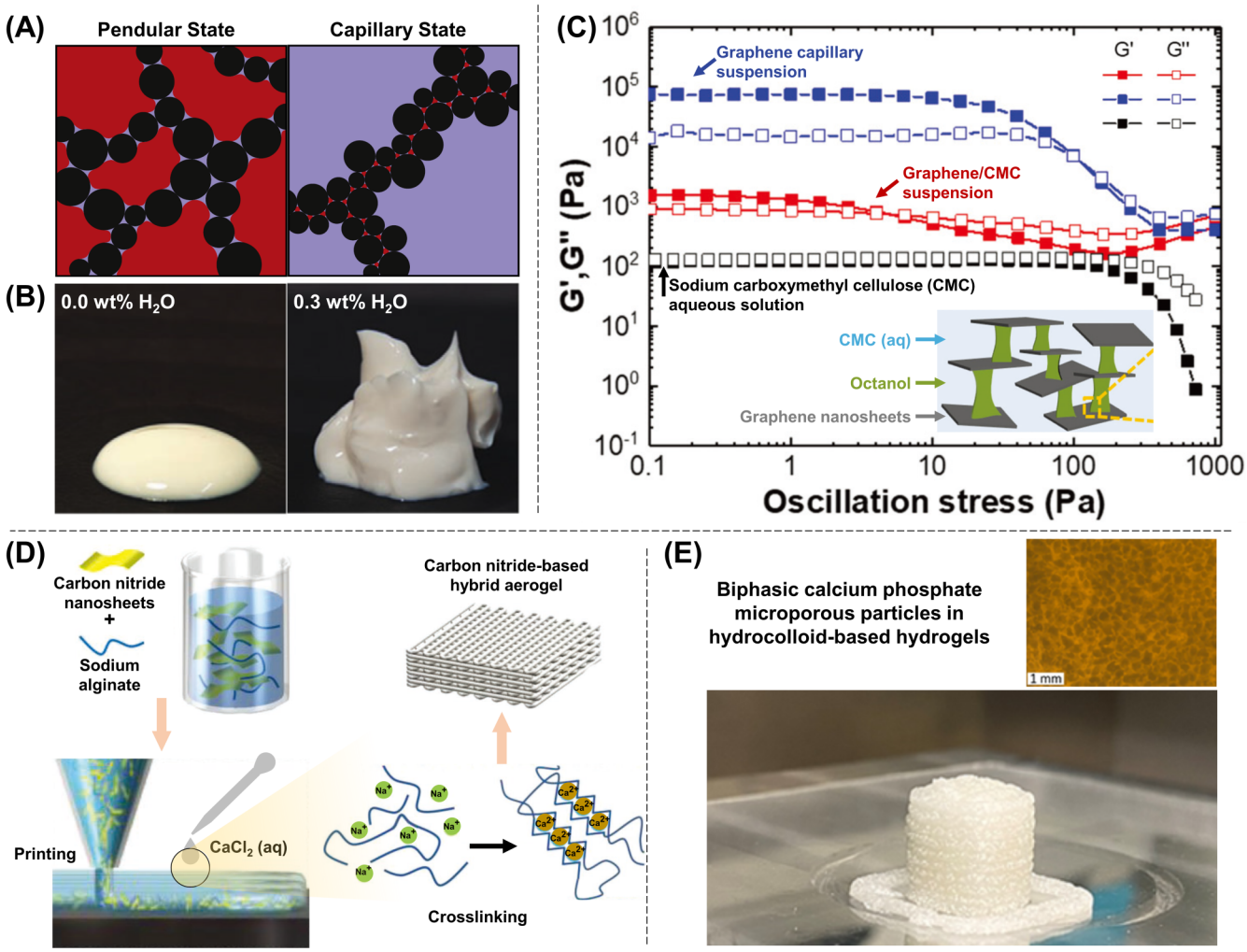

FIG. 26. (a) Two states of capillary suspensions: the pendular state, in which the minority liquid preferentially wets the particles, and the capillary state, in which the majority liquid preferentially wets the particles, both of which lead to particle aggregation.[215] (b) Adding a small amount of water to a suspension of hydrophobically modified calcium carbonate/diisononyl phthalate produces gel-like behavior.[214] (c) Influence of adding graphene and 2 vol. % octanol to a carboxymethyl cellulose suspension on the storage and loss modulus.[218] (d) DIW of hybrid particle-hydrogel ink, crosslinking, and resulting printed aerogel.[220] (e) Printed porous bone scaffold made from hybrid particle-hydrogel ink.[140] Reproduced with permission from Koos *et al.*, Curr. Opin. Colloid Interface Sci. **19**(6), 575–584 (2014). Copyright 2014 Elsevier; Koos *et al.*, Science **331**(6019), 897–900 (2011). Copyright 2011 American Association for the Advancement of Science; Ding *et al.*, Nanoscale **12**(21), 11440–11447 (2020). Copyright 2020 The Royal Society of Chemistry; He *et al.*, Adv. Funct. Mater. **28**(29), 1801121 (2018). Copyright 2018 John Wiley and Sons; Herrada-Manchón *et al.*, Gels **8**(1), 28 (2022). Copyright 2022 Author(s), licensed under a Creative Commons Attribution (CC BY) license.

offer the unique opportunity to tune ink rheology with only slight modifications to ink composition.

2. Hybrid inks

With the demand for new functional inks, inks composed of different types of the aforementioned fluids have also been reported. For example, He *et al.* reported an ink composed of carbon nitride nanosheets and sodium alginate hydrogel, with both components contributing to the rheological properties of the ink as displayed in Fig. 26(d). After printing, the obtained object was submerged in an aqueous solution of $CaCl_2$ to crosslink the sodium alginate, then supercritically dried to yield a hybrid aerogel.[220] In a similar vein, Aguilar and co-workers developed an ink of biphasic calcium phosphate particles in a hydrogel matrix which showed promise for highly porous, custom-fit bone replacements, with an example print shown in Fig. 26(e).[140] In general, the factors that influence the rheology of hybrid inks are combinations of the factors we mentioned in each category. This area requires more research to account for competing effects and truly quantify the printability of complex compositions.

V. EVOLVING TECHNIQUES ON LINKING RHEOLOGICAL BEHAVIORS TO PRINTABILITY

As discussed above, the composition of DIW inks varies widely from fluid matrices filled with granular particles[23,29,34–37,68,126–128,131,141,143,163,221,222] or LDPs[13,14,16,18,19,60,117,166,169–175,180–182] to emulsions,[38–42,70,117,187] foams,[59,183,189] hydrogels,[5–11,38,43,45,55,61,62,123–125,140,191,196,204,205,223] and liquid metals.[47–50,206,213] Different factors influence the rheology of each class of ink, so establishing the link between rheological behaviors and DIW printability can be challenging. Fortunately, opportunities to probe fundamental relationships arise as new computational techniques emerge. In the past few decades, computational simulations and machine learning have significantly advanced to the point where they can facilitate research in many fields, including the 3D printing realm. This section will briefly discuss how these evolving techniques accelerate the development of DIW inks.

A. Recovery rheology

Rheological studies typically describe the mechanical deformations of materials using the stress, σ, and the total strain and its rate of change, γ and $\dot{\gamma}$, respectively. However, a more comprehensive understanding can be achieved by acknowledging the composite nature of strain. As first proposed by Weissenberg[224] and Reiner[225] and illustrated in Eq. (4), strain can be experimentally decomposed into a recoverable or elastic strain, γ_{rec}, and an unrecoverable or plastic strain, γ_{unrec}. The two components are determined by measurement of the strain response to a zero-stress step, known as the "recovery step." The recoverable strain refers to the amount of strain recovered by the material, while the unrecoverable strain is the remaining portion of the total strain.

In recent years, several studies have used an iterative method, known as "recovery rheology," to decompose a range of rheological responses into recoverable and unrecoverable behaviors.[88,100,114,115,226] This method is unique because it does not rely on any mathematical formulation but rather on the separability of the strain components. As we have discussed before, most studies on DIW rheology focus on large-amplitude oscillatory shear tests and plots of the dynamic moduli as a function of strain amplitude.

A common observation among all the categories of DIW inks discussed in this review is that they exhibit an overshoot in the loss modulus. Recently, a study utilizing oscillatory shear recovery tests showed that this behavior was the result of a gradual change in the strain acquisition behavior, from predominantly recoverable at small amplitudes to predominantly unrecoverable at larger amplitudes.[114] Dinkgreve *et al.* showed that no fewer than five distinct metrics have been proposed to determine the yield point. However, the work of Donley *et al.* showed that there is no single identifiable yield point from an amplitude and that yielding is a gradual transition.

The findings of Donley *et al.* led to the development of a model for yield stress fluids that unify their rheological behavior above and below the yield stress.[100] This model employs a single differential equation to account for both the linear and nonlinear rheology without incorporating the sudden yielding threshold of the Oldroyd–Prager formalism. This accurately predicts the steady shear behavior as well as the transient rheology that is responsible for successful printing. As shown in Fig. 27, this includes a gradual

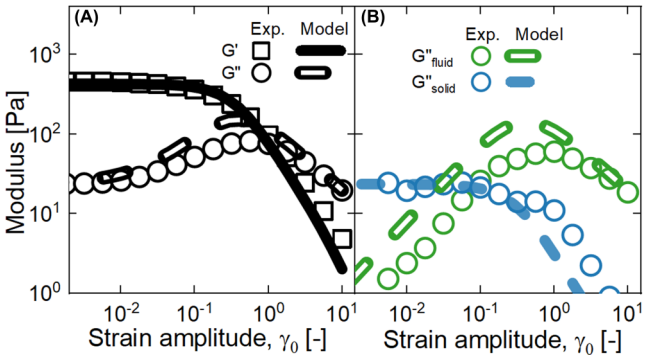

FIG. 27. Oscillatory shear and recovery tests on Carbopol 980 gel. (a) Dynamic moduli as a function of strain amplitude. Symbols are experiments and lines are model predictions. (b) Components of the loss modulus as a function of strain amplitude.[100] Reproduced with permission from Kamani *et al.*, Phys. Rev. Lett. **126**(21), 218002 (2021). Copyright 2021 American Physical Society.

overshoot in the loss modulus observed for DIW inks, as shown in Sec. IV, and the transient large-amplitude oscillatory shear responses. This model indicates that rapid elastic deformation aids plastic deformation. In terms of DIW printing, this means that the rate at which a filament is laid on another will affect the shape of the lower layer. The recovery rheology framework was also recently used to identify the sequence of processes that a simple yield stress fluid goes through during transient large-amplitude oscillatory shear behavior.[88] While this model has yet to be directly applied to DIW situations, its ability to accurately describe the transient nonlinear rheology of a wide array of yield stress fluids leads us to propose it as an excellent candidate for DIW studies.

B. Computational modeling

Computational modeling is a powerful tool for understanding the printing process, with two major directions being the most prominent for DIW. The first is to simulate particle movement and interaction under shearing to help understand the behavior of the inks under shear deformation. Most of the reported simulation approaches focus solely on particle/matrix composites; with the advent of new categories of inks, rapid advances in this area are expected in the near future. The second direction is the simulation of the microscopic behavior of ink in the nozzle, which is of tremendous benefit for identifying printable inks and optimizing ink composition. Finite element models and computational fluid dynamics are extensively used to simulate fluid flow behavior and properties of molten polymer in the nozzle in FDM.[227] Moreover, the combination of microfluidic devices and flow simulation techniques can offer crucial insights into the transient nonlinear rheology that occurs during DIW.[227] These models give insight into the influence of the printing parameters, such as pressure drop, shear rate profiles, and the shape of the extrudate during the process, and offer a handle for further improvement.[228,229]

Unlike FDM, studies modeling the rheology of DIW inks remain scarce. In 2017, Liu *et al.*[7] developed a cell-laden bioink for

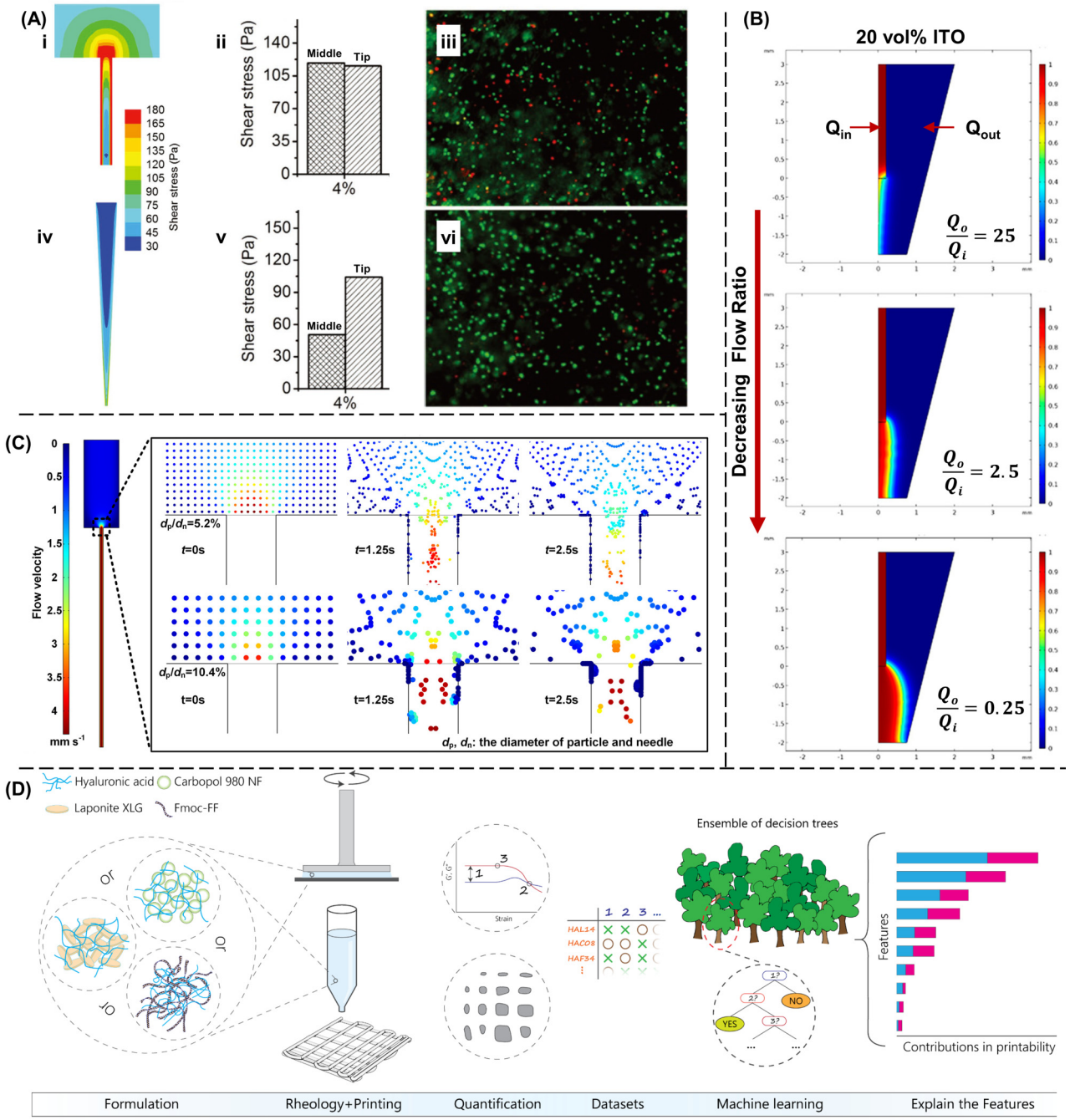

FIG. 28. (a) The effect of the bioprinting process on cell viability. (i) and (iv) are the shear stress distribution maps during the printing process using a straight nozzle and a cone-shaped nozzle, respectively. (ii) and (v) are the quantification of shear stress at the middle and tip of two nozzles. (iii) and (vi) are the live/dead staining (red indicates dead cells) of the cell-laden constructs bioprinted using two different nozzles.[7] (b) Flow simulations of the ITO particles across a range of flow rate ratios.[230] (c) Flow velocity field in a simulated syringe showing the particle aggregation at the needle entrance for inks with different sizes of particles (d_p and d_n are the diameters of the particle and nozzle, respectively).[16] (d) Schematic of machine learning to predict printability of DIW inks.[232] Reproduced with permission from Liu *et al.*, Adv. Healthc. Mater. **6**, 1601451 (2017). Copyright 2017 John Wiley and Sons; Cipollone *et al.*, ACS Appl. Mater. Interfaces **14**(21), 24897–24907 (2022). Copyright 2022 American Chemical Society; Ao *et al.*, ACS Appl. Energy Mater. **5**(6), 6970–6979 (2022). Copyright 2022 American Chemical Society; Nadernezhad *et al.*, Adv. Sci. **9**(29), 2202638 (2022). Copyright 2022 John Wiley and Sons.

DIW and investigated the effect of the extrusion process on cell viability. They used computational fluid dynamics to simulate the stress distributions of inks within straight and cone-shaped nozzles. As shown in Figs. 28(ai) and 28(aii), the use of a straight nozzle would generate high stress along the entire nozzle length. In comparison, when a cone-shaped nozzle was employed, the high σ only existed at the tip [Figs. 28(aiv) and 28(av)]. The live/dead staining of the cell-laden bioinks extruded from two different nozzles is shown in Figs. 28(aiii) and 28(avi). Clearly, the cells printed with a cone-shaped nozzle have a higher viability than those printed with a straight nozzle, which is in good agreement with the computational study of the shear stress distribution during printing.

Simulations are also very useful in facilitating the development of novel printing techniques. For example, Cipollone *et al.*[230] used COMSOL to simulate co-flow behavior during coaxial printing of indium tin oxide (ITO)-alumina particle core–shell ink and analyzed the core deformations and eccentricity of the printed filament. As shown in Fig. 28(b), the simulations indicate that the core diameter increases logarithmically with a decreasing ratio of the volumetric flow rates between the outer and inner phases. This finding guided the later experimental control of the printing of core–shell architectures. Apart from obtaining the shear stress distribution, researchers have also studied the mechanism of congestion during extrusion, which can help solve the issue of nozzle clogging, a leading cause of inefficient and unsuccessful DIW printing. A few studies employ mathematical models to predict the printability of inks.[16,117,231] Factors including nozzle diameters, filler sizes and contents, ink viscosity, and extrusion pressure are considered to result in the bridging and aggregation of particles at the nozzle inlet. The Bao group[16] simulated particle transport and liquid motion in the ink flow field with COMSOL-coupled computational fluid dynamics to support the fact that smaller particles are less likely to clog the nozzle inlet. As shown in Fig. 28(c), when the particle/nozzle diameter ratio decreased, the ratio between the maximum horizontal length of accumulated particles and the nozzle diameter (i.e., the relative clog size) also decreased.

C. Machine learning and materiomics

Recently, machine learning (ML) techniques have gained significant interest in the DIW process. For example, Nadernezhad and Groll's recent study[232] employed machine learning principles to relate the printability of hydrogels induced by addition of rheology modifiers, as shown in Fig. 28(d). They established the printability of formulations containing various rheology modifiers so that the model's decision-making process is understandable and interpretable by a user familiar with rheology and 3D printing. First, inks were prepared from aqueous hyaluronic acid and different particles additives. Rheological characterization and printability studies were quantified to develop datasets. A random forest ML algorithm was trained from these data sets to produce a model to predict printability. The model was then analyzed to elucidate the influence of particular variables on the decision-making process of the model. This generic map makes possible the design of new formulations based on data-driven correlations from inherently different systems and provides a guideline for multiple systems.

Currently, most machine learning algorithms are purely statistical in their foundation and, therefore, rely heavily on an abundance of data to reach accuracy in their predictions. More often, studies that use such an approach concentrate on optimizing a specific aspect of the printing process, including line morphology optimization, printed line width control, ink printability, and process drift calibration.[233,234] Alternatively, physics-based ML frameworks require fewer data inputs by directly integrating physical governing laws. Recent studies have used this approach to successfully predict velocity fields and fully resolved flow fields for complex fluids under different flow conditions.[235–238] However, physics-based machine learning methods have not yet been used to study the process of DIW 3D printing.

Building a materiomics platform and leveraging the ML technique to establish quantitative relationships have become hot topics across the field of materials science. Materiomics is defined as the holistic study of material systems, which examines links between physicochemical material properties and material characteristics and function. The focus of materiomics is system functionality and behavior rather than a piecewise collection of properties. In the case of DIW printing, the same research pattern can be used to link rheological behaviors to printability. Although no model has yet been established to correlate the ink rheology and printability with the above formulation parameters, it is a promising direction in this field.

VI. SUMMARY AND OUTLOOKS

Direct ink writing could be considered a mature technique from the standpoint of ink development but also young technique from the standpoint of understanding fundamental structure–function relationships. Although DIW was established and full-fledged in the late 1990s,[3,127,221] it is still the most popular 3DP platform for developing novel materials (e.g., composition). With the rapid technological and material advances being made in this field, standardization of materials formulation, printing, and characterization is increasingly important,[62,223] yet getting more challenging. For example, although there is consensus on the importance of accurately controlling high-resolution features in DIW printing, to date, "printability" remains a widely used yet poorly defined term. Most researchers, including our own research group, still assess printability qualitatively by an ink's ability to hold its shape upon a spatula or by describing the fidelity with macroscopic imaging. Quantitatively, this corresponds to the criterion laid out in Eq. (3), $\rho gh/2\sigma_y < 1$, indicating that the yield stress is large enough to withstand forces due to gravity for a substantial amount of material.

As mentioned above, the stress is tensorial and contains both shear and extensional components. Most of the work on the rheology of DIW inks has focused on shear rheology. Comparatively little has been done to investigate the extensional effects. We think that there remains work to be done to determine the full effects of extensional fields on the physical properties of printed objects, and a deeper understanding of the rheology of DIW inks should lead to better printing outcomes. As long as an ink has a sufficiently large yield stress to withstand the force due to gravity [Eq. (3)], such as is observed when an ink holds its shape on a spatula, it should be

printable, although the quality of the print will depend on the details of how the ink yields and unyields. The transient rheology of yield stress fluids is, therefore, a central problem to further development of DIW outcomes. A deeper understanding of yield stress fluid rheology should allow for new processes to be designed that take advantage of the complexities observed. That this is not yet possible comes down to our incomplete understanding of what factors determine how and when an ink yields and unyields. Rapid progress is being made, however, in determining this complex rheology, and the future should see new models being used to great effect to both predict outcomes and design new processes.

In this review, we provide an overview of the rheological requirements of DIW inks and discuss quantitative assessments of the ink printability using rheology and print resolution. We also propose a classification for ink composition based on the origin of their complex rheological behaviors, and the factors influencing the rheology of different types of inks are discussed respective to each class of inks. Techniques that could have a significant impact on the field in the near future include computational studies, high-throughput rheological measurements, machine learning, and materiomics, are also discussed to illustrate the future directions of materials development for DIW.

Although considerable achievements related to DIW have been made in the past decade, there is still a knowledge gap to predict printability based on the physical and chemical properties of each component. In view of this fact, we further propose some perspectives based on our experience, summarized in Fig. 29. We hope that these viewpoints may help this field develop.

1. The rheology and DIW communities should work together to provide universal models for ink formulation and development, such as the model proposed by Kamani *et al.*[100] DIW researchers tend to formulate inks by a guess-and-check approach and use simple characterization methods to examine flow effects corresponding to Weissenberg number rheology but neglect the transience described by Deborah number variations. Supplementing this knowledge of printability with more thorough and robust transient nonlinear rheological characterization would promote more informed and more rapid ink development.
2. The community should standardize how printability is determined and assess the printability quantitatively (from both the rheology perspective and fidelity perspective) to enable meaningful comparisons between different studies. We propose that the dimensionless group formed by the ratio of gravitational forces to the yield stress be used as a measure of printability, and that a simple criterion of this number being less than unity could be used to define "printable" [see Eq. (3)]. Different researchers currently adopt distinct methods to measure the workability and buildability of feedstocks for extrusion-based 3D printing. These various standards result in non-connected and piecemeal recommended values within the literature, making it challenging to define optimum ranges for rheological properties.
3. Physics-based automated analysis systems, such as artificial intelligence and machine learning algorithms, should be applied to assist in the development of DIW. The rapid development in this field will bring about many new ink compositions and to consummate the application of materiomics to the rheology of DIW inks, high-throughput rheological measurements that can automatically and standardly measure many ink samples with different compositions are critical. Therefore, it is also critical that a standard set of experiments be determined for such studies. Given the way in which both the Weissenberg and Deborah numbers change during large-amplitude oscillatory shear experiments, we suggest that these may form an excellent starting point. Physics-guided machine learning could then be used to analyze the data and better predict and optimize inks suitable for printing.

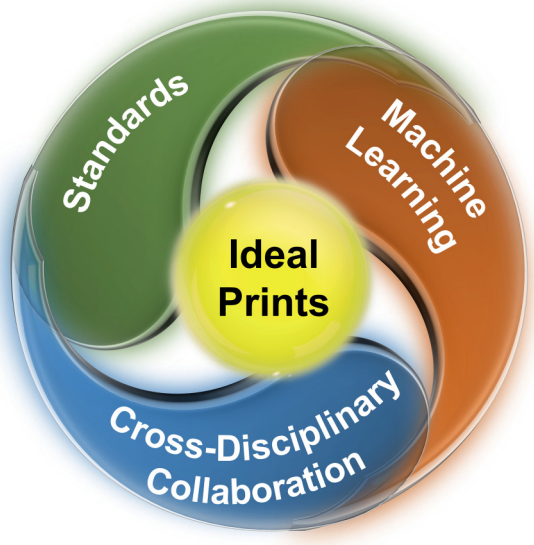

FIG. 29. Proposed perspectives to promote DIW toward ideal printing.

Overall, significant steps have been taken in the evaluation of extrudability, printability, and shape fidelity in DIW printing, which is also driven by understanding the correlation between the shape fidelity, rheological, and physicochemical properties of inks. Combining theoretical models and straightforward quantitative tests will be an important and powerful step toward further improving shape fidelity of DIW-printed constructs, which will help to drive the field into the next stage to fully predictable printability and optimized print processes.

ACKNOWLEDGMENTS

P.W. and C.C. acknowledge Yifei Wang and Yunchong Yang for providing suggestions. P.W. would like to acknowledge Muhuai Wei for bringing happiness and hope to P.W.'s life. This work was funded by NSF DMR (Grant No. 2103182) and Texas A&M. C.C. was supported by a NASA Space Technology Graduate Research Opportunity. K.K. and S.R. acknowledge support from NSF (Grant No. 1847389). P.W and C.C. contributed equally to this work.

AUTHOR DECLARATIONS

Conflict of Interest

The authors have no conflicts to disclose.

Author Contributions

Peiran Wei: Conceptualization (equal); Writing – original draft (equal); Writing – review & editing (equal). **Ciera Cipriani:** Conceptualization (equal); Writing – original draft (lead); Writing – review & editing (lead). **Chia-Min Hsieh:** Writing – original draft (supporting); Writing – review & editing (supporting). **Krutarth Kamani:** Writing – original draft (supporting); Writing – review & editing (supporting). **Simon Rogers:** Conceptualization (supporting); Funding acquisition (supporting); Writing – review & editing (supporting). **Emily Pentzer:** Conceptualization (equal); Funding acquisition (equal); Writing – review & editing (equal).

NOMENCLATURE

3D	Three-dimensional
DIW	Direct ink writing
3DP	3D printing
FDM	Fused deposition modeling
σ	Shear stress
η	Viscosity
$\dot{\gamma}$	Shear rate
σ_y	Yield stress
G^*	Complex modulus
G'	Storage modulus
G''	Loss modulus
σ_0	Stress amplitude
γ_0	Strain amplitude
δ	Phase lag
η^*	Complex viscosity
ω	Angular frequency
3ITT	Three-interval thixotropy test
d_1, d_2, d_3, …	Filament diameter
F_s	Force of filament opposing gravity
θ	Angle of deflection
L	Half the distance between pillars in filament collapse test
C_f	Collapse area factor
ρ	Material density
g	Gravitational acceleration
C_f^l	Lateral area collapse factor
A_t^l	Theoretical area of pore formed from printing
A_a^l	Actual area of pore formed from printing
F_d	Distance between printed filaments
L_t	Theoretical printed layer thickness
F_s	Length of fused portion of adjacent filaments
P_r	Printability index
d_f	Theoretical filament radius
η_0	Matrix viscosity
$[\eta]$	Intrinsic viscosity
Φ	Volume fraction of solid particles
k_H	Huggins coefficient
Φ_{max}	Maximum solid fraction
AR	Aspect ratio
$[\eta]_\infty$	Lower bound of intrinsic viscosity
s	Degree of sphericity
R_{HS}	Hard-sphere particle radius
D	Interparticle surface-to-surface distance
R_{eff}	Effective particle radius
r	Thickness of layer on particle surface
ST	Shear-thinning
1D	One-dimensional
2D	Two-dimensional
LDP	Low-dimensional particle
PEDOT	Poly(3,4-ethylenedioxythiophene)
PSS	Polystyrene sulfonate
Φ^*	Critical volume fraction
h	LDP thickness
d	LDP diameter
κ^{-1}	Debye screening length
GO	Graphene oxide
PVA	Polyvinyl alcohol
Ct	Critical transition concentration
HIPE	High internal phase emulsion
PPGDMA	Poly(propylene glycol) dimethacrylate
DUDMA	Diurethane dimethacrylate
C7	Sodium 1-heptane sulfonate
κ-CA	κ-carrageenan
HA	Hyaluronic acid
ND	Nanodiamond
ND–COOH	Carboxylated nanodiamond
ND–OH	Hydroxylated nanodiamond
LM	Liquid metal
EGaIn	Eutectic gallium indium
ITO	Indium tin oxide
γ_{rec}	Recoverable or elastic strain
γ_{unrec}	Unrecoverable or plastic strain
d_p	Particle diameter
d_n	Nozzle diameter
ML	Machine learning

DATA AVAILABILITY

The data that support the findings of this study are available within this article.

REFERENCES

[1]V. G. Rocha, E. Saiz, I. S. Tirichenko, and E. García-Tuñón, "Direct ink writing advances in multi-material structures for a sustainable future," J. Mater. Chem. A **8**(31), 15646–15657 (2020).
[2]J. Cesarano, "A review of robocasting technology," MRS Proc. **542**, 133–139 (1998).
[3]J. N. Stuecker, J. E. Miller, R. E. Ferrizz, J. E. Mudd, and J. Cesarano, "Advanced support structures for enhanced catalytic activity," Ind. Eng. Chem. Res. **43**, 51–55 (2004).
[4]J. A. Lewis, "Direct ink writing of 3D functional materials," Adv. Funct. Mater. **16**(17), 2193–2204 (2006).
[5]L. Ouyang, R. Yao, Y. Zhao, and W. Sun, "Effect of bioink properties on printability and cell viability for 3D bioplotting of embryonic stem cells," Biofabrication **8**(3), 035020 (2016).

[6]M. Sarker and X. B. Chen, "Modeling the flow behavior and flow rate of medium viscosity alginate for scaffold fabrication with a three-dimensional bioplotter," J. Manuf. Sci. Eng. **139**, 081002 (2017).
[7]W. Liu, M. A. Heinrich, Y. Zhou, A. Akpek, N. Hu, X. Liu, X. Guan, Z. Zhong, X. Jin, A. Khademhosseini, and Y. S. Zhang, "Extrusion bioprinting of shear-thinning gelatin methacryloyl bioinks," Adv. Healthc. Mater. **6**, 1601451 (2017).
[8]J. Franco, P. Hunger, M. E. Launey, A. P. Tomsia, and E. Saiz, "Direct write assembly of calcium phosphate scaffolds using a water-based hydrogel," Acta Biomater. **6**, 218–228 (2010).
[9]Y. Maazouz, E. B. Montufar, J. Guillem-Marti, I. Fleps, C. Öhman, C. Persson, and M. P. Ginebra, "Robocasting of biomimetic hydroxyapatite scaffolds using self-setting inks," J. Mater. Chem. B **2**, 5378–5386 (2014).
[10]P. Jiang, C. Yan, Y. Guo, X. Zhang, M. Cai, X. Jia, X. Wang, and F. Zhou, "Direct ink writing with high-strength and swelling-resistant biocompatible physically crosslinked hydrogels," Biomater. Sci. **7**, 1805–1814 (2019).
[11]R. Ajdary, G. Reyes, J. Kuula, E. Raussi-Lehto, T. S. Mikkola, E. Kankuri, and O. J. Rojas, "Direct ink writing of biocompatible nanocellulose and chitosan hydrogels for implant mesh matrices," ACS Polym. Au **2**, 97–107 (2022).
[12]H. Yuk, B. Lu, S. Lin, K. Qu, J. Xu, J. Luo, and X. Zhao, "3D printing of conducting polymers," Nat. Commun. **11**, 1604 (2020).
[13]R. Haney, P. Tran, E. B. Trigg, H. Koerner, T. Dickens, and S. Ramakrishnan, "Printability and performance of 3D conductive graphite structures," Addit. Manuf. **37**, 101618 (2021).
[14]K. Xu, N. Zhao, Y. Li, P. Wang, Z. Liu, Z. Chen, J. Shen, and C. Liu, "3D printing of ultrathick natural graphite anodes for high-performance interdigitated three-dimensional lithium-ion batteries," Electrochem. Commun. **139**, 107312 (2022).
[15]Z. Wang, Q. Zhang, S. Long, Y. Luo, P. Yu, Z. Tan, J. Bai, B. Qu, Y. Yang, J. Shi, H. Zhou, Z.-Y. Xiao, W. Hong, and H. Bai, "Three-dimensional printing of polyaniline/reduced graphene oxide composite for high-performance planar supercapacitor," ACS Appl. Mater. Interfaces **10**, 10437–10444 (2018).
[16]S. Ao, Z. Guo, Y. Song, D. Fang, and Y. Bao, "Clog-free, low-cost, and uniform electrode inks for 3D printed lithium-ion batteries," ACS Appl. Energy Mater. **5**(6), 6970–6979 (2022).
[17]M. Abshirini, M. C. Saha, M. C. Altan, and Y. Liu, "3D printed flexible micro-scaled porous conductive polymer nanocomposites for piezoresistive sensing applications," Adv. Mater. Technol. **7**, 2101555 (2022).
[18]B. G. Compton and J. A. Lewis, "3D-printing of lightweight cellular composites," Adv. Mater. **26**, 5930–5935 (2014).
[19]G. Franchin, L. Wahl, and P. Colombo, "Direct ink writing of ceramic matrix composite structures," J. Am. Ceram. Soc. **100**(10), 4397–4401 (2017).
[20]F. Bos, R. Wolfs, Z. Ahmed, and T. Salet, "Additive manufacturing of concrete in construction: Potentials and challenges of 3D concrete printing," Virt. Phys. Protyp., **11**(3), 209–225 (2016).
[21]A. Paolini, S. Kollmannsberger, and E. Rank, "Additive manufacturing in construction: A review on processes, applications, and digital planning methods," Addit. Manuf. **30**, 100894 (2019).
[22]K. Shen, J. Ding, and S. Yang, "3D printing quasi-solid-state asymmetric micro-supercapacitors with ultrahigh areal energy density," Adv. Energy Mater. **8**, 1800408 (2018).
[23]C. E. Cipriani, T. Ha, O. B. Martinez Defilló, M. Myneni, Y. Wang, C. C. Benjamin, J. Wang, E. B. Pentzer, and P. Wei, "Structure–processing–property relationships of 3D printed porous polymeric materials," ACS Mater. Au **1**(1), 69–80 (2021).
[24]Q. Ge, A. H. Sakhaei, H. Lee, C. K. Dunn, N. X. Fang, and M. L. Dunn, "Multimaterial 4D printing with tailorable shape memory polymers," Sci. Rep. **6**, 31110 (2016).
[25]A. J. Young, R. Guillet-Nicolas, E. S. Marshall, F. Kleitz, A. J. Goodhand, L. B. L. Glanville, M. R. Reithofer, and J. M. Chin, "Direct ink writing of catalytically active UiO-66 polymer composites," Chem. Commun. **55**, 2190–2193 (2019).
[26]A. Saha, T. G. Johnston, R. T. Shafranek, C. J. Goodman, J. G. Zalatan, D. W. Storti, M. A. Ganter, and A. Nelson, "Additive manufacturing of catalytically active living materials," ACS Appl. Mater. Interfaces **10**, 13373–13380 (2018).
[27]X. Li, Y. Xue, R. Dehoff, C. Tsouris, and P. Taboada-Serrano, "Hierarchically-Structured Ti/TiO_2 electrode for hydrogen evolution synthesized via 3D printing and anodization," J. Energy Power Technol. **2**(2), 7 (2020).
[28]"Web of Science," Clarivate, www.webofscience.com/wos/woscc/basic-search (accessed 22 July 2023).
[29]P. Wei, C. E. Cipriani, and E. B. Pentzer, "Thermal energy regulation with 3D printed polymer-phase change material composites," Matter **4**(6), 1975–1989 (2021).
[30]I. Hager, A. Golonka, and R. Putanowicz, "3D printing of buildings and building components as the future of sustainable construction?," Proc. Eng. **151**, 292–299 (2016).
[31]M. E. Mackay, "The importance of rheological behavior in the additive manufacturing technique material extrusion," J. Rheol. **62**(6), 1549–1561 (2018).
[32]S.S. Crump, "Apparatus and method for creating three-dimensional objects," U.S. Patent No. 5,121,329 (9 June 1992).
[33]G. Gomez-Gras, R. Jerez-Mesa, J. A. Travieso-Rodriguez, and J. Lluma-Fuentes, "Fatigue performance of fused filament fabrication PLA specimens," Mater. Des. **140**, 278–285 (2018).
[34]L. del-Mazo-Barbara and M. P. Ginebra, "Rheological characterisation of ceramic inks for 3D direct ink writing: A review," J. Eur. Ceram. Soc. **41**(16), 18–33 (2021).
[35]P. Wei, H. Leng, Q. Chen, R. C. Advincula, and E. B. Pentzer, "Reprocessable 3D-printed conductive elastomeric composite foams for strain and gas sensing," ACS Appl. Polym. Mater. **1**(4), 885–892 (2019).
[36]C. E. Cipriani, N. C. Starvaggi, K. J. Edgehouse, J. B. Price, S. L. Vivod, and E. B. Pentzer, "Additive manufacturing: Modular platform for 3D printing fluid-containing monoliths," Mol. Syst. Des. Eng. **7**, 1039–1044 (2022).
[37]P. Wei, G. A. Bhat, C. E. Cipriani, H. Mohammad, K. Schoonover, E. B. Pentzer, and D. J. Darensbourg, "3D printed CO_2-based triblock copolymers and post-printing modification," Angew. Chem. Int. Ed. **61**(37), e202208355 (2022).
[38]N. A. Sears, T. S. Wilems, K. A. Gold, Z. Lan, S. N. Cereceres, P. S. Dhavalikar, R. Foudazi, and E. M. Cosgriff-Hernandez, "Hydrocolloid inks for 3D printing of porous hydrogels," Adv. Mater. Technol. **4**(2), 1800343 (2019).
[39]N. A. Sears, P. S. Dhavalikar, and E. M. Cosgriff-Hernandez, "Emulsion inks for 3D printing of high porosity materials," Macromol. Rapid Commun. **37**(16), 1369–1374 (2016).
[40]C. Minas, D. Carnelli, E. Tervoort, and A. R. Studart, "3D printing of emulsions and foams into hierarchical porous ceramics," Adv. Mater. **28**(45), 9993–9999 (2016).
[41]M. R. Sommer, L. Alison, C. Minas, E. Tervoort, P. A. Rühs, and A. R. Studart, "3D printing of concentrated emulsions into multiphase biocompatible soft materials," Soft Matter **13**(9), 1794–1803 (2017).
[42]L. Alison, S. Menasce, F. Bouville, E. Tervoort, I. Mattich, A. Ofner, and A. R. Studart, "3D printing of sacrificial templates into hierarchical porous materials," Sci. Rep. **9**, 409 (2019).
[43]S. Wüst, M. E. Godla, R. Müller, and S. Hofmann, "Tunable hydrogel composite with two-step processing in combination with innovative hardware upgrade for cell-based three-dimensional bioprinting," Acta Biomater. **10**(2), 630–640 (2014).
[44]Q. Lin, L. Li, M. Tang, S. Uenuma, J. Samanta, S. Li, X. Jiang, L. Zou, K. Ito, and C. Ke, "Kinetic trapping of 3D-printable cyclodextrin-based poly(pseudo) rotaxane networks," Chem **7**(9), 2442–2459 (2021).
[45]Z. Chen, D. Zhao, B. Liu, G. Nian, X. Li, J. Yin, S. Qu, and W. Yang, "3D printing of multifunctional hydrogels," Adv. Funct. Mater. **29**(20), 1900971 (2019).
[46]A. M. Watson, A. B. Cook, and C. E. Tabor, "Electrowetting-assisted selective printing of liquid metal," Adv. Eng. Mater. **21**(10), 1900397 (2019).
[47]C. Ladd, J.-H. So, J. Muth, and M. D. Dickey, "3D printing of free standing liquid metal microstructures," Adv. Mater. **25**(36), 5081–5085 (2013).
[48]T. V. Neumann and M. D. Dickey, "Liquid metal direct write and 3D printing: A review," Adv. Mater. Technol. **5**(9), 2000070 (2020).

[49]U. Daalkhaijav, O. D. Yirmibesoglu, S. Walker, and Y. Mengüç, "Rheological modification of liquid metal for additive manufacturing of stretchable electronics," Adv. Mater. Technol. **3**, 1700351 (2018).
[50]A. Haake, R. Tutika, G. M. Schloer, M. D. Bartlett, and E. J. Markvicka, "On-demand programming of liquid metal-composite microstructures through direct Ink write 3D printing," Adv. Mater. **34**(20), 2200182 (2022).
[51]R. Tu and H. A. Sodano, "Additive manufacturing of high-performance vinyl ester resin via direct ink writing with UV-thermal dual curing," Addit. Manuf. **46**, 102180 (2021).
[52]D. A. Rau, J. Herzberger, T. E. Long, and C. B. Williams, "Ultraviolet-assisted direct ink write to additively manufacture all-aromatic polyimides," ACS Appl. Mater. Interfaces **10**(41), 34828–34833 (2018).
[53]C. B. Arrington, D. A. Rau, C. B. Williams, and T. E. Long, "UV-assisted direct ink write printing of fully aromatic poly(amide imide)s: Elucidating the influence of an acrylic scaffold," Polymer **212**, 123306 (2021).
[54]Z. J. Smith, D. R. Barsoum, Z. L. Arwood, D. Penumadu, and R. C. Advincula, "Characterization of micro-sandwich structures via direct ink writing epoxy based cores," J. Sandw. Struct. Mater. **25**(1), 112–127 (2023).
[55]C. Hu, M. S. Haider, L. Hahn, M. Yang, and R. Luxenhofer, "Development of a 3D printable and highly stretchable ternary organic–inorganic nanocomposite hydrogel," J. Mater. Chem. B **9**(22), 4535–4545 (2021).
[56]Q. Chen, T. Sukmanee, L. Rong, M. Yang, J. Ren, S. Ekgasit, and R. Advincula, "A dual approach in direct ink writing of thermally cured shape memory rubber toughened epoxy," ACS Appl. Polym. Mater. **2**(12), 5492–5500 (2020).
[57]I. D. Robertson, M. Yourdkhani, P. J. Centellas, J. E. Aw, D. G. Ivanoff, E. Goli, E. M. Lloyd, L. M. Dean, N. R. Sottos, P. H. Geubelle, J. S. Moore, and S. R. White, "Rapid energy-efficient manufacturing of polymers and composites via frontal polymerization," Nature **557**, 223–227 (2018).
[58]J. Malda, J. Visser, F. P. Melchels, T. Jüngst, W. E. Hennink, W. J. A. Dhert, J. Groll, and D. W. Hutmacher, "25th anniversary article: Engineering hydrogels for biofabrication," Adv. Mater. **25**(36), 5011–5028 (2013).
[59]M. Costantini, J. Jaroszewicz, Ł. Kozoń, K. Szlązak, W. Święszkowski, P. Garstecki, C. Stubenrauch, A. Barbetta, and J. Guzowski, "3D-printing of functionally graded porous materials using on-demand reconfigurable microfluidics," Angew. Chem. Int. Ed. **131**, 7702–7707 (2019).
[60]W. Yang, J. Yang, J. J. Byun, F. P. Moissinac, J. Xu, S. J. Haigh, M. Domingos, M. A. Bissett, R. A. W. Dryfe, and S. Barg, "3D printing of freestanding MXene architectures for current-collector-free supercapacitors," Adv. Mater. **31**(37), 1902725 (2019).
[61]M. Müller, J. Becher, M. Schnabelrauch, and M. Zenobi-Wong, "Nanostructured Pluronic hydrogels as bioinks for 3D bioprinting," Biofabrication **7**(3), 035006 (2015).
[62]M. E. Cooke and D. H. Rosenzweig, "The rheology of direct and suspended extrusion bioprinting," APL Bioeng. **5**(1), 011502 (2021).
[63]B. Rodier, A. De Leon, C. Hemmingsen, and E. Pentzer, "Controlling oil-in-oil pickering-type emulsions using 2D materials as surfactant," ACS Macro Lett. **6**(11), 1201–1206 (2017).
[64]R. Foudazi, "HIPEs to PolyHIPEs," React. Funct. Polym. **164**, 104917 (2021).
[65]M. A. S. R. Saadi, A. Maguire, N. T. Pottackal, M. S. H. Thakur, M. M. Ikram, A. J. Hart, P. M. Ajayan, and M. M. Rahman, "Direct ink writing: A 3D printing technology for diverse materials," Adv. Mater. **34**(28), 2108855 (2022).
[66]A. Maguire, N. Pottackal, M. A. S. R. Saadi, M. M. Rahman, and P. M. Ajayan, "Additive manufacturing of polymer-based structures by extrusion technologies," Oxf. Open Mater. Sci. **1**(1), itaa004 (2020).
[67]S. Tagliaferri, A. Panagiotopoulos, and C. Mattevi, "Direct ink writing of energy materials," Mater. Adv. **2**, 540–563 (2021).
[68]A. M'Barki, L. Bocquet, and A. Stevenson, "Linking rheology and printability for dense and strong ceramics by direct ink writing," Sci. Rep. **7**, 6017 (2017).
[69]H. A. Barnes, "Thixotropy—A review," J. Non-Newton. Fluid Mech. **70**, 1–33 (1997).
[70]J. C. Conrad, S. R. Ferreira, J. Yoshikawa, R. F. Shepherd, B. Y. Ahn, and J. A. Lewis, "Designing colloidal suspensions for directed materials assembly," Curr. Opin. Colloid Interface Sci. **16**, 71–79 (2011).
[71]E. C. Bingham, *Fluidity and Plasticity* (McGraw-Hill, 1922).
[72]N. Casson, "Flow equation for pigment-oil suspensions of the printing ink-type," in *Rheology of Disperse Systems* (Pergamon Press, 1959), pp. 84–104.
[73]W. H. Herschel and R. Bulkley, "Konsistenzmessungen von gummi-benzollösungen," Kolloid-Z. **39**, 291–300 (1926).
[74]J. Feng, B.-L. Su, H. Xia, S. Zhao, C. Gao, L. Wang, O. Ogbeide, J. Feng, and T. Hasan, "Printed aerogels: Chemistry, processing, and applications," Chem. Soc. Rev. **50**(6), 3842–3888 (2021).
[75]I. Gibson, D. Rosen, and B. Stucker, *Additive Manufacturing Technology* (Springer, New York, 2019), pp. 147–173.
[76]J. J. Stickel and R. L. Powell, "Fluid mechanics and rheology of dense suspensions," Annu. Rev. Fluid Mech. **37**, 129–149 (2005).
[77]T. Tadros, "Correlation of viscoelastic properties of stable and flocculated suspensions with their interparticle interactions," Adv. Colloid Interface Sci. **68**, 97–200 (1996).
[78]T. Tadros, "Interparticle interactions in concentrated suspensions and their bulk (rheological) properties," Adv. Colloid Interface Sci. **168**(1), 263–277 (2011).
[79]D.-C. Kong, M.-H. Yang, X.-S. Zhang, Z.-C. Du, Q. Fu, X.-Q. Gao, and J.-W. Gong, "Control of polymer properties by entanglement: A review," Macromol. Mater. Eng. **306**(12), 2100536 (2021).
[80]R. S. Porter and J. F. Johnson, "The entanglement concept in polymer systems," Chem. Rev. **66**(1), 1–27 (1966).
[81]R. Porter and J. Johnson, "Shear viscosities of polyisobutene systems—A study of polymer entanglement," Polymer **3**, 11–16 (1962).
[82]N. Pashias, D. V. Boger, J. Summers, and D. J. Glenister, "A fifty cent rheometer for yield stress measurement," J. Rheol. **40**(6), 1179–1189 (1996).
[83]R. Hibbeler, *Mechanics of Materials* (Maxwell Macmillan International, New York, 1991).
[84]J. L. White, "Dynamics of viscoelastic fluids, melt fracture, and the rheology of fiber spinning," J. Appl. Polym. Sci. **8**(5), 2339–2357 (1964).
[85]S. A. Rogers, J. D. Park, and C.-W. J. Lee, "Instantaneous dimensionless numbers for transient nonlinear rheology," Rheol. Acta **58**, 539–556 (2019).
[86]R. J. Poole, "The Deborah and weissenberg numbers," Rheol. Bull. **53**(2), 32–39 (2012).
[87]P. K. Singh, J. C.-W. Lee, K. A. Patankar, and S. A. Rogers, "Revisiting the basis of transient rheological material functions: Insights from recoverable strain measurements," J. Rheol. **65**, 129–144 (2021).
[88]K. M. Kamani, G. J. Donley, R. Rao, A. M. Grillet, C. Roberts, A. Shetty, and S. A. Rogers, "Understanding the transient large amplitude oscillatory shear behavior of yield stress fluids," J. Rheol. **67**(2), 331–352 (2023).
[89]J. M. Dealy, "Weissenberg and Deborah numbers—Their definition and use," Rheol. Bull. **79**(2), 14–18 (2010).
[90]H. A. Barnes and K. Walters, "The yield stress myth?," Rheol. Acta **24**, 323–326 (1985).
[91]E. C. Bingham, *An Investigation of the Laws of Plastic Flow* (US Government Printing Office, 1917).
[92]J. G. Oldroyd, *Mathematical Proceedings of the Cambridge Philosophical Society* (Cambridge University Press, 1947), pp. 100–105.
[93]K. Hohenemser and W. Prager, "Über die Ansätze der Mechanik isotroper Kontinua," Z. Für Angew. Math. Mech. **12**(4), 216–226 (1932).
[94]W. Prager, *Introduction to Mechanics of Continua* (Ginn, Boston, 1961).
[95]P. Coussot and S. A. Rogers, "Oldroyd's model and the foundation of modern rheology of yield stress fluids," J. Non-Newton. Fluid Mech. **295**, 104604 (2021).
[96]P. Saramito, "A new elastoviscoplastic model based on the Herschel–Bulkley viscoplastic model," J. Non-Newton. Fluid Mech. **158**(1), 154–161 (2009).
[97]P. Saramito, "A new constitutive equation for elastoviscoplastic fluid flows," J. Non-Newton. Fluid Mech. **145**, 1–14 (2007).
[98]C. J. Dimitriou and G. H. McKinley, "A canonical framework for modeling elasto-viscoplasticity in complex fluids," J. Non-Newton. Fluid Mech. **265**, 116–132 (2019).
[99]S. M. Fielding, "Elastoviscoplastic rheology and aging in a simplified soft glassy constitutive model," J. Rheol. **64**(3), 723–738 (2020).

[100]K. Kamani, G. J. Donley, and S. A. Rogers, "Unification of the rheological physics of yield stress fluids," Phys. Rev. Lett. **126**(21), 218002 (2021).
[101]L. M. Sherman, "Rheometers: Which type is right for you?," *Plastics Technology*, www.ptonline.com/articles/rheometers-which-type-is-right-for-you (accessed 24 April 2023).
[102]Y. Shao, R. Han, X. Quan, and K. Niu, "Study on ink flow of silicone rubber for direct ink writing," J. Appl. Polym. Sci. **138**(33), 50819 (2021).
[103]S. Venkatraman, M. Okano, and A. Nixon, "A comparison of torsional and capillary rheometry for polymer melts: The Cox-Merz rule revisited," Polym. Eng. Sci. **30**(5), 308–313 (1990).
[104]A. U. Khan, N. Mahmood, and A. A. Bazmi, "Direct comparison between rotational and extrusion rheometers," Mater. Res. **12**(4), 477–481 (2009).
[105]H. A. Barnes, *A Handbook of Elementary Rheology* (The University of Wales Institute of Non-Newtonian Fluid Mechanics, Aberystwyth, 2000).
[106]P. R. d. S. Mendes, A. A. Alicke, and R. L. Thompson, "Parallel-plate geometry correction for transient rheometric experiments," Appl. Rheol. **24**(5), 1–10 (2014).
[107]R. H. Ewoldt, P. Winter, J. Maxey, and G. H. McKinley, "Large amplitude oscillatory shear of pseudoplastic and elastoviscoplastic materials," Rheol. Acta **49**, 191–212 (2010).
[108]M. M. Cross and A. Kaye, "Simple procedures for obtaining viscosity/shear rate data from a parallel disc viscometer," Polymer **28**(3), 435–440 (1987).
[109]Z. Fahimi, C. P. Broedersz, T. H. S. van Kempen, D. Florea, G. W. M. Peters, and H. M. Wyss, "A new approach for calculating the true stress response from large amplitude oscillatory shear (LAOS) measurements using parallel plates," Rheol. Acta **53**, 75–83 (2014).
[110]M. T. Shaw and Z. Z. Liu, "Single-point determination of nonlinear rheological data from parallel-plate torsional flow," Appl. Rheol. **16**(2), 70–79 (2006).
[111]K. Geiger, "Weissenberg-Rabinowitsch evaluation of flow curves measured with the parallel-disk rotational rheometer using a Carreau-type flow formula," Rheol. Acta **27**(2), 209–211 (1988).
[112]B. Rabinowitsch, "Über die viskosität und elastizität von solen," Z. Für Phys. Chem. **145**(1), 1–26 (1929).
[113]G. Wypych, *Handbook of Fillers* (ChemTec Publishing, Toronto, 2016).
[114]G. J. Donley, P. K. Singh, A. Shetty, and S. A. Rogers, "Elucidating the G″ overshoot in soft materials with a yield transition via a time-resolved experimental strain decomposition," Proc. Natl. Acad. Sci. U.S.A. **117**(36), 21945–21952 (2020).
[115]J. C.-W. Lee, K. M. Weigandt, E. G. Kelley, and S. A. Rogers, "Structure-property relationships via recovery rheology in viscoelastic materials," Phys. Rev. Lett. **122**(24), 248003 (2019).
[116]M. Dinkgreve, J. Paredes, M. M. Denn, and D. Bonn, "On different ways of measuring 'the' yield stress," J. Non-Newton. Fluid Mech. **238**, 233–241 (2016).
[117]A. Corker, H. C.-H. Ng, R. J. Poole, and E. García-Tuñón, "3D printing with 2D colloids: Designing rheology protocols to predict 'printability' of soft-materials," Soft Matter **15**(6), 1444–1456 (2019).
[118]J. Mewis, "Thixotropy—A general review," J. Non-Newton. Fluid Mech. **6**, 1–20 (1979).
[119]J. Mewis and N. J. Wagner, *Colloidal Suspension Rheology* (Cambridge University Press, New York, 2012).
[120]R. G. Larson and Y. Wei, "A review of thixotropy and its rheological modeling," J. Rheol. **63**(3), 477–501 (2019).
[121]T. Divoux, V. Grenard, and S. Manneville, "Rheological hysteresis in soft glassy materials," Phys. Rev. Lett. **110**(1), 18304 (2013).
[122]D. Therriault, S. R. White, and J. A. Lewis, "Rheological behavior of fugitive organic inks for direct-write assembly," Appl. Rheol. **17**(1), 10112 (2007).
[123]A. Ribeiro, M. M. Blokzijl, R. Levato, C. W. Visser, M. Castilho, W. E. Hennink, T. Vermonden, and J. Malda, "Assessing bioink shape fidelity to aid material development in 3D bioprinting," Biofabrication **10**, 014102 (2018).
[124]A. Habib, V. Sathish, S. Mallik, and B. Khoda, "3D printability of alginate-carboxymethyl cellulose hydrogel," Materials **11**(3), 454 (2018).
[125]N. Soltan, L. Ning, F. Mohabatpour, P. Papagerakis, and X. Chen, "Printability and cell viability in bioprinting alginate dialdehyde-gelatin scaffolds," ACS Biomater. Sci. Eng. **5**(6), 2976–2987 (2019).
[126]J. Archez, S. Maitenaz, L. Demont, M. Charrier, R. Mesnil, N. Texier-Mandoki, X. Bourbon, S. Rossignol, and J. F. Caron, "Strategy to shape, on a half-meter scale, a geopolymer composite structure by additive manufacturing," Open Ceram. **5**, 100071 (2021).
[127]J. Cesarano III, R. Segalman, and P. Calvert, "Robocasting provides moldless fabrication from slurry deposition," Ceram. Ind. **148**(4), 94 (1998).
[128]C. P. Lee, M. Takahashi, S. Arai, C.-L. K. Lee, and M. Hashimoto, "3D printing of Okara ink: The effect of particle size on the printability," ACS Food Sci. Technol. **1**(11), 2053–2061 (2021).
[129]S. L. Voon, J. An, G. Wong, Y. Zhang, and C. K. Chua, "3D food printing: A categorised review of inks and their development," Virtual Phys. Prototyp. **14**(3), 203–218 (2019).
[130]A. Bhardwaj, A. M. Rahman, X. Wei, Z. Pei, D. Truong, M. Lucht, and N. Zou, "3D printing of biomass–fungi composite material: Effects of mixture composition on print quality," J. Manuf. Mater. Process. **5**(4), 112 (2021).
[131]A. Dolganov, M. T. Bishop, G. Z. Chen, and D. Hu, "Rheological study and printability investigation of titania inks for direct ink writing process," Ceram. Int. **47**(9), 12020–12027 (2021).
[132]C. J. C. Nocheseda, F. P. Liza, A. K. M. Collera, E. B. Caldona, and R. C. Advincula, "3D printing of metals using biodegradable cellulose hydrogel inks," Addit. Manuf. **48**, 102380 (2021).
[133]H. A. Barnes, "Rheology of emulsions—A review," Colloids Surf. A Physicochem. Eng. Asp. **91**, 89–95 (1994).
[134]A. Einstein, "On the Movement of Small Particles Suspended in a Stationary Liquid Demanded by the Molecular-Kinetic Theory of Heat," Ann. Phys. **322**, 549–560 (1905).
[135]G. K. Batchelor, "The effect of Brownian motion on the bulk stress in a suspension of spherical particles," J. Fluid Mech. **83**(1), 97–117 (1977).
[136]I. M. Krieger and T. J. Dougherty, "A mechanism for non-Newtonian flow in suspensions of rigid spheres," Trans. Soc. Rheol. **3**, 137–152 (1959).
[137]M. M. Rueda, M.-C. Auscher, R. Fulchiron, T. Périé, G. Martin, P. Sonntag, and P. Cassagnau, "Rheology and applications of highly filled polymers: A review of current understanding," Prog. Polym. Sci. **66**, 22–53 (2017).
[138]H. Woods, *Rheology and Characterization of High-Solids Suspensions for Direct Ink Writing of Energetic Materials* (Georgia Institute of Technology, 2019).
[139]J. Y. Moon, S. Dai, L. Chang, J. S. Lee, and R. I. Tanner, "The effect of sphere roughness on the rheology of concentrated suspensions," J. Non-Newton. Fluid Mech. **223**, 233–239 (2015).
[140]H. Herrada-Manchón, D. Rodríguez-González, M. A. Fernández, N. W. Kucko, F. B. D. Groot, and E. Aguilar, "Effect on rheological properties and 3D printability of biphasic calcium phosphate microporous particles in hydrocolloid-based hydrogels," Gels **8**(1), 28 (2022).
[141]J. Maurath and N. Willenbacher, "3D printing of open-porous cellular ceramics with high specific strength," J. Eur. Ceram. Soc. **37**(15), 4833–4842 (2017).
[142]"The influence of particles on suspension rheology," Anton Paar Wiki, www.wiki.anton-paar.com/en/the-influence-of-particles-on-suspension-rheology (accessed 24 April 2023).
[143]K. Huang, H. Elsayed, G. Franchin, and P. Colombo, "3D printing of polymer-derived SiOC with hierarchical and tunable porosity," Addit. Manuf. **36**, 101549 (2020).
[144]C. E. Cipriani, Y. Shu, E. B. Pentzer, and C. C. Benjamin, "Viscoelastic and thixotropic characterization of paraffin/photopolymer composites for extrusion-based printing," Phys. Fluids **34**(9), 093106 (2022).
[145]W. Pabst, E. Gregorová, and C. Berthold, "Particle shape and suspension rheology of short-fiber systems," J. Eur. Ceram. Soc. **26**, 149–160 (2006).
[146]S. Mueller, E. W. Llewellin, and H. M. Mader, "The rheology of suspensions of solid particles," Proc. R. Soc. A Math. Phys. Eng. Sci. **466**, 1201–1228 (2009).
[147]Z. An, Y. Zhang, Q. Li, H. Wang, Z. Guo, and J. Zhu, "Effect of particle shape on the apparent viscosity of liquid–solid suspensions," Powder Technol. **328**, 199–206 (2018).
[148]B. J. Konijn, O. B. J. Sanderink, and N. P. Kruyt, "Experimental study of the viscosity of suspensions: Effect of solid fraction, particle size and suspending liquid," Powder Technol. **266**, 61–69 (2014).

[149]C. Ancey, "Role of lubricated contacts in concentrated polydisperse suspensions," J. Rheol. **45**(6), 1421 (2001).
[150]D. J. Jeffrey and A. Acrivos, "The rheological properties of suspensions of rigid particles," AIChE J. **22**(3), 417–432 (1976).
[151]S. A. Rogers, P. T. Callaghan, G. Petekidis, and D. Vlassopoulos, "Time-dependent rheology of colloidal star glasses," J. Rheol. **54**(1), 133–158 (2010).
[152]J. Mewis, W. J. Frith, T. A. Strivens, and W. B. Russel, "The rheology of suspensions containing polymerically stabilized particles," AIChE J. **35**(3), 415–422 (1989).
[153]L. C. Hsiao, S. Jamali, E. Glynos, P. F. Green, R. G. Larson, and M. J. Solomon, "Rheological state diagrams for rough colloids in shear flow," Phys. Rev. Lett. **119**(15), 158001 (2017).
[154]A. Singh, R. Mari, M. M. Denn, and J. F. Morris, "A constitutive model for simple shear of dense frictional suspensions," J. Rheol. **62**(2), 457–468 (2018).
[155]R. Seto, A. Singh, B. Chakraborty, M. M. Denn, and J. F. Morris, "Shear jamming and fragility in dense suspensions," Granul. Matter **21**, 1–8 (2019).
[156]A. Singh, C. Ness, R. Seto, J. J. de Pablo, and H. M. Jaeger, "Shear thickening and jamming of dense suspensions: The 'roll' of friction," Phys. Rev. Lett. **124**(24), 248005 (2020).
[157]S. Pradeep, M. Nabizadeh, A. R. Jacob, S. Jamali, and L. C. Hsiao, "Jamming distance dictates colloidal shear thickening," Phys. Rev. Lett. **127**(15), 158002 (2021).
[158]R. I. Tanner and S. Dai, "Particle roughness and rheology in noncolloidal suspensions," J. Rheol. **60**(4), 809–818 (2016).
[159]R. V. More and A. M. Ardekani, "Effect of roughness on the rheology of concentrated non-Brownian suspensions: A numerical study," J. Rheol. **64**, 67–80 (2020).
[160]Y. Lin, Y. Wang, H. Qin, D. Pan, and J. Chen, "Surface roughness effect on the shear thinning of non-colloidal suspensions," Phys. Fluids **33**(4), 043104 (2021).
[161]J. J. Cai and R. Salovey, "Model filled rubber. II. Particle composition dependence of suspension rheology," J. Polym. Sci. Part B Polym. Phys. **37**(8), 815–824 (1999).
[162]F. W. Laird, "Sedimentation of colloidal particles," J. Phys. Chem. **31**(7), 1034–1049 (1927).
[163]K. Cai, B. Román-Manso, J. E. Smay, J. Zhou, M. I. Osendi, M. Belmonte, and P. Miranzo, "Geometrically complex silicon carbide structures fabricated by robocasting," J. Am. Ceram. Soc. **95**(8), 2660–2666 (2012).
[164]G. Yang, Y. Sun, L. Qin, M. Li, K. Ou, J. Fang, and Q. Fu, "Direct-ink-writing (DIW) 3D printing functional composite materials based on supra-molecular interaction," Compos. Sci. Technol. **215**, 109013 (2021).
[165]L. Meng, A. S. Ivanov, S. Kim, X. Zhao, N. Kumar, A. Young-Gonzales, T. Saito, W. Bras, K. Gluesenkamp, and V. Bocharova, "Alginate–sodium sulfate decahydrate phase change composite with extended stability," ACS Appl. Polym. Mater. **4**(9), 6563–6571 (2022).
[166]Y. Jiang, Z. Xu, T. Huang, Y. Liu, F. Guo, J. Xi, W. Gao, and C. Gao, "Direct 3D printing of ultralight graphene oxide aerogel microlattices," Adv. Funct. Mater. **28**(16), 1707024 (2018).
[167]M. Escamilla, K. Pachuta, K. Huang, M. Klingseisen, H. Cao, H. Zhang, A. Sehirlioglu, and E. Pentzer, "Polymer particles armored with cobalt oxide nanosheets for the catalytic degradation of bisphenol A," Mater. Adv. **3**, 2354–2363 (2022).
[168]K. Pachuta, H. Volkova, B. Hirt, M.-H. Berger, E. Pentzer, and A. Sehirlioglu, "Liquid-phase exfoliation method to access cobalt oxide nanosheets in pH-neutral solutions," J. Am. Ceram. Soc. **105**(3), 1904–1912 (2022).
[169]Q. Sun, Y. Peng, X. Georgolamprou, D. Li, and R. Kiebach, "Synthesis and characterization of a geopolymer/hexagonal-boron nitride composite for free forming 3D extrusion-based printing," Appl. Clay Sci. **199**, 105870 (2020).
[170]S. S. L. Chan, R. M. Pennings, L. Edwards, and G. V. Franks, "3D printing of clay for decorative architectural applications: Effect of solids volume fraction on rheology and printability," Addit. Manuf. **35**, 101335 (2020).
[171]Y. Lakhdar, C. Tuck, A. Terry, C. Spadaccini, and R. Goodridge, "Direct ink writing of boron carbide monoliths," J. Eur. Ceram. Soc. **41**(16), 76–92 (2021).
[172]J. S. Pelz, N. Ku, W. T. Shoulders, M. A. Meyers, and L. R. Vargas-Gonzalez, "Multi-material additive manufacturing of functionally graded carbide ceramics via active, in-line mixing," Addit. Manuf. **37**, 101647 (2021).
[173]M. Greaves, M. Mende, J. Wang, W. Yang, and S. Barg, "Investigating the rheology of 2D titanium carbide (MXene) dispersions for colloidal processing: Progress and challenges," J. Mater. Res. **36**(22), 4578–4600 (2021).
[174]S. A. Mirkhani, A. Shayesteh Zeraati, E. Aliabadian, M. Naguib, and U. Sundararaj, "High dielectric constant and low dielectric loss via poly(vinyl alcohol)/$Ti_3C_2T_x$ MXene nanocomposites," ACS Appl. Mater. Interfaces **11**(20), 18599–18608 (2019).
[175]X. Zang, J. N. Hohman, K. Yao, P. Ci, A. Yan, M. Wei, T. Hayasaka, A. Zettl, P. J. Schuck, J. Wu, and L. Lin, "Metallo-hydrogel-assisted synthesis and direct writing of transition metal dichalcogenides," Adv. Funct. Mater. **29**(27), 1807612 (2019).
[176]C. M. Wang, Y. Y. Zhang, Y. Xiang, and J. N. Reddy, "Recent studies on buckling of carbon nanotubes," Appl. Mech. Rev. **63**(3), 030804 (2010).
[177]V. R. Dugyala, T. G. Anjali, S. Upendar, E. Mani, and M. G. Basavaraj, "Nano ellipsoids at the fluid–fluid interface: Effect of surface charge on adsorption, buckling and emulsification," Faraday Discuss. **186**, 419–434 (2016).
[178]S. M. Jogun and C. F. Zukoski, "Rheology and microstructure of dense suspensions of plate-shaped colloidal particles," J. Rheol. **43**(4), 847–871 (1999).
[179]J. Li, P. C. Ma, W. S. Chow, C. K. To, B. Z. Tang, and J.-K. Kim, "Correlations between percolation threshold, dispersion state, and aspect ratio of carbon nanotubes," Adv. Funct. Mater. **17**(16), 3207–3215 (2007).
[180]B. Chen, Y. Jiang, X. Tang, Y. Pan, and S. Hu, "Fully packaged carbon nanotube supercapacitors by direct ink writing on flexible substrates," ACS Appl. Mater. Interfaces **9**(34), 28433–28440 (2017).
[181]F. Zhang, K. Wu, X. Xu, W. Wu, X. Hu, K. Yu, and C. Liang, "3D printing of graphite electrode for lithium-ion battery with high areal capacity," Energy Technol. **9**(11), 2100628 (2021).
[182]J. Zhang, S. Uzun, S. Seyedin, P. A. Lynch, B. Akuzum, Z. Wang, S. Qin, M. Alhabeb, C. E. Shuck, W. Lei, E. Caglan Kumbur, W. Yang, X. Wang, G. Dion, J. M. Razal, and Y. Gogotsi, "Additive-free MXene liquid crystals and fibers," ACS Cent. Sci. **6**(2), 254–265 (2020).
[183]J. T. Muth, P. G. Dixon, L. Woish, L. J. Gibson, and J. A. Lewis, "Architected cellular ceramics with tailored stiffness via direct foam writing," Proc. Natl. Acad. Sci. U.S.A. **114**(8), 1832–1837 (2017).
[184]J. Paredes, M. A. J. Michels, and D. Bonn, "Rheology across the zero-temperature jamming transition," Phys. Rev. Lett. **111**(1), 15701 (2013).
[185]M. Dinkgreve, J. Paredes, M. A. J. Michels, and D. Bonn, "Universal rescaling of flow curves for yield-stress fluids close to jamming," Phys. Rev. E **92**(1), 12305 (2015).
[186]J. Sjoblom, *Emulsions and Emulsion Stability* (Taylor & Francis Group, LLC, Boca Raton, 2005).
[187]S. S. L. Chan, M. L. Sesso, and G. V. Franks, "Direct ink writing of hierarchical porous alumina-stabilized emulsions: Rheology and printability," J. Am. Ceram. Soc. **103**(10), 5554–5566 (2020).
[188]L. M. Prince, "A theory of aqueous emulsions I.: Negative interfacial tension at the oil/water interface," J. Colloid Interface Sci. **23**(2), 165–173 (1967).
[189]C. W. Visser, D. N. Amato, J. Mueller, and J. A. Lewis, "Architected polymer foams via direct bubble writing," Adv. Mater. **31**(46), 1904668 (2019).
[190]B. Herzhaft, "Rheology of aqueous foams: A literature review of some experimental works," Oil Gas Sci. Technol. **54**(5), 587–596 (1999).
[191]Y. Cheng, K. H. Chan, X.-Q. Wang, T. Ding, T. Li, X. Lu, and G. W. Ho, "Direct-ink-write 3D printing of hydrogels into biomimetic soft robots," ACS Nano **13**(11), 13176–13184 (2019).
[192]T. Xu, K. Liu, N. Sheng, M. Zhang, W. Liu, H. Liu, L. Dai, X. Zhang, C. Si, H. Du, and K. Zhang, "Biopolymer-based hydrogel electrolytes for advanced energy storage/conversion devices: Properties, applications, and perspectives," Energy Storage Mater. **48**, 244–262 (2022).
[193]Y. Guo, J. Bae, Z. Fang, P. Li, F. Zhao, and G. Yu, "Hydrogels and hydrogel-derived materials for energy and water sustainability," Chem. Rev. **120**(15), 7642–7707 (2020).
[194]V. G. Muir, S. Weintraub, A. P. Dhand, H. Fallahi, L. Han, and J. A. Burdick, "Influence of microgel and interstitial matrix compositions on granular hydrogel composite properties," Adv. Sci. **10**, 2206117 (2023).
[195]V. G. Muir, T. H. Qazi, S. Weintraub, B. O. Torres Maldonado, P. E. Arratia, and J. A. Burdick, "Sticking together: Injectable granular hydrogels with

increased functionality via dynamic covalent inter-particle crosslinking," Small **18**(36), 2201115 (2022).
[196]X. Cui, J. Li, Y. Hartanto, M. Durham, J. Tang, H. Zhang, G. Hooper, K. Lim, and T. Woodfield, "Advances in extrusion 3D bioprinting: A focus on multicomponent hydrogel-based bioinks," Adv. Healthc. Mater. **9**(15), 1901648 (2020).
[197]S. Uman, A. Dhand, and J. A. Burdick, "Recent advances in shear-thinning and self-healing hydrogels for biomedical applications," J. Appl. Polym. Sci. **137**(25), 48668 (2020).
[198]D. B. Emiroglu, A. Bekcic, D. Dranseikiene, X. Zhang, T. Zambelli, A. J. DeMello, and M. W. Tibbitt, "Building block properties govern granular hydrogel mechanics through contact deformations," Sci. Adv. **8**(50), eadd8570 (2022).
[199]J. R. Seth, M. Cloitre, and R. T. Bonnecaze, "Elastic properties of soft particle pastes," J. Rheol. **50**(3), 353–376 (2006).
[200]J. R. Seth, L. Mohan, C. Locatelli-Champagne, M. Cloitre, and R. T. Bonnecaze, "A micromechanical model to predict the flow of soft particle glasses," Nat. Mater. **10**(11), 838–843 (2011).
[201]L. Mohan and R. T. Bonnecaze, "Short-ranged pair distribution function for concentrated suspensions of soft particles," Soft Matter **8**(15), 4216–4222 (2012).
[202]F. Khabaz, B. F. Di Dio, M. Cloitre, R. T. Bonnecaze, F. Khabaz, R. T. Bonnecaze, and M. Cloitre, "Transient dynamics of soft particle glasses in startup shear flow: Part II: Memory and aging," J. Rheol. **66**(4), 717–730 (2022).
[203]F. Khabaz, B. F. Di Dio, M. Cloitre, and R. T. Bonnecaze, "Transient dynamics of soft particle glasses in startup shear flow: Part I: Microstructure and time scales," J. Rheol. **65**(2), 241–255 (2021).
[204]E. Mancha Sánchez, J. C. Gómez-Blanco, E. López Nieto, J. G. Casado, A. Macías-García, M. A. Díaz Díez, J. P. Carrasco-Amador, D. Torrejón Martín, F. M. Sánchez-Margallo, and J. B. Pagador, "Hydrogels for bioprinting: A systematic review of hydrogels synthesis, bioprinting parameters, and bioprinted structures behavior," Front. Bioeng. Biotechnol. **8**, 776 (2020).
[205]D. G. Lim, E. Kang, and S. H. Jeong, "pH-dependent nanodiamonds enhance the mechanical properties of 3D-printed hyaluronic acid nanocomposite hydrogels," J. Nanobiotechnol. **18**, 88 (2020).
[206]M. D. Dickey, R. C. Chiechi, R. J. Larsen, E. A. Weiss, D. A. Weitz, and G. M. Whitesides, "Eutectic gallium-indium (EGaIn): A liquid metal alloy for the formation of stable structures in microchannels at room temperature," Adv. Funct. Mater. **18**(7), 1097–1104 (2008).
[207]J.-H. Kim, S. Kim, J.-H. So, K. Kim, and H.-J. Koo, "Cytotoxicity of gallium-indium liquid metal in an aqueous environment," ACS Appl. Mater. Interfaces **10**(20), 17448–17454 (2018).
[208]J. E. Chandler, H. H. Messer, and G. Ellender, "Cytotoxicity of gallium and indium ions compared with mercuric ion," J. Rent. Res. **73**(9), 1554–1559 (1994).
[209]J. N. Koster, "Directional solidification and melting of eutectic GaIn," Cryst. Res. Technol. **34**(9), 1129–1140 (1999).
[210]A. R. Jacob, D. P. Parekh, M. D. Dickey, and L. C. Hsiao, "Interfacial rheology of gallium-based liquid metals," Langmuir **35**(36), 11774–11783 (2019).
[211]E. S. Elton, T. C. Reeve, L. E. Thornley, I. D. Joshipura, P. H. Paul, A. J. Pascall, and J. R. Jeffries, "Dramatic effect of oxide on measured liquid metal rheology," J. Rheol. **64**, 119–128 (2020).
[212]Q. Xu, N. Oudalov, Q. Guo, H. M. Jaeger, and E. Brown, "Effect of oxidation on the mechanical properties of liquid gallium and eutectic gallium-indium," Phys. Fluids **24**(6), 063101 (2012).
[213]B. Ma, C. Xu, J. Chi, J. Chen, C. Zhao, H. Liu, B. Ma, C. Xu, J. Chi, J. Chen, C. Zhao, and H. Liu, "A versatile approach for direct patterning of liquid metal using magnetic field," Adv. Funct. Mater. **29**(28), 1901370 (2019).
[214]E. Koos and N. Willenbacher, "Capillary forces in suspension rheology," Science **331**(6019), 897–900 (2011).
[215]E. Koos, "Capillary suspensions: Particle networks formed through the capillary force," Curr. Opin. Colloid Interface Sci. **19**(6), 575–584 (2014).
[216]E. Koos, J. Johannsmeier, L. Schwebler, and N. Willenbacher, "Tuning suspension rheology using capillary forces," Soft Matter **8**(24), 6620–6628 (2012).
[217]S. Roh, D. P. Parekh, B. Bharti, S. D. Stoyanov, and O. D. Velev, "3D printing by multiphase silicone/water capillary inks," Adv. Mater. **29**(30), 1701554 (2017).
[218]H. Ding, S. Barg, and B. Derby, "Direct 3D printing of graphene using capillary suspensions," Nanoscale **12**(21), 11440–11447 (2020).
[219]J. Dittmann, J. Maurath, B. Bitsch, and N. Willenbacher, "Highly porous materials with unique mechanical properties from smart capillary suspensions," Adv. Mater. **28**(8), 1689–1696 (2016).
[220]P. He, X. Tang, L. Chen, P. Xie, L. He, H. Zhou, D. Zhang, and T. Fan, "Patterned carbon nitride-based hybrid aerogel membranes via 3D printing for broadband solar wastewater remediation," Adv. Funct. Mater. **28**(29), 1801121 (2018).
[221]J. I. Cesarano and P. D. Cavert, "Freeforming objects with low-binder slurry," U.S. Patent No. 6,027,329 (22 February 2000).
[222]M. Chen, H. Li, L. Yang, S. Wang, P. Zhao, Y. Huang, L. Lu, G. Yue, and Q. Li, "Rheology and shape stability control of 3D printed calcium sulphoaluminate cement composites containing paper milling sludge," Addit. Manuf. **54**, 102781 (2022).
[223]A. Schwab, R. Levato, M. D'Este, S. Piluso, D. Eglin, and J. Malda, "Printability and shape fidelity of bioinks in 3D bioprinting," Chem. Rev. **120**(19), 11028–11055 (2020).
[224]K. Weissenberg, "A continuum theory of rhelogical phenomena," Nature **159**, 310–311 (1947).
[225]M. Reiner, "The Deborah number," Phys. Today **17**(1), 62–62 (1964).
[226]J. J. Griebler and S. A. Rogers, "The nonlinear rheology of complex yield stress foods," Phys. Fluids **34**(2), 23107 (2022).
[227]S. Varchanis, S. J. Haward, C. C. Hopkins, A. Syrakos, A. Q. Shen, Y. Dimakopoulos, and J. Tsamopoulos, "Transition between solid and liquid state of yield-stress fluids under purely extensional deformations," Proc. Natl. Acad. Sci. U.S.A. **117**(23), 12611–12617 (2020).
[228]A. Das, E. L. Gilmer, S. Biria, M. J. Bortner, E. L. Gilmer, S. Biria, and M. J. Bortner, "Importance of polymer rheology on material extrusion additive manufacturing: Correlating process physics to print properties," ACS Appl. Polym. Mater. **3**(3), 1218–1249 (2021).
[229]J. An, J. E. M. Teoh, R. Suntornnond, and C. K. Chua, "Design and 3D printing of scaffolds and tissues," Engineering **1**(2), 261–268 (2015).
[230]D. Cipollone, J. A. Mena, K. Sabolsky, E. M. Sabolsky, and K. A. Sierros, "Coaxial ceramic direct ink writing on heterogenous and rough surfaces: Investigation of core-shell interactions," ACS Appl. Mater. Interfaces **14**(21), 24897–24907 (2022).
[231]H. Yuk and X. Zhao, "A new 3D printing strategy by harnessing deformation, instability, and fracture of viscoelastic inks," Adv. Mater. **30**(6), 1704028 (2018).
[232]A. Nadernezhad and J. Groll, "Machine learning reveals a general understanding of printability in formulations based on rheology additives," Adv. Sci. **9**(29), 2202638 (2022).
[233]H. Zhang and S. K. Moon, "Reviews on machine learning approaches for process optimization in noncontact direct ink writing," ACS Appl. Mater. Interfaces **13**(45), 53323–53345 (2021).
[234]Y. Liu, T. Zhao, W. Ju, and S. Shi, "Materials discovery and design using machine learning," J. Materiomics **3**(3), 159–177 (2017).
[235]M. Mahmoudabadbozchelou, M. Caggioni, S. Shahsavari, W. H. Hartt, G. Em Karniadakis, and S. Jamali, "Data-driven physics-informed constitutive metamodeling of complex fluids: A multifidelity neural network (MFNN) framework," J. Rheol. **65**(2), 179–198 (2021).
[236]M. Mahmoudabadbozchelou and S. Jamali, "Rheology-informed neural networks (RhINNs) for forward and inverse metamodelling of complex fluids," Sci. Rep. **11**, 12015 (2021).
[237]M. Mahmoudabadbozchelou, G. E. Karniadakis, and S. Jamali, "nn-PINNs: Non-newtonian physics-informed neural networks for complex fluid modeling," Soft Matter **18**, 172–185 (2021).
[238]M. Mahmoudabadbozchelou, K. M. Kamani, S. A. Rogers, and S. Jamali, "Digital rheometer twins: Learning the hidden rheology of complex fluids through rheology-informed graph neural networks," Proc. Natl. Acad. Sci. **119**(20), e2202234119 (2022).